AN ABSTRACT OF THE THESIS OF

D. Kurt Gaskill for the degree of Doctor of Philosophy in Physics presented on July 10, 1984.

Title: Perturbed Angular Correlation Measurements of Hyperfine Fields in Liquid and Amorphous Selenium-Tellurium Alloys

Redacted for Privacy

Abstract approved: John A. Gardner

The correlation time of fluctuating hyperfine fields in liquid Se_xTe_{1-x} has been measured, for the temperature range of about 260°C to 980°C and throughout the composition range, using the perturbation of angular correlations (PAC) of dissolved dilute ^{111}Cd impurities. The angular correlation of ^{111}Cd was exponentially damped and consistent with the effect of either a randomly fluctuating electric field gradient (EFG) or a paramagnetic relaxation mechanism (PRM). The measured attenuation factor is not consistent with any simple EFG fluctuation, since that model would imply bond lifetimes too short for large rotating molecules or an atomic jump frequency faster than phonon frequencies for small molecules. The PRM model is consistent with experiment provided the Cd is bonded to a small paramagnetic molecule or ion. Good scaling between the measured attenuation factor and the correlation time of fluctuating

spins measured in liquid Se by Warren and Dupree supports this contention and gives a value for the hyperfine coupling parameter, $\langle\omega_S^2\rangle_{E.A.} = 9.05 \times 10^{17}\ s^{-2}$. The existence of small paramagnetic Cd - chalcogen molecules with a hyperfine coupling of this size is consistent with a modification of Cutler's bond equilibrium theory. By assuming that the coupling parameter is concentration-independent, the PAC data yield spin correlation times which decrease as the Te composition and temperature are increased, consistent with the midrange alloy NMR data of Kirby. The shortest time calculated, 10^{-13}s, was measured at the highest temperature in Te, about 450°C, and the longest time, about 10^{-11}s, for the lowest measured temperature in $Se_{0.5}Te_{0.5}$, about 350°C. The spin correlation time τ_S scaled reasonably well with the spin density. Some concentration-dependent effects were seen but these are tentatively attributed to changes in the effective coupling constant. τ_S is approximately proportional to the spin density at high densities and to the square root of the spin density at low densities. The data imply a Te-Te bond strength of 1.1(1)eV and an upper limit to the rotation time of Cd-containing molecules of 10^{-10} to 10^{-11}s. The data supply an estimate of the defect spin density in liquid tellurium, supercooled below 350°C. Additionally, the data imply that In is insoluble in Se below about 450°C but soluble to at least a ppm in Te at 260°C.

Perturbed Angular Correlation Measurements of Hyperfine Fields in Liquid and Amorphous Selenium-Tellurium Alloys

by

D. Kurt Gaskill

A THESIS

submitted to

Oregon State University

in partial fulfillment of
the requirements for the
degree of

Doctor of Philosophy

Completed July 10, 1984

Commencement June 1985

APPROVED:

Redacted for Privacy

Professor of Physics in charge of major

Redacted for Privacy

Chairman of the department of Physics

Redacted for Privacy

Dean of Graduate School

Date thesis is presented July 10, 1984

Typed by Katherine Haag for D. Kurt Gaskill

ACKNOWLEDGEMENT

The helpful efforts of the faculty, staff, and students of Oregon State University, and in particular the Department of Physics, are sincerely appreciated. Special thanks to Dr. Kenneth Krane for helping me with the electronics of the spectrometer, Lou Klahn for answering questions about electronics in general, and Dr. Melvin Cutler for useful and stimulating discussions.

Also, special thanks to Dr. Robert Rasera (UMBC) for his guiding insight in using the spectrometer and the theory of PAC, Dr. Horst Radscheit (Heidelburg) for his useful criticisms and Dr. William Warren, Jr. (Bell Lab) for extremely useful discussions about his measurements, my measurements, and the connection between the two.

I acknowledge the support of the Office of Naval Research and the OSU Department of Physics for my enjoyable stay in Corvallis.

Sincere thanks to the great effort by Kathy Haag in typing this thesis.

Heartfelt thanks to my advisor, Dr. John Gardner, for his support, help and guidance in producing this work and physics in general.

And one million grateful thank-you's to my wife, Cheryl, for putting up with all this ____ throughout the country and the years. This is our thesis, Cher.

TABLE OF CONTENTS

LIST OF FIGURES

LIST OF TABLES

PERTURBED ANGULAR CORRELATION MEASUREMENTS OF HYPERFINE FIELDS IN LIQUID AND AMORPHOUS SELENIUM-TELLURIUM ALLOYS

I. INTRODUCTION

Either by themselves, or alloyed with other elements, the liquid chalcogen elements, O, S, Se, Te, and Po, exhibit a wide range of physical and electronic properties continuously variable with composition. For example, S is a polymeric, nearly insulating liquid with a ring phase at temperatures just above its melting point, Se is a liquid semiconductor containing 2-fold bonded chains, liquid Te is a poor metal and is roughly 3-fold coordinated, and Po is a 6-fold coordinated liquid metal. The electronic properties are a consequence of the physical structure of these materials and depend on the existence of various types of thermally generated bond defects. Good introductory sources on liquid semiconductors and chalcogens are Cutler[1] and Glazov et al.[2] Current research endeavors can be found in the proceedings of the International Conference of Liquid and Amorphous Semiconductors and the International Conference of Liquid and Amorphous Metals, both of which are held every two years.

1.1 Physical Properties of Se_xTe_{1-x}

Liquid selenium-tellurium alloys, the subject of this work, are particularly interesting systems to study. By continuously changing the composition from selenium to tellurium, the structure

continuously changes from long chains[2], of about 10^5 atoms[3], that are mainly 2-fold coordinated[4,5], to a mainly 3-fold coordinated[6,7] structure[2]. (Selenium and tellurium are completely miscible with melting points of 217°C and 450°C respectively[8].) For pure Se the existence of a ring-like phase is doubtful[9] and for pure Te the coordination number increases continuously to 5 at a temperature of approximately 1600°C[6]. The increase in the density of the alloy system[10,11], the decrease in viscosity[12], and a reduction in the thermal expansion coefficient[11,13] with increasing tellurium composition and temperature are consistent with the change to 3-fold bonding and shorter mean chain length.

The observed change in near neighbor coordination is also associated with the thermal generation of additional or "defect" bonding states[14], which can be understood in the following way. The predominant covalent 2-fold bonding of selenium and selenium-tellurium alloys is due to the atomic configuration s^2p^4. The two s-state electrons do not participate in the bonding. Two of the p-state electrons are used to form part of the covalent bonds with two adjacent neighbor chalcogens. The other two p-state electrons enter into a nonbonding "lone pair" state. The empty p-states, at higher energies, are antibonding states. The resulting chain structure is actually helical, because of the orientation of the p-orbitals, in the solid trigonal crystal and is probably

preserved in the liquid[4]. The symbol D_2 is often used to describe the 2-fold bonding at the chalcogen sites.

At elevated temperatures one of the bonds may not be satisfied. The unpaired electron is in the so-called "dangling" bond state and the symbol D_1^* is often used to designate this configuration. The addition of an electron effectively reduces the energy of the dangling bond, through electron pairing, forming a D_1^- center[15].

The 2-fold coordinated chain can be modified by additional bonding, forming a 3-fold center by using one of the lone pair electrons as one-half of a bonding pair, leaving an unpaired electron in the lone pair state. These states are designated D_3^*. Removing the electron remaining in the lone pair state lowers the energy of the 3-fold center by eliminating the lone pair-covalent bond interaction. This combination is called a D_3^+ center.

It has been suggested that the D_1^- and D_3^+ centers are the most stable bonding states and the D_1^* and D_3^* centers are the thermally generated states[15,16]. The D_3^+ center may be one of the dominant bonding states in tellurium. The energies and concentrations of these defects are matters of significant research interest and some controversy at present. However, it is generally accepted that the D^*, D_1^-, and D_3^+ defects should exist in significant concentrations.

1.2 Electronic and Magnetic Properties Se_xTe_{1-x}

Detailed measurements of the conductivity of Se_xTe_{1-x} alloys have been carried out by Perron[17,18] and Rasolondramanitra[19]. The conductivity of selenium at the melting point is about $10^{-5}\Omega^{-1}cm^{-1}$. The conductivity increases (to approximately $10^{3}\Omega^{-1}cm^{-1}$ for high-temperature tellurium) as the tellurium content and temperature is increased. The alloys exhibit semiconducting properties in the lower temperature regions, with the onset of metallic conductivity occurring at high temperatures and decreasing with tellurium content. Ionic conduction is not a dominant conductivity mechanism in these materials but can play a small role, especially at low temperatures and selenium-rich compositions[19]. To observe semiconducting properties of tellurium, it must be supercooled at least 100°C, because it is essentially metallic at the melting point. Very little experimental data exist for such extreme supercooled material, and it has not been definitively shown that tellurium is semiconducting at all.

The thermopower measurements of Perron and of Rasolondramanitra decrease with increasing tellurium content and temperature, where the cutoff from simple activated behavior occurs at roughly the same temperature as the semiconducting region ends. These electrical properties are generally consistent with an increase in the concentration of D_1^- centers, determined from a model based on bond equilibrium theory (BET)[19], extensively developed by Cutler[1,20], and Cutler and Bez[21].

Conductivity and thermopower measurements of monovalent doping in Se_xTe_{1-x} alloys have been made by Radscheit et al.[22] and Fischer et al.[23] Using an extension of BET, the data are consistent with a model in which the metal atoms are bonded to chalcogen atoms, and about one half are associated with diatomic metal-chalcogen negative ions, denoted D_M^- centers.

It is worthwhile to mention that oxygen impurities greatly influence the conductivities of the alloys. This subject is extensively reviewed and treated by Rasolondramanitra[19].

The density of states is qualitatively similar to that of the solid except that band tailing occurs and singularities are smoothed by the effects of long range disorder and potential fluctuations[2]. The deep band-tail states are localized and cannot readily conduct electrical current. They are believed to merge relatively abruptly, at an energy called the mobility edge, with extended states which participate in electrical conduction.

The distance between the mobility edges at the conductivity and valence bands is called the mobility gap and is analogous to a band gap in a crystalline semiconductor. The s-states and bonding p-states of the chalcogen form deep valence bands, the non-bonding p-electrons form the valence band, and the anti-bonding p-states and higher-lying s-states form the conduction band.

The acceptor states in the mobility gap are predicted by BET to be caused by formation of D_1^- centers, and the donor states by D_3^+

centers. Since the density of defects can change with temperature and composition, the Fermi level can move throughout a large portion of the mobility gap. Rasolondramanitra[19] indicates that the electrical transport properties are mainly governed by an increase in the number of acceptor states with increasing tellurium content and temperature. Fischer et al.[23] find that monovalent doping results in a growth of the acceptor band through an increase in the concentration of D_M^- centers.

Magnetic susceptibility measurements have been carried out by Gardner and Cutler in Se_xTe_{1-x} alloys[24]. The data exhibit an activated temperature dependence in the semiconducting region at low temperatures. Unpaired electrons in the D_1^* (and possibly D_3^*) centers contribute a Curie law susceptibility per spin, and the data yield the concentration of defect centers. Calculated values of spin concentration are about 10^{-4} for low temperature selenium to approximately 10^{-1} at the semiconductor-metal transition. The activation energy is one-half the energy required to break a 2-fold bond to form the D_1^* centers.

As the tellurium content and temperature is increased, the activated behavior ceases and the susceptibility begins to saturate, indicating spin-spin interactions are becoming important.

Nuclear magnetic resonance (NMR) on selenium was first performed by Brown et al.[25], and more extensively by Warren and Dupree[26] at various pressures. The NMR results were used by

Warren and Dupree[26] to calculate the correlation time of spin fluctuations. The correlation time decreases with increasing temperature and pressure, but apparently depends only on the density of spins and not explicitly on pressure or temperature. Kirby[27] made NMR measurements on $Se_{0.5}Te_{0.5}$ and $Se_{0.4}Te_{0.6}$ and found correlation times the same order of magnitude as Warren and Dupree and decreasing as the tellurium composition and temperature increases.

1.3 Perturbed Angular Correlations in Se_xTe_{1-x}

It is not exactly clear what roles the various defect centers play in the physical and electrical properties of Se_xTe_{1-x}. The time scales, reaction mechanisms, electronic, and magnetic interactions of these bonding defects have been subject of informed speculation but relatively little hard data.

The microscopic technique of perturbed angular correlations (PAC) gives the experimenter the ability to sample the fluctuating hyperfine fields at the site of the PAC probe. The dominant hyperfine fields were expected to be electric field gradients whose random fluctuations are due to thermal generation of defect centers. Hyperfine fields due to magnetic interactions with a nearby spin are also present, but these were expected to be small, since the density of electronic spins is small. If the spins are randomly distributed with respect to the PAC probe, this mechanism would contribute negligibly to the PAC relaxation.

As the reader will find, the above expectation was apparently incorrect for this experiment. The probe apparently is chemically bound with high probability to a magnetic molecule and thus the magnetic interaction is much larger than anticipated. Also the electric quadrupolar interaction is much weaker than expected with the result that the magnetic interaction dominates. The data provide significant new information about the dynamics of the electron-spin and suggest that the dynamics depend only on electron spin interactions. These results have important implications on other magnetism research both in the selenium-tellurium alloys and on some general problems in many-body physics.

CHAPTER II

THEORY OF ANGULAR CORRELATIONS

2.1 Angular Correlation

There are many examples of the decay of excited nuclear states to ground states or meta-stable states by the emission of successive particles and/or radiations.[28] The observed characteristics of these decays are the spin, parity, energy of the participating levels, and the multipolarities of the emitted radiation.

Knowing the characteristics of the levels involved in a decay by successive emission from an excited state, calculations can be done to determine the probability that the i^{th} particle or radiation is observed at the angular coordinates θ_i, ϕ_i with respect to the first particle or radiation emitted. The probability is called the angular correlation function of the successive decay. This work will focus on the angular correlation of two successive gamma radiations from ^{111}Cd, shown schematically in figure 2-1. Details and properties of the decay are listed in table 2-1.

For the ^{111}Cd case, the probability that a nucleus decaying through the cascade by emitting γ_1, into the solid angle $d\Omega_1$, and then γ_2 into the solid angle $d\Omega_2$, is the angular correlation function, $W(\vec{K}_1,\vec{K}_2)d\Omega_1 d\Omega_2$, where $\vec{K}_1$ and $\vec{K}_2$ are the directions of the two successive gamma decays.

Discrepancies between theory and experiment are accounted for by the presence of external perturbing fields acting on the

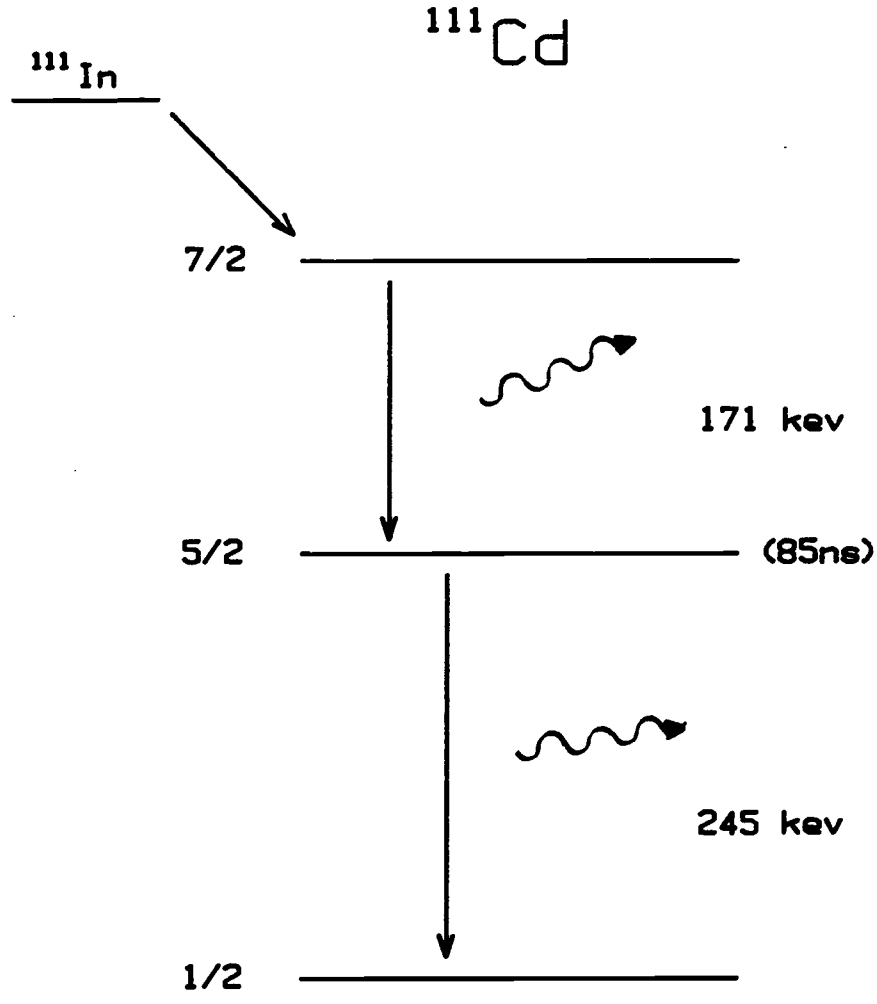

Figure 2-1 Decay scheme of ^{111}Cd.

Table 2-1 Characteristics of ^{111}Cd

Parent $^{111}In \xrightarrow{\beta} {}^{111}Cd$, $\tau_{\frac{1}{2}}$ = 2.83d.

	Initial State	Intermediate State	Final State
spin	$7/2^+$	$5/2^+$	$1/2^+$
energy	416.70(10)keV	245.42(1)keV	0.0
branching ratio	99.17%	100%	----
half life ($\tau_{\frac{1}{2}}$)	120(30)ps	85.0(7)ns	stable
Quadrupole moment (Q)	?	+0.77(12)b	none
Magnetic moment (μ)	?	-0.7656(25)	-0.5948856(9)
Gamma energy		171.3 KeV	245.4 KeV
multipolarity		M1, E2	E2
mixing ratio (δ)		-0.144(3)	--

Values taken from Nuc. Data 27 (1979)[29]

nucleus. Knowledge of the magnitude and geometry of the perturbing fields at the nuclear site is gained by comparing experiment with the calculated effects for the particular field.

The physical reason for the angular correlation is as follows. The first radiation, γ_1, is emitted with no directional preference because the nuclei are randomly oriented in the sample. By observing γ_1 in the direction $\vec{K}_1$ those nuclei that are oriented preferentially for the emission of γ_1 in that direction are observed. The nuclei are now in the intermediate state with some relative (in general, unequal) population of m states. (The direction $\vec{K}_1$ can serve as a convenient quantization axis.) Upon decaying to the ground state, the relative m state population plus the selection rules of the decay (determined by the multipolarity and mixing ratios of the emitted γ_2) determine the probability that γ_2 will be emitted into the direction $\vec{K}_2$.

Without the effect of external perturbing fields, the unperturbed angular correlation function has the following form: (The mathematics for unperturbed angular correlation is covered in the Appendix, sections A through C)

$$W(\vec{K}_1,\vec{K}_2) = \sum_{\substack{k=0 \\ (\text{even } k)}}^{k_{MAX}} A_k(\gamma_1)A_k(\gamma_2)P_k(\cos\theta) \qquad 2\text{-}1$$

where:

1) θ is the angle between $\vec{K}_1$ and $\vec{K}_2$.

2) The parameter $A_k(\gamma_1)=A_k(L_1L_1'I_iI)$ is a number which depends only on the multipolarity of the emitted radiation, L_1 and

L_1', and the spins of nuclear states involved in the transition. (Note: A_0=1 for overall normalization.) Tabulations can be found in references such as 30.

3) The parameter $A_k(\gamma_2)=A_k(L_2L_2'I_fI)$ is a number similar to that above involving the multipolarities and spins of the second radiation.

4) The sum is finite with $k_{MAX}=MIN(2I, L_1+L_1', L_2+L_2')$.

5) The sum is over only even k values.

6) Circular polarization of the radiations are not observed (directional correlation only).

The physical reasons behind this result are:

1) The initial m state populations are equal because local quantization axes of the fields sensed by the excited nuclei are randomly distributed throughout the sample.

2) The decay depends only on nuclear transition parameters, e.g., spins, multipolarities. The connection between successive decays is through the Legendre polynomial term, $P_k(\cos\theta)$, which comes about from the unequal m state populations in the intermediate state.

3) The index k represents the coupling of angular momentum and must satisfy the triangle condition with the vector sets $(\vec{I}, \vec{I}, \vec{k})$, $(\vec{L_1}, \vec{L_1}', \vec{k})$ and $(\vec{L_2}, \vec{L_2}', \vec{k})$. Thus k has the maximum value given above.

4) Not observing the circular polarization of the emitted radiation imposes the constraint that only even values of k need be considered.

5) External perturbations are not present.

For the ^{111}Cd isotope, $k_{MAX}=4$. Thus, $A_2(\gamma_1)A_2(\gamma_2)$ and $A_4(\gamma_1)A_4(\gamma_2)$ need be considered. The best values for these terms as of this writing are: $A_2(\gamma_1)A_2(\gamma_2)=-0.180(2)$ and $A_4(\gamma_1)A_4(\gamma_2)=+0.002(3)$.[31]

2.2 Perturbations - Static

When considering the effect of externally applied perturbations with Hamiltonian K(t) (whether intrinsic crystal or dipolar fields or laboratory-generated magnetic fields), the perturbation is assumed to act on the intermediate state from the instant it is formed until the moment of the emission of the second radiation. It is unnecessary to consider perturbations acting on the initial state since the observation of the first gamma chooses those nuclei that are preferentially oriented whether or not a perturbing field is present.

The formalism used in the case of perturbing fields is that of the time evolution operator, $\Lambda(t)=\exp[\frac{-i}{\hbar}\int_0^t K(t')\,dt']$. This operator acts on the m states of the intermediate state causing transitions amongst themselves. The perturbed angular correlation function in this case becomes

$$W(\vec{K}_1,\vec{K}_2,t) =$$

$$\sum_{\substack{k_1,N_1\\k_2,N_2}} A_{k_1}(\gamma_1)A_{k_2}(\gamma_2)(\hat{k}_1\hat{k}_2)\; G^{N_1N_2}_{k_1k_2}(t)\; Y^{N_1}_{k_1}{}^{*}(\theta_1,\phi_1)Y^{N_2}_{k_2}(\theta_2,\phi_2) \qquad 2\text{-}2$$

where the attenuation factor $G_{k_1k_2}^{N_1N_2}(t)$ has the form

$$G_{k_1k_2}^{N_1N_2}(t) = \sum_{m_a,m_b} (-1)^{2I+m_a+m_b}(\hat{k}_1\hat{k}_2)^{\frac{1}{2}}\begin{pmatrix} I & I & k_1 \\ m_a' & -m_a & N_1 \end{pmatrix}\begin{pmatrix} I & I & k_2 \\ m_b' & -m_b & N_2 \end{pmatrix}$$

$$\langle Im_b|\Lambda(t)|Im_a\rangle\langle I\, m_b'|\Lambda(t)|Im_a'\rangle^* \qquad 2\text{-}3$$

and (θ_i,ϕ_i) are the emission directions of the respective photons. The notation $\hat{k}=2k+1$ is used.

(Mathematical details on the effect of perturbing fields can be found in the Appendix, sections D through H.) The two cases of most interest are where the excited nuclear state is present in a single crystal or powdered sample. For the single crystal case the attenuation factor becomes

$$G_{k_1k_2}^{N_1N_2}(t) = \sum_{\substack{m_a,m_b \\ n,n'}} (-1)^{2I+m_a+m_b}(\hat{k}_1\hat{k}_2)^{\frac{1}{2}}\begin{pmatrix} I & I & k_1 \\ m_a' & -m_a & N_1 \end{pmatrix}\begin{pmatrix} I & I & k_2 \\ m_b' & -m_b & N_2 \end{pmatrix}$$

$$\langle n|m_b\rangle^*\langle n|m_a\rangle\langle n'|m_b'\rangle\langle n'|m_a'\rangle^* \exp[-i(E_n-E_{n'})t/\hbar] \qquad 2\text{-}4$$

and the terms $\langle n|m_a\rangle$ are the matrix elements

$$\langle n|m_a\rangle = \langle In|U|Im_a\rangle \quad , \qquad 2\text{-}5$$

where U is the unitary operator which diagonalizes the interaction Hamiltonian.

For the limiting case of an axially symmetric perturbing field, U=1 and the symmetry axis is taken as the quantizing z axis. The perturbation factor becomes

$$G_{k_1k_2}^{N_1N_2}(t) = \sum_{m,m'} (\hat{k}_1\hat{k}_2) \begin{pmatrix} I & I & k_1 \\ m' & -m & N_1 \end{pmatrix} \begin{pmatrix} I & I & k_2 \\ m' & -m & N_1 \end{pmatrix}$$

$$\exp\left[-i(E_m - E_{m'})t/\hbar\right] \delta_{N_1,N_2} \quad . \qquad 2\text{-}6$$

If the crystal is aligned with its symmetry axis parallel to the axis of one of the detectors,

$$G_{k_1k_2}^{N_1N_2}(t) = \delta_{k_1,k_2}\, \delta_{N_1,N_2}\, \delta_{N_1,0} \quad , \qquad 2\text{-}7$$

which produces

$$W(\vec{K}_1,\vec{K}_2,t) = \sum_k A_k(\gamma_1)A_k(\gamma_2)P_k(\cos\theta) \quad . \qquad 2\text{-}1$$

Physically, the perturbing field causes transitions among the m states. If the symmetry axis of the crystal is aligned with the axis of one of the detectors, then the perturbing field cannot cause transitions among the m states and no perturbation is observed.

In considering the case of the powdered sample, the sample is assumed to be made up of a large number of microcrystals which are randomly oriented. The probe nuclei are embedded in each of the microcrystals. The total attenuation factor, $G_{k_1k_2}^{N_1N_2}(t)$, is found by averaging over all the equally possible orientations of the microcrystals in the sample. The appropriate unitary matrix to diagonalize the interaction Hamiltonian must be used as before. Also a rotation operator is applied to rotate each microcrystal's coordinate system to the angular correlation (lab) coordinate

system. The Euler angles describing this rotation, α, β, γ, take on all possible values because the microcrystals are randomly oriented throughout the sample. (Complete mathematical details can be found in the Appendix, section D.) The result is

$$\overline{G_{k_1k_2}^{N_1N_2}(t)} = \delta_{k_1,k_2}\,\delta_{N_1,N_2}\sum_{m,m'} S_{m\,m'}^{k_1k_1}\cos[(E_m-E_{m'})t/\hbar]$$

$$\equiv G_{k_1k_1}(t) \quad , \tag{2-8}$$

where

$$S_{mm'}^{k_1k_2} = \sum_{n_1,n_2,n_1'} (-1)^{2I+n_1+n_2}\langle m|n_1\rangle^*\langle m|n_2\rangle\langle m'|n_1'\rangle\langle m'|n_2'\rangle^*$$

$$\begin{pmatrix} I & I & k_1 \\ n_2' & -n_2 & P \end{pmatrix}\begin{pmatrix} I & I & k_2 \\ n_1' & -n_1 & P \end{pmatrix} \quad , \tag{2-9}$$

and $\langle m|n_1\rangle$ are the elements of the unitary matrix which diagonalizes the interaction Hamiltonian in the principal axis system (similar to equation 2-5). Furthermore, equation 2-8 yields the simple result,

$$W(\vec{k}_1,\vec{k}_2,t) = \sum_k A_k(\gamma_1)A_k(\gamma_2)G_{kk}(t)\,P_k(\cos\theta) \quad . \tag{2-10}$$

That is, the effect of the perturbation in the powdered sample is a multiplicative factor which modulates or reduces the unperturbed angular correlation.

Physically, the non-diagonal ($k_1\neq k_2$) terms do not contribute since all possible Euler angle combinations enter into the averaging process and cancel individual contributions "pairwise" - the

orthogonality of the rotation matrices only allow diagonal terms to contribute. (An analogy would be the calculation of an electric field from a volume of space charge with high symmetry.) The resulting Kronecker deltas greatly simplify the expression that produces equation 2-10.

The perturbing Hamiltonian due to a static electric field gradient (EFG) interacting with the quadrupole moment of the intermediate state of the excited nucleus has the form

$$K_Q = \frac{4\pi}{5} T^{(2)} V^{(2)} = \frac{4\pi}{5} \sum_q (-1)^q T_q^{(2)} V_{-q}^{(2)} \quad , \qquad 2\text{-}11$$

where $T_q(2)$ is the q^{th} component of the nuclear quadrupole operator and $V_q(2)$ is the q^{th} component of the tensor operator of the EFG due to the lattice point charges surrounding the excited nucleus. (The Appendix, section E, contains the mathematical details in evaluating this interaction.)

Evaluation of the energy eigenvalues in the principal axis system is needed to apply the formulas presented in equation 2-6 for a single crystal or equations 2-8 and 2-9 for a powdered sample. In this system the EFG tensor has the form

$$V_0^{(2)} = \frac{1}{4} \sqrt{\frac{5}{\pi}} V_{zz}$$

$$V_{\pm 1}^{(2)} = 0$$

$$V_{\pm 2}^{(2)} = \frac{1}{4} \sqrt{\frac{5}{6\pi}} \eta V_{zz} \quad , \qquad 2\text{-}12$$

where V_{zz} is the second derivative with respect to z of the potential due to lattice point charges at the site of the excited nucleus in the principal axis system, and η is the asymmetry parameter which describes the symmetry of the EFG at the nuclear site and is defined by

$$\eta = \frac{(V_{xx}-V_{yy})}{V_{zz}} \quad , \quad |V_{xx}| \leq |V_{yy}| \leq |V_{zz}| \quad . \qquad 2\text{-}13$$

The asymmetry parameter takes on all values between 0 (axially symmetric EFG) and 1 (extreme asymmetry of EFG).

The eigenvalues of the resulting interaction Hamiltonian matrix depend on the spin, I, of the intermediate state and the value of η. This matrix is difficult to diagonalize in general and the problem is simplified to the I=5/2 case represented in this work. The interaction matrix then takes the form

$$\underset{\sim}{K}_Q = \frac{eQV_{zz}}{4I(2I-1)} \begin{bmatrix} 10 & 0 & \eta\sqrt{10} & 0 & 0 & 0 \\ 0 & -2 & 0 & \eta 3\sqrt{2} & 0 & 0 \\ \eta\sqrt{10} & 0 & -8 & 0 & \eta 3\sqrt{2} & 0 \\ 0 & \eta 3\sqrt{2} & 0 & -8 & 0 & \eta\sqrt{10} \\ 0 & 0 & \eta 3\sqrt{2} & 0 & -2 & 0 \\ 0 & 0 & 0 & \eta\sqrt{10} & 0 & 10 \end{bmatrix} . \qquad 2\text{-}14$$

The quadrupole moment of the intermediate state is defined through

$$eQ = \langle II| \sum_p e_p (3z_p^2 - r_p^2) |II\rangle = 4\left(\frac{\pi}{5}\right) \langle II|T_o^{(2)}|II\rangle \quad . \qquad 2\text{-}15$$

Also note that the interaction Hamiltonian is diagonal for axially symmetric (η=0) EFG's.

The energy eigenvalues, in units of $\frac{eQV_{zz}}{4I(2I-1)} = \hbar\omega_Q$, are solutions of

$$\left(\frac{\lambda}{2}\right)^3 - 7\left(\frac{\lambda}{2}\right)(3+\eta^2) - 20(1-\eta^2) = 0 \quad . \qquad 2\text{-}16$$

Note that the interaction Hamiltonian is degenerate with respect to ± m states. The solutions are best calculated numerically for a given value of η. Figure A-1 graphically displays the three solutions as a function of η.

Equation 2-8 can be written in the form

$$G_{k_1k_1}(t) = \sum_n S^{k_1k_1}(\omega_n)\cos(\omega_n t) \quad , \qquad 2\text{-}17$$

where the sum is over all possible energy differences between the m states. Again the degeneracy of the eigenvalues allows for only three values in energy differences. Using the form $\Delta E=h\omega$, defining $\omega_0=0$, and letting ω_1 be the smallest of the three energy differences followed by ω_2 and ω_3, then the coefficient can be written

$$S^{k_1k_2}(\omega_n) = \sum_{m,m'} S^{k_1k_2}_{mm'} \quad , \qquad 2\text{-}18$$

where the sum is restricted to those values of m, m' which produce the desired energy difference ω_n. Note that $\omega_1 + \omega_2 = \omega_3$.

A more transparent solution is afforded by the axially symmetric EFG case. This produces the attenuation factor

$$G_{kk}(t) = \sum_{m,m'} \begin{pmatrix} I & I & k \\ m' & -m & P \end{pmatrix}^2 \cos[(m^2-m'^2)3\omega_Q t] \quad , \qquad 2\text{-}19$$

which is true for any value of I. This can be rewritten as

$$G_{kk}(t) = \sum_n s_n^{k_1 k_1} \cos(n\omega_f t) \quad , \qquad 2\text{-}20$$

where

$$s_n^{k_1 k_2} = \sum_{m,m'} \begin{pmatrix} I & I & k_1 \\ m' & -m & P \end{pmatrix} \begin{pmatrix} I & I & k_2 \\ m' & -m & P \end{pmatrix} \quad . \qquad 2\text{-}21$$

The index n are the positive integer values of $|m^2-m'^2|$ for integer I and $1/2|m^2-m'^2|$ for half integer I. Also $\omega_f=3\omega_Q$ for integer I and $6\omega_Q$ for half integer I.

In particular, the I=5/2 case yields the form

$$G_{kk}(t) = \frac{1}{5} + \frac{13}{35}\cos\omega_f t + \frac{10}{35}\cos 2\omega_f t + \frac{5}{35}\cos 3\omega_f t \quad . \qquad 2\text{-}22$$

If the excited nuclei occupy sites of different EFG symmetry and strength then the net attenuation factor is

$$G_{kk}(t) = \sum_i f_i \, G_{kk}^i(t) \quad , \qquad 2\text{-}23$$

where the sum is taken over all the inequivalent sites, each with some fractional occupation, f_i, and attenuation factor, $G_{kk}^i(t)$.

Because the EFG may vary in magnitude and symmetry from site to site in a given sample, the energy differences take on a distributed set of values. By assuming that the energy differences are normally distributed about a mean frequency, the net effect is to change the attenuation factor to

$$\overline{G_{kk}(t)} = \sum_n S^{kk}(\omega_n) \cos(\omega_n t) \, e^{-\delta^2\omega_n^2 t^2/2} \quad , \qquad 2\text{-}24$$

where $\delta=\sigma/\omega_f$ and σ is the standard deviation of the distribution about the mean value ω_f. (Recall that $\omega_1=\omega_f$.)

2.3 Time Dependent Perturbations

When the perturbing field fluctuates randomly in time, some average local field configuration exists at any time t. This field then randomly reorients its direction as time passes. If many reorientations occur during the lifetime of the intermediate state then there exists no macroscopic preferred direction for the sample. Thus, a convenient quantization axis is chosen to simplify equations 2-2 and 2-3. This axis is chosen to coincide with the propagation direction of one (the first) of the radiations. The perturbed angular correlation function takes the form

$$W(\vec{K}_1,\vec{K}_2,t) = \sum_{k_1,k_2} A_{k_1}(\gamma_1)A_{k_2}(\gamma_2)G^{00}_{k_1k_2}(t)P_{k_2}(\cos\theta) \qquad 2\text{-}25$$

and

$$G^{00}_{k_1k_2}(t) = \sum_{m,m'} (-1)^{2I+m+m'}(\hat{k}_1\hat{k}_2)^{\frac{1}{2}} \begin{pmatrix} I & I & k_1 \\ m & -m & 0 \end{pmatrix} \begin{pmatrix} I & I & k_2 \\ m' & -m' & 0 \end{pmatrix} \left|\langle Im' \left| \Lambda(t) \right| Im\rangle\right|^2 , \qquad 2\text{-}26$$

where the term involving the time evolution operator, $\Lambda(t)$, is the probability of a transition from the state $|Im\rangle$ at t=0 to the state $|Im'\rangle$ at time t. Let this be $W_{mm'}(t)$. (Details on evaluating this probability can be found in Appendix A, section F.)

Using first-order time-dependent perturbation theory, the transition rate for the sample is

$$Q_{mm'}(t) = \frac{\langle W_{mm'}(t)\rangle_{E.A.}}{t} = \frac{2\tau_c}{h^2}\langle|K_{mm'}(0)|^2\rangle_{E.A.} \quad , \qquad 2\text{-}27$$

where the brackets and "E.A." indicate a statistical or ensemble average over the sample. The term τ_c is the correlation time of the fluctuating interacting field,

$$\langle K_{mm'}(t)\, K^*_{mm'}(t-\tau)\rangle_{E.A.} = \langle|K_{mm'}(0)|^2\rangle_{E.A.}\, e^{-|\tau|/\tau_c} \quad . \qquad 2\text{-}28$$

The assumptions in the above two expressions are as follows:

1) The fluctuating perturbing fields are stationary random fields, independent of the origin of time, t.

2) The value of the correlation function, $\langle K_{mm'}(t)K_{mm'}{}^*(t-\tau)\rangle_{E.A.}$, is independent of the direction in which time is measured (an even function of τ). Hence the correlation function is real, positive and decreasing with τ.

3) The exponential damping term, given by equation 2-28, is the form of the correlation function. (This assumption is used in Abragam's Brownian motion model[32] and Slichter's fluctuating spin model.[33])

4) The experimental observation time (the lifetime of the intermediate state) is long compared to the correlation time of the field.

5) The motional narrowing approximation is used where the rate of fluctuations is fast compared to the transition frequency, $W_{mm'} \ll 1/\tau_c$.

First order perturbation theory cannot be used when the transition probability is not small compared to unity. Then the master equation must be solved to find the occuption probability of a state $|m\rangle$, P_m, as a function of time,

$$\frac{dP_m}{dt} = \sum_{m'=-I}^{+I} Q_{mm'} (P_{m'}-P_m) \quad . \qquad 2\text{-}29$$

Solutions to this equation are valid when the transition rate is small compared to the field fluctuation rate, $Q_{mm'} << 1/\tau_c$.

The form of $\langle|K_{mm'}(0)|^2\rangle_{E.A.} = \langle|K_{mm'}(t)|^2\rangle_{E.A.}$ needs to be known before an explicit solution to the master equation can be found. Two possible models are: a random fluctuating EFG and a paramagnetic relaxation model due to random flipping of a spin coupled to the intermediate state.

For the randomly fluctuating EFG in the laboratory system, the interaction Hamiltonian is,

$$K_Q(t) = \frac{4\pi}{5} \sum_q (-1)^q T_q^{(2)} V_{-q}^{(2)} (z,t) \quad . \qquad 2\text{-}30$$

The EFG tensor is best described in the time independent coordinates of the principal axis system, z'. The connection between the two coordinate systems is through the Euler angles, $\alpha(t)$, $\beta(t)$, $\gamma(t)$, which describe the random reorientation of a local field with time. Using the rotation operator the interaction Hamiltonian becomes

$$K_Q(t) = \frac{4\pi}{5} \sum_{q,q'} (-1)^q T_q^{(2)} D^{(2)}_{-q'-q}(\alpha(t),\beta(t),\gamma(t)) V^{(2)}_{-q'}(z'). \qquad 2\text{-}31$$

The prescription is to form the quantity $|K_{mm'}(t)|^2$, then to take

the ensemble average by averaging over all the possible angles, α, β, γ, remembering that the average value of the EFG is to be used. This gives the result

$$\langle|\langle Im|K_Q(t)|Im'\rangle|^2\rangle_{E.A.}$$

$$= \frac{\pi}{80}(eQ)^2 V^2_{z'z'}(1+\eta^2/6)\begin{pmatrix} I & 2 & I \\ -I & 0 & I \end{pmatrix}^{-2} \sum_q \begin{pmatrix} I & 2 & I \\ -m & q & m' \end{pmatrix}^2 \quad . \quad 2\text{-}32$$

(Complete mathematical details can be found in the Appendix, section G for this and the following.) Note that the term $V_{z'z'}(1 + n^2/6)$ is the average of the square of the local EFG.

Inserting the above expression into equation 2-27 and solving the master equation, equation 2-29, gives the important result

$$G^{00}_{k_1k_2}(t) = e^{-\lambda_{k_1} t}\,\delta_{k_1,k_2} \quad , \qquad 2\text{-}33$$

with the attenuation constant

$$\lambda_k = \frac{3}{80}\tau_c\left(\frac{eQ}{\hbar}\right)^2 \frac{V^2_{z'z'}(1+\eta^2/6)k(k+1)}{I^2(2I-1)}\,[4I(I+1)-k(k+1)-1] \quad , \qquad 2\text{-}35$$

which implies that the perturbed angular correlation function has the form

$$W(\vec{k}_1,\vec{k}_2,t) = \sum_k A_k(\gamma_1)A_k(\gamma_2)G^{00}_{kk}(t)P_k(\cos\theta) \quad . \qquad 2\text{-}34$$

As the time t between the two radiations increases, the more opportunity the perturbation has to randomize the populations of the intermediate m states and thus destroy the angular correlation. Also notice that for $\tau_c \to 0$ the attenuation factor remains close

to unity for a fixed time t. This is because the EFG is changing so quickly that the quadrupolar interaction cannot induce significant transitions during the correlation timescale. As τ_c increases in value, the fluctuating EFG becomes more effective in inducing transitions and reducing the angular correlation.

Qualitative behavior of how the angular correlation pattern is influenced by still further increasing τ_c is as follows. For some value of τ_c the attenuation factor is essentially zero for all time t. As τ_c is further increased until it is on the order of the intermediate state lifetime, t_N, the random fluctuating EFG becomes less effective or "liquid-like" and takes on the characteristics of a static EFG, albeit one with a large distribution of ω_f. As τ_c becomes greater than t_N, the sample appears solid to the intermediate state and the static EFG results previously mentioned become overwhelmingly dominant. It is not clear whether the correlation function model of Abragam or Slichter is applicable for $\tau_c \lesssim t_N$.

The last case of interest is the model Hamiltonian for a paramagnetic interaction between the intermediate state of the nucleus and a nearby unpaired spin, which may be on a neighboring atom. It is assumed that the spins of the sample are randomly oriented in all directions and randomly fluctuating in time. This fluctuation may be due to the motion of the atom the spin resides on next to the ^{111}Cd nucleus or a spin flipping relaxation mechanism between it and other atoms with unpaired spins. This model will be referred to as the paramagnetic relaxation model (PRM).

The model Hamiltonian in the laboratory system is,

$$K_s(t) = a_s \vec{I}(z) \cdot \vec{S}(z,t) \quad , \qquad 2\text{-}36$$

where a_s is the coupling constant of the interaction which is strongly distance dependent. Justification for the model is given by Abragam[32].

Just as in the randomly fluctuating EFG case, the Hamiltonian is rewritten so the spin can be evaluated in its own time independent coordinate system, designated by z',

$$K_s(t) = a_s \sum_{n,n'} (-1)^n I_n^{(1)}(z) D^{(1)}_{-n',-n}(\alpha(t),\beta(t),\gamma(t)) S^{(1)}_{-n'}(z') \quad . \qquad 2\text{-}37$$

The Euler angles $\alpha(t)$, $\beta(t)$, $\gamma(t)$, represent the rotation from the nuclear coordinates z to the spin coordinates z'. They depend on time because of the continual reorientation of the spin with respect to the nucleus.

Again, as in the EFG case, the energy matrix elements are taken. The ensemble average is performed over all possible spin configurations and the following is obtained

$$\left\langle \left| \langle Im | K_s(t) | Im' \rangle \right|^2 \right\rangle_{E.A.}$$

$$= \frac{\left\langle |a_s|^2 \right\rangle_{E.A.}}{3} S(S+1)I(I+1)(2I+1) \sum_n \begin{pmatrix} I & 1 & I \\ -m' & n & m \end{pmatrix}^2 \quad , \qquad 2\text{-}38$$

where the term $\left\langle |a_s|^2 \right\rangle_{E.A.}$ is the average coupling strength for the interaction in the sample. (Refer to Appendix A, section H for complete mathematical details for this and the following.)

With this result the master equation can be solved and the attenuation factor is

$$G^{00}_{k_1 k_2}(t) = e^{-\lambda_{k_1} t} \delta_{k_1,k_2} \quad , \qquad 2\text{-}39$$

with

$$\lambda_k = \frac{1}{3} \tau_c \omega_s^2 S(S+1)\ k(k+1) \qquad 2\text{-}40$$

using the notation $\langle |a_s|^2 \rangle_{E.A.} = \hbar^2 \langle \omega_s^2 \rangle_{E.A.}$.

The correlation time of the spin fluctuation, τ_c, is the timescale of the paramagnetic spin reorienting itself. All the assumptions and interpretations given for the randomly fluctuating EFG case apply to this result.

CHAPTER III

EXPERIMENTAL EQUIPMENT AND SAMPLES

3.1 Electronics

The equipment in a perturbed angular correlation experiment must be able to identify the type and energy of radiation emitted, the time interval between the detection of the first and next radiation (or whatever is being observed), and the angle between the radiations. This work is concerned with the two gamma cascade from ^{111}Cd. (See table 2-1 for the particulars of the decay.) Thus the detection equipment must be able to differentiate the 171 kev gamma from the 245 kev gamma as well as from the Compton background, have a time resolution much less than the half life of 85 ns and have a well defined geometry. After identifying the angle and time interval between two successive gammas this information must be quickly stored so that sufficient statistics can be accumulated in a short period of time.

The experimental geometry consists of four detectors arranged in 90° intervals about the sample (see figure 3-1). This geometry is chosen to maximize the anisotropy of the angular correlation function. The reader is encouraged to consult the block diagram in figure 3-1 to facilitate following the explanation presented below.

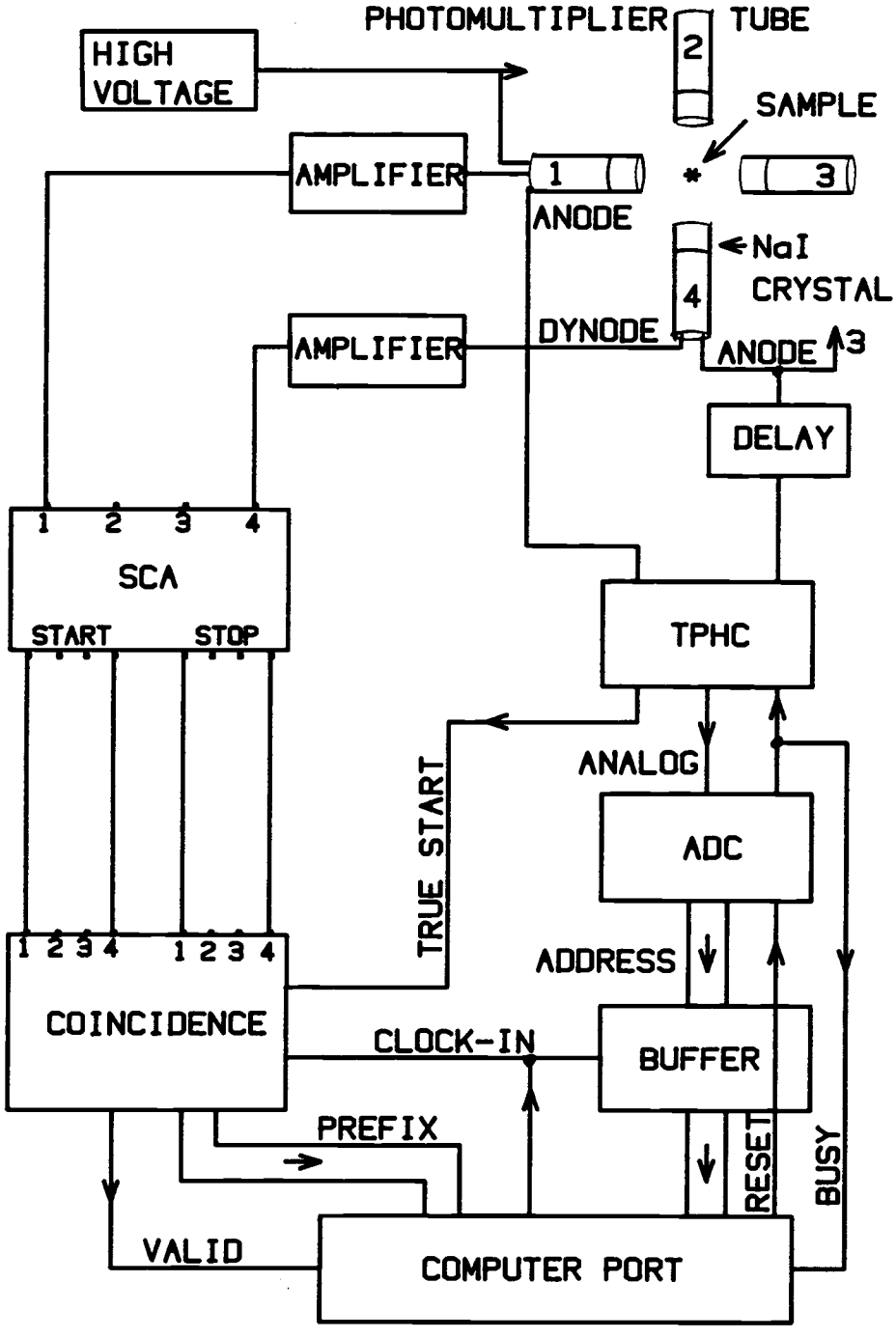

Figure 3-1 Block diagram of PAC experimental geometry and electronics.

Each detector consists of a 1 1/2" x 1 1/2" NaI crystal which fluoresces at approximately 400 nm with an intensity proportional to the energy of absorbed gamma, optically coupled with Dow Corning 20-057 optical coupling compound to an RCA 8575 photomultiplier tube. The assembly was covered with black masking tape to block any stray light. The fluorescent light ejects from the photocathode of the photomultiplier tube electrons which then are multiplied by the dynode chain. The photomultiplier tubes use -2500 V from a regulated high-voltage d.c. power supply manufactured by Northeast Scientific Corporation of Acton, ME. Part of the pulse at the next to the last dynode is taken off and used for energy resolution in the "slow" circuit. The pulse at the anode is used to start and stop the "clock" in the "fast" circuit. Standard RG58, 50Ω cable is used to carry all pulses.

The slow circuit operates in the following manner. The dynode pulse is amplified by either a Canberra 2012, Ortec 575, or Tennelec 213 amplifier unit. The height of the pulse is proportional to the energy of the absorbed photon. The pulse is fed into two laboratory-built single channel analyzers (SCA) which produce a TTL pulse of variable duration if the initial voltage lies between two energy cutoffs forming a window. One SCA has its window set on the low energy gamma from the ^{111}Cd and the other on the higher energy. The size of the window is sufficiently narrow so no overlap occurs between the two energies. The variable output pulse length,

typically 1 μs, is used to produce the desired total experimental time scale length of about 1.5 μs. The electronic delay associated with the amplifier-SCA chain is on the order of 1 μs. Power is supplied to this and the equipment following by Ortec M250/N and 401A NIMBINs.

The fast circuit operates in the following manner. The anode pulse is amplified by a Hewlett-Packard Model 460AR wide band fast amplifier. The output is fed into an Ortec 436 100MHz discriminator which was set to trigger just above the noise level because the initial portion of the leading edge of the fast pulse contains the timing information. The output is fed into an Ortec 437A time to pulse height converter (TPHC). The fast pulses from two of the detectors are fed into the start of the TPHC. The other two outputs are put into an Ortec 416 Gate and Delay Generator to introduce approximately 1 μs of delay to match the delay introduced by the slow circuit. The output is then fed into the stop input of the TPHC.

When the TPHC is triggered, its output pulse is sent to a Northern NS-629 analog to digital converter (ADC). The ADC puts out a BUSY signal which disables the TPHC from any further pulse pairs. The BUSY signal is also sent to the Radio Shack Color Computer (CoCo) through a computer port, which is a 6522 VIA chip, triggering an interrupt. The digitized ADC output is then set up on a buffer card.

Simultaneous with the TPHC output is a TRUE START pulse which locks in the contents of the coincidence status from the slow circuit pulses in the laboratory built coincidence module. The coincidence module is designed to accept only one valid coincidence. It produces a VALID signal and an addressing prefix associated with the valid coincidence, which identifies the detector pairs involved in the coincidence.

The program running in the CoCo contains an interrupt service routine which sends out a CLOCK-IN signal to the buffer and the coincidence module, which clocks the digitized time interval and geometry information into the computer port. As the information on the port is accessed, a handshake line comes on which produces a RESET pulse for the ADC. This clears the ADC BUSY line, sets it for the next event, and enables the TPHC. The act of clocking in the geometrical data from the coincidence module unlocks this device and enables it for the next coincidence.

The VALID signal is examined by the interrupt routine of the CoCo. For valid interrupts the routine treats the geometry prefix as an origin address to select a memory bank and the ADC data as an offset to determine the memory location which will be incremented by one count. The routine then returns to the previous programming activities. For an invalid interrupt, the routine also returns to Basic.

The recovery time of the photomultiplier-NaI crystal determines the maximum singles rate at which the experiment can collect data without encountering difficulties such as pulse pile up, pulse rejection, timing, mismatching, etc. For this equipment, a singles rate of $5\text{-}10\text{x}10^3$ s^{-1} is the limit. Typically experimental runs are made with a singles rate of 0.5 to $2\text{x}10^3$ s^{-1}.

The connections of the fast circuit to the TPHC produces the following result. For those coincidences whose start pulse originates from a detector which observes a low energy gamma, a normal spectrum is produced. If the start detector observes a high energy gamma, then the timing information is reversed, and a time reversed spectrum is observed, as shown in figure 3-2a, b. The timing location corresponding to zero time interval between the low and high energy gamma, t_o, is placed in the middle of the memory bank, as indicated in figure 3-2c, d, for the spectra in this work.

The accidental coincidence counts, or background counts, for each spectrum are found on the side opposite (reflect about t_o) to the data containing the true coincidence counts, where the data are approximately constant. The background counts showed a slight slope decreasing away from t_o. The size of this variation is typically 5% of the average value of the background counts. It is not clear what the electronic source for this problem is, but it may be due to errors in gating or pulse length asymmetries. These second order effects would increase the average background counts

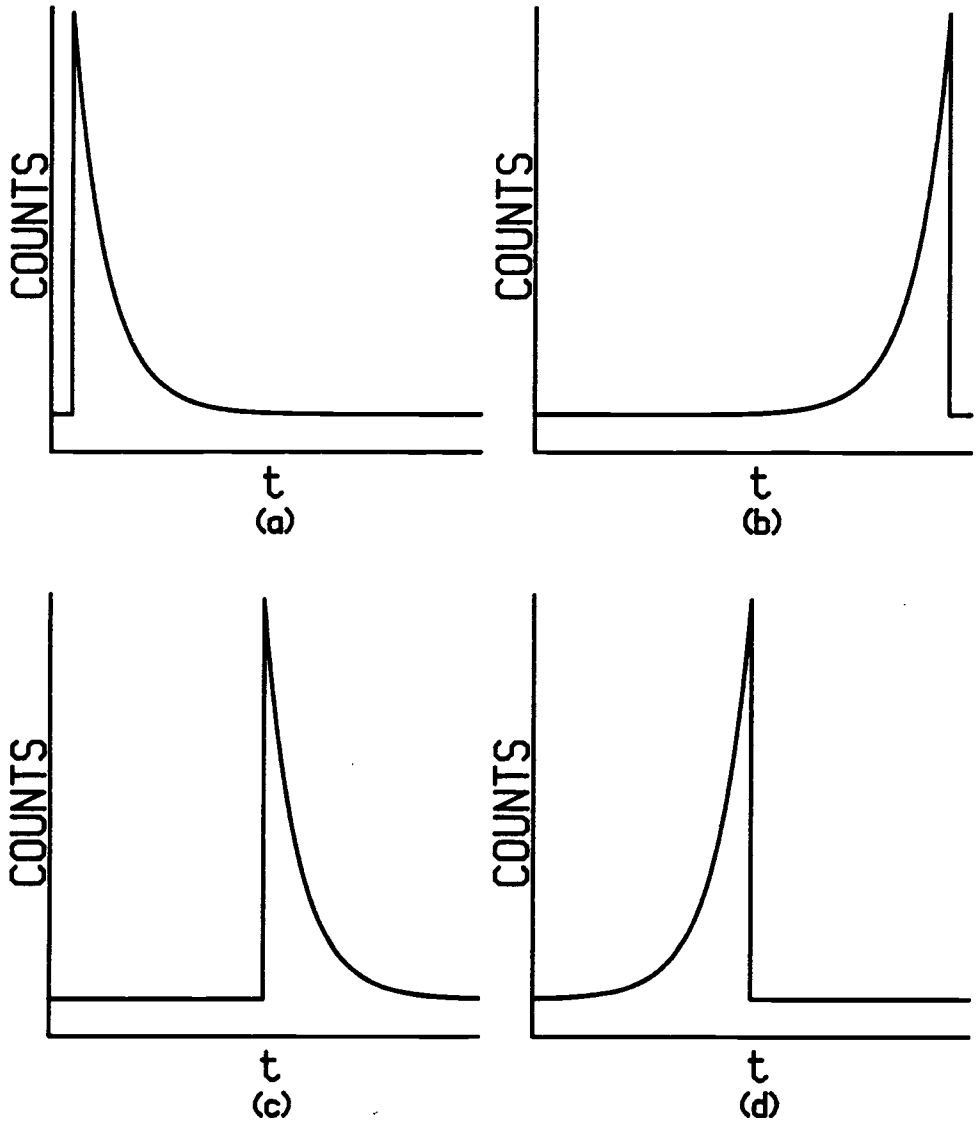

Figure 3-2 Accumulated coincidence spectrum for a typical spectrometer system. Figure 3a is the forward spectrum and 3b, the time reversed. Figure 3c shows forward spectra and 3d a time reversed spectra with t_0 in the middle, representative of this work.

near t_o, where the frequency of coincidences is highest. Thus the background average was taken as far away as possible from t_o where the background is the flattest. See Chapter IV for further details on this aspect.

The frequency of coincidence events, signalled by interrupts, was a few hundred events per second. This allowed the CoCo to have a Basic program running quasi-continuously, because the interrupt service routine can put Basic on "hold" while handling the interrupt. The Basic program was written to allow the user to determine the form of the accumulated spectrum as a function of detector pairs and to make a rough calculation of the form of the perturbation factor, $G_{22}(t)$, as the experiment progresses. This real-time analysis gives the experimenter additional information to make decisions concerning the quality of a particular experimental run and determine future courses of action.

After the data is accumulated, it is transferred to a DEC PDP 11/23 computer for storage and analysis using a data transfer program.

3.2 Equipment

The detectors, consisting of a NaI crystal, photomultiplier tube and associated electronics for the dynode chain, are mechanically fastened to an aluminum plate with grooves so that the detectors are free to slide at varying distances from the sample at

a fixed angle. Rulers are attached to the plate next to each detector so the experimenter can position each detector at a known distance from the center of the plate, where the sample is placed. This allows the user to adjust the count rate that the detectors see to improve data accumulation time. The distance from the front of the NaI crystal to the center of the plate was the same for all detectors, lying typically in the range 5-8 cm with a 1 mm error, during the course of data accumulation.

At the center of the plate is the furnace, surrounded by its water cooled jacket, containing the sample. The furnace consists of an alumina tube of approximately 3/8" O.D. with 22 gauge nichrome wire, wound from the bottom for approximately 75% of its length, as the resistive heating element. The nichrome is covered with Saureisen Electrotemp Cement No. 8 which supports the wires and prevents accidental shorting due to thermal expansion of the heating element. The furnace is then placed in a water cooled jacket with power leads introduced through vacuum feed-throughs. The jacket also has O-rings to seal against atmospheric pressure, and the interior is pumped on using a Cenco Hyvac 7 forepump. This decreases the thermal conductivity to the jacket and increases the lifetime of the nichrome windings by reducing the concentration of gaseous oxidizing agents. The structure is then placed so a sample will be centered with respect to the detectors. The reproducibility of this positioning is approximately 2 mm.

The furnace tube exhibited a temperature gradient along its length. The gradient was found to be closest to zero approximately 1.5 cm from the bottom of the tube. At this location the temperature variation was approximately 2°C for a length of 1 cm. A small alumina pellet, of about 0.5 cm radius, placed at the bottom of the tube centered the sample in this region.

The power for the furnace is a laboratory-built off-on a.c. power supply. The thermocouple element on the sample (see the sample subsection below) provides a voltage that a Model 49 Proportioning Control, Omega Engineering, temperature controller uses to control the temperature of the furnace.

3.3 Samples

The samples used in this work were selenium-tellurium alloys of varying composition. The selenium raw material was 99.999% pellets. The tellurium raw material was 99.999% chunks. Both elements were produced by ASARCO and United Mineral and Chemical Corporation.

The alloys were made in the following way. A quartz tube, supplied by Fused Silica, Fremont, CA, of size 10x12 mm and length approximately 50 cm, was cleaned by an HCl solution, rinsed with distilled, deionized water and allowed to dry. It was then sealed at one end by a oxygen-hydrogen torch. Quartz was selected because of its high melting temperature, approximately 1350°C, and relative immunity to attack by most materials such as moderately corrosive

high temperature selenium-tellurium liquids. The appropriate amounts of selenium and tellurium were weighed out on a Mettler balance, with a worst case precision of 0.005 g, and added to the bottom of the quartz tube. The sample portion of the tube was immersed in a water bath while the portion of the tube just above the sample is "necked off" with the torch. The tube was then evacuated by a forepump, with a protective glass wool filter inserted in the pump line. After a few minutes of pumping, the sample was sealed at the neck with the torch.

The sample was heated to a temperature of at least 100°C above the melting point of the alloy composition by using a resistance furnace monitored by thermocouple or, after experience was gained, by gently heating the sample directly with the torch. The sample was then shaken and allowed to quench to room temperature by quickly immersing it in a bucket of water. This insures that no large-scale segregation of the alloy takes place during the cooling process.

The sample capsule was opened when needed and the alloyed material broken into convenient chunks. Most alloys were used quickly during the course of the experiment. Those used over a longer term were stored in an evacuated desiccator.

The radioactive tracer was supplied by New England Nuclear, Boston, MA in 3 mCi quantities dissolved in a 0.05 M HCl solution of volume 0.3 ml. The manufacturer claimed the product to be 99.99%

carrier-free ^{111}In. Because of the short (2.8 d) half life, the tracer was purchased in 3-4 week intervals.

The alloy, approximately 50-100 mg, was deposited at the bottom of a 2 x 4 mm quartz tube, sealed at one end by the torch. The tracer was then introduced in the following way. A stainless steel tube (manufactured by the Hamilton Co., Reno, NV) with dimensions 0.25 x 0.47 mm and approximately 15 cm long was epoxied to a No. 20 syringe needle. Using an ordinary syringe, approximately 2 μCi of the tracer solution was drawn into the shaft of the steel tubing. The liquid was then injected into bottom of the quartz sample tube.

The quartz tube was then attached to a forepump with a filter in the line. The forepump vacuum was used to evaporate the HCl carrier solution. The forepump was vented through the laboratory hood, with an additional particle filter in the line, for overall safety. (The particle filter showed no signs of radioactive contamination.)

The sample was then sealed under moderate vacuum with an oxygen-acetylene torch with a small #4 nozzle (manufactured by Tescom Corporation, Minneapolis, MN). The sample capsule, approximately 1 cm long, had a 30 cm length of 2 mm quartz rod attached to serve as a handle. The sample was then transported, via a steel pipe container with a lead bottom, to the spectrometer laboratory.

It was observed that some samples did not show a spectrum characteristic of a liquid. (The spectra appeared like an overdamped solid.) It was found that using quartz supplied by Fused Silica alleviated this problem, implying that poor quality quartz was at the root of the problem.

The estimated misalignment for the liquid samples in the furnace is less than 2 mm. Mechanical misalignment, previously indicated, is about 2 mm. The count rates recorded at each detector were typically within 10% of each other, for the same energy, indicating that the sample was well centered.

A Pt-Pt + 10% Rh thermocouple was attached to the sample with a small amount of masking tape, making physical contact with the capsule near the middle. The thermocouple wires were encased in ceramic to prevent any accidental shorting. It was found that the masking tape had disintegrated upon heating, but the thermocouple was still making physical contact or was in close proximity to the sample capsule. Thus the thermocouple reading is a good measure of the sample temperature. The thermocouple was attached to thermocouple compensating wires and the voltage read by a Hewlett-Packard 3465B Digital Multimeter.

The samples were heated to over 900°C before collecting any data to allow the tracer to become homogeneously mixed with the sample. It was found that approximately four hours was enough time to do this.

The glass splats used in the EFG studies were made with the following device. (The device was originally designed and used by M. Cutler and W. Osmun. Modifications were made with the assistance of S.-S. Kao and F. Bell.) A catapult with a carbon crucible on the end was set by a catch inside a nichrome wound furnace. The catapult was released when the material in the crucible was in the desired state, striking a copper target cooled by liquid nitrogen.

The apparatus was kept in a glass bell jar that had been previously evacuated to approximately 15 mtorr and then back-filled with nitrogen gas, commercially supplied by Industrial Welding and Supply, Albany, OR, to a pressure of 300-400 torr. Pressures were read by a Magnevac vacuum gauge type GMA-140C by CVC, Rochester, NY. The system was pumped through a glass wool filter and a cold trap and the pump was vented into a laboratory hood. Figure 3-3 shows a block diagram of the apparatus.

The samples were made by using previously prepared alloy and approximately five times the needed activity of ^{111}In and then sealing as if it were a liquid alloy sample. The sample was heated to well over the boiling point and quenched in water. The capsule was broken and about twice the necessary amount of radioactive alloy (4 μCi) was removed and deposited in a new crucible attached to the catapult. After pumpdown of the splat apparatus, the sample was heated until vapor was observed, indicating that the boiling point had been reached at the ambient pressure in the bell jar, and the

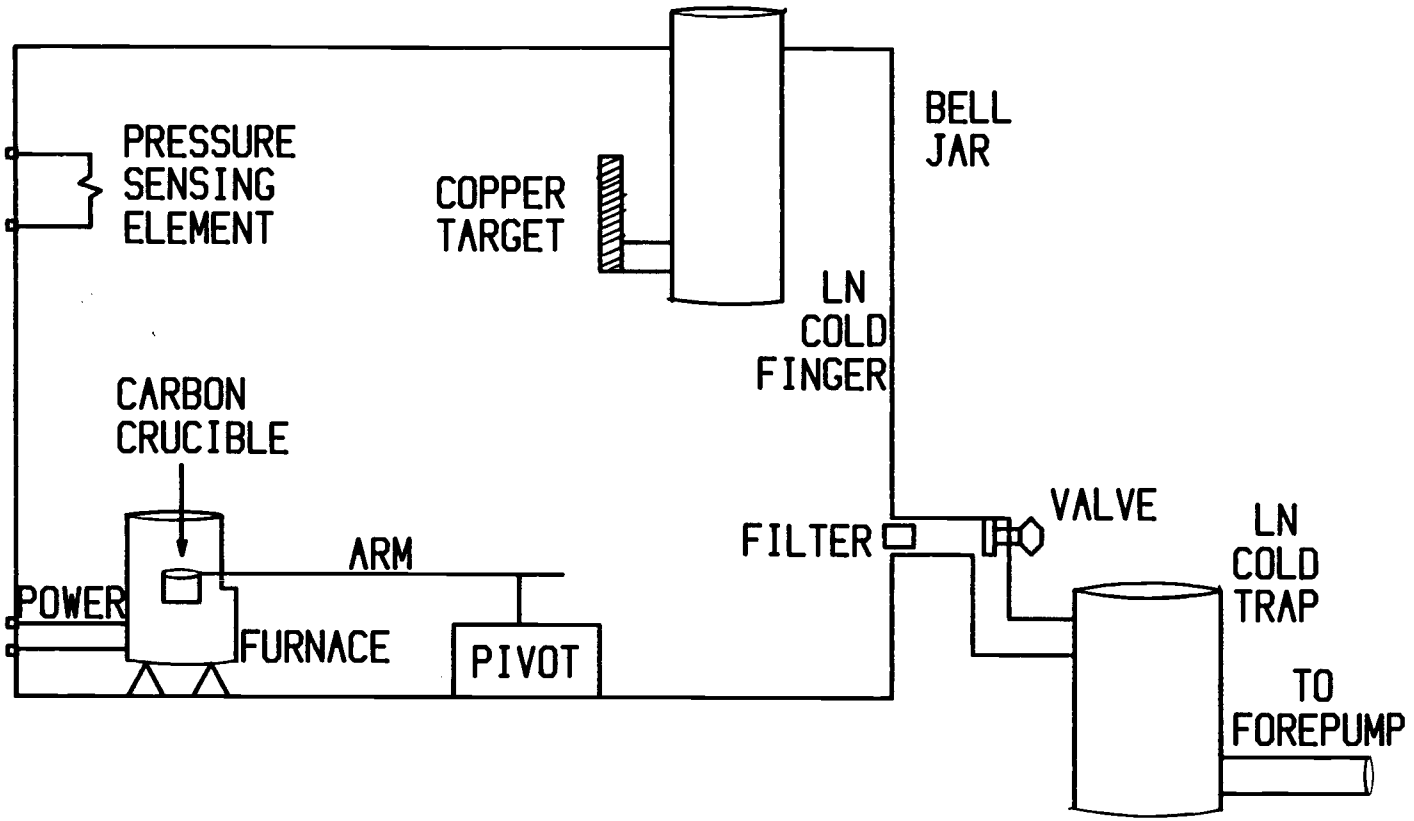

Figure 3-3 Diagram of the splat apparatus.

catapult catch was released. Splattering losses reduced the initial activity to about the appropriate level.

After pumping the poisonous radioactive vapor out of the bell jar, the sample was extracted, placed in a plastic vial and immersed in a dewar filled with liquid nitrogen. Great care was used to insure that the sample did not come into contact with any warm surfaces. The splat samples produced had a very shiny metallic look to them and were exceedingly brittle, often crumbling upon the slightest contact.

The catapult had been tested to have a velocity of $\approx$ 5 m/s. The splats produced had thicknesses of 50-100 microns. Both of these parameters are consistent with a quenching rate of approximately $0.5\text{-}1.0\times10^{6}$ K/s.

The samples were placed into the approximate center of a dewar (actually a thermos liner manufactured by Aladdin Industries, Nashville, TN) replacing the furnace at the spectrometer site. Because the count rate between detectors varied up to 50%, it is clear that sample misalignment occurred in some instances. The geometry of the dewar was such that the sample could not be misaligned by more than the size of the plastic vial, 0.5 cm. The resulting error in counting cancels through second order as will be discussed in the Data Reduction section of Chapter IV.

The dewar used at the spectrometer site needed refilling at three day intervals. This time scale was convenient so the sample was never moved during data-taking runs.

CHAPTER IV

EXPERIMENTAL DATA

4.1 Data Reduction

The data collected and stored in the CoCo was digitized at a rate that the TPHC-ADC combination determined, through the output voltage height of the TPHC and the countdown clock rate of the ADC. To determine the time difference between adjacent ADC addresses, or channels, an Ortec 462 Time Calibrator Unit was employed. The resulting time calibration for the system, typically 3 ns, was checked every few months or after a new TPHC or ADC was added. No significant long term changes of the time calibration were observed except when the TPHC or ADC was changed.

The linearity of the response of the TPHC-ADC combination was checked using a Honeywell MTP-2030 Pulse Generator with the start pulse from the Time Calibrator, which fires randomly in time. The observed spectrum accumulated was flat with time except for the first 10 channels or so. This nonlinearity is due to the initial nonlinearity of the TPHC-typical for these types of units.

The above calibration procedures were done for all detector combination pairs at least once to check for overall system response. No deviations were observed between detector pairs.

The photomultiplier tubes were set at a high bias, the fast pulse was acted on by the Hewlett-Packard Wide Band Amplifier, and

the discriminator was set at a low level to get the sharpest possible resolution, or full width at half maximum, from the NaI crystals. The measured resolution for each detector was between 2.4 and 2.6 ns, nearly equal to the best published performance for NaI crystals.[34] Because of the sharpness of the time resolution, it was unnecessary to convolute the data with a time resolution function.

The data was analyzed according to the following formula,

$$R(t) = \frac{2}{3}\left[\frac{W_1(180°)W_2(180°)}{W_1(90°)W_2(90°)}\right] - 1$$

and

$$A_2G_{22}(t) = \frac{R(t)}{1 - \frac{1}{2}R(t)} \quad , \qquad 4\text{-}1$$

where two sets of 180° spectra and two sets of 90° spectra are used, all belonging to either the forward or to the time reversed type of spectra (see figure 3-2c, d). The average background associated with each spectrum was subtracted before applying equation 4-1.

This data reduction scheme has certain advantages as pointed out by A. R. Arends et al.[35] The sample half life, detector efficiencies, and differences in the coincidence resolving times and accumulation livetimes between detector pairs cancel exactly. Furthermore, solid angle deviations cancel through first order in the solid angle differences or second order in the sample detector distances. As pointed out in Chapter III, the worst case

misalignment was 0.5 cm compared to sample detector distances of 5-8 cm. Misalignment of t_0 for the four forward or four reverse spectra cancels through second order. For the equipment used in this work, misalignment of t_0 was less than 0.4 ns which should be contrasted to the time calibration of about 3.0 ns.

Potential error sources that will have major effects on this experiment are source self absorbtion and average background errors. P. C. Lopiparo and R. L. Rasera point out[36,37] that source self absorbtion is negligible for the small samples used in this work. The effect of the background nonlinearities mentioned in Chapter III was found by observing the $A_2G_2(t)$ function for samples that should have $G_2(t)=1$, such as liquids with fast τ_c or static EFG's with cubic symmetry. Background errors would cause deviations from straight line behavior for these samples. Deviations were observed for very active samples where the average background count rate was larger than 300 counts per channel per day. Samples with a smaller average background count rate had deviations from straight line behavior of the $A_2G_2(t)$ function within the statistical error of the data. Typical average background count rates were 10-150 counts per channel per day. For this reason, data were taken only when the prepared sample activity had this strength. This strength corresponds to 2μCi. See the last paragraph of this section for additional details.

Since radioactive decays are random events, the error associated with N counts is $\sqrt{N}$, which represents one standard deviation. All errors were calculated according to this rule.

The complexity of the perturbation factor for static EFG's and the possibility of fitting the data to a local minimum necessitated the use of a Fourier transform program. This program gave the experimenter information on the number of sites and estimates of the frequencies associated with each site.

The values of $A_2G_2(t)$ were then fit to either an exponential damping formula, $A_2e^{-\lambda_2 t}$, or to a generalized static EFG model,

$$\sum_j A_2 f_j [S_o + \sum_{i=1}^{3} S_i \cos \omega_i t \; e^{-(\delta_i \omega_i t)^2/2}] \quad , \qquad 4\text{-}2$$

by a generalized FIT program. This program allowed for the A_2, λ_2, f_j, $S_{o,i}$, ω_i and δ_i values to be fit parameters or constants at the user's discretion. Also built in was the option to fit three sites of different EFG symmetry or strengths and to model solid-liquid mixtures. The principle of operation of the fit program is to minimize the square of the residual between the model and the data. The program slightly changes the values of the adjustable parameters, by using a modified polygon search routine. The program is constrained to find those values which satisfy the sum rules $S_o + \sum_{i=1}^{3} S_i = 1$ and $\omega_1 + \omega_2 = \omega_3$. When the program found a minimum, it reported the values of the adjustable parameters with a one standard deviation error. If the program reported unphysical

values such as negative S_i or ω_i values, the results of the fit were not used. This often meant that the model to fit the data was incorrect.

The fit values for the forward and reversed spectra were then averaged together with the error calculated in the usual statistical manner. If both values were not within this error about the average, the error is reported as half the distance between the values.

A data collection run consisted of 25 K to 100 K counts in the channel with the maximum counts and took 15 to 72 hours. The low end was used to determine rough values of the sample characteristics and the upper end was used to collect highly accurate values for those samples where the characteristics were difficult to measure, e.g., small λ_2 values. Typically a run took 24 hours with 32 K in the channel with the maximum counts.

It was observed that fitted values for λ_2 and ω_i were slightly larger for reversed spectra as compared to the forward spectra. This difference was typically well within the one standard deviation error for runs with many counts (32 K or better in the maximum count channel). As pointed out in the last chapter, this discrepancy is felt to be a second order electronics effect probably affecting the average background of the spectra.

4.2 Liquid Se_xTe_{1-x} Data

Figure 4-1 presents the λ_2 vs. 1000/T(K) data collected for the liquid alloy Se_xTe_{1-x} where x = 1.000, 0.750(2), 0.626(1), 0.500(5), 0.275(2), and 0.000.

Values of λ_2 less than about 5×10^5 s^{-1} (high temperature region) cannot be measured because of the shallowness of the exponential slope for the time calibration used. (Improvement can be gained if the time calibration is doubled, but the run time also must be doubled. This would imply run times on the order of one week or more, which was not done.) Note that measurable values of λ_2 for the tellurium sample could only be observed for the supercooled liquid.

The other extreme is limited by the solubility of the tracers in the liquid. For pure selenium, the indium tracer precipitates completely below about 450° C. This indicates that the solubility of indium in liquid selenium is less than one part per million, the concentration of the tracer, below 450° C. The data indicate that the solubility improves as the tellurium content is increased.

To observe possible hysteretic temperature effects, data runs were made going up and down with temperature in a random manner. This was done for all compositions. The data do not exhibit any hysteretic effects and no effort is made to identify data runs with the direction that the temperature was changed.

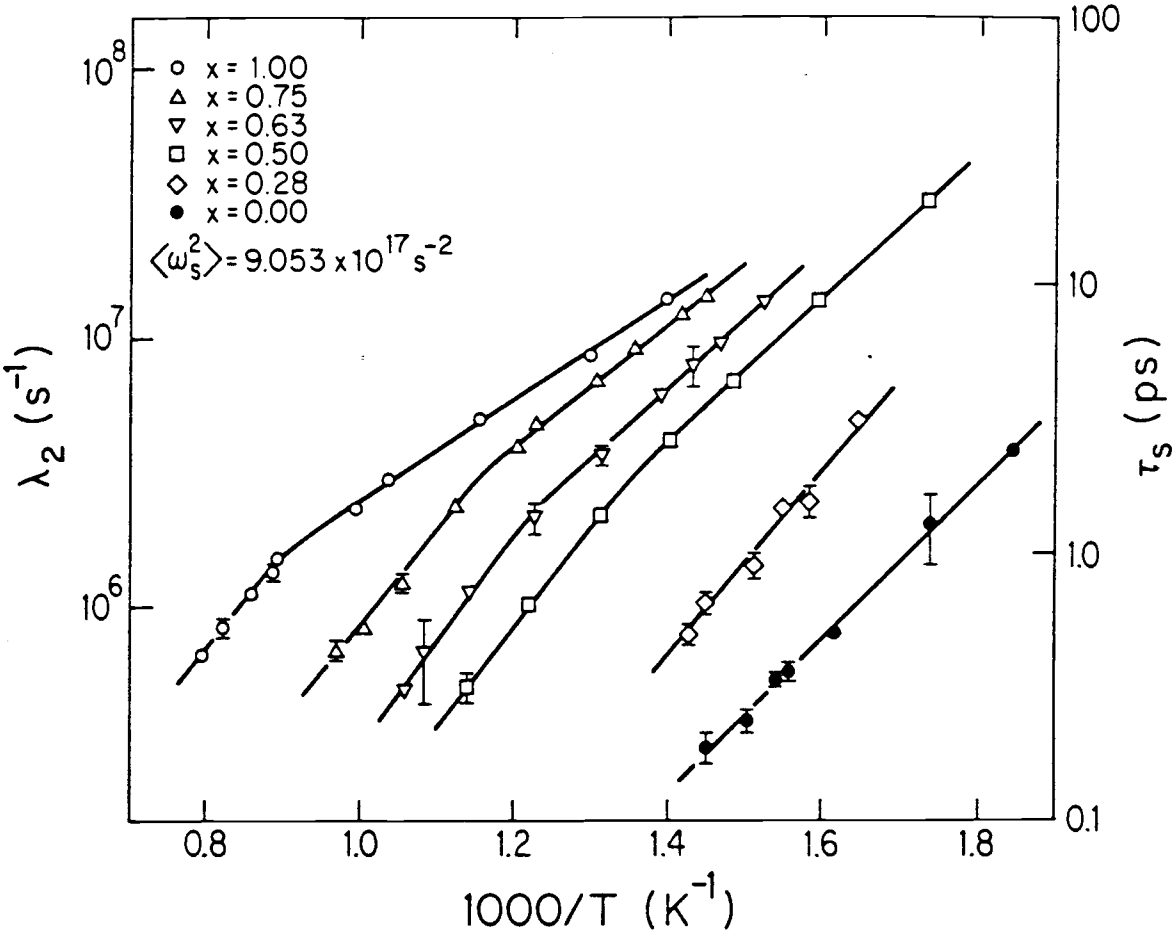

Figure 4-1 Values of λ_2 and τ_S vs. 1000/T(K). The solid lines are a guide to the eye.

The data demonstrate that λ_2 decreases with increasing temperature and increasing tellurium composition. Each set of data appears to have two linear regions, suggesting that the process producing λ_2 may be an activated one. The activation energies are approximately 0.68 eV in the high temperature region and about one-half that value in the low temperature regions.

The data agree well with the λ_2 values of selenium by Rasera and Gardner,[38] which were prepared with a larger indium concentration, about 1-2 atomic percent.

4.3 Amorphous Se_xTe_{1-x} Data

The amorphous Se_xTe_{1-x} splats were made from a melt at the boiling temperature of the alloys at a pressure of 300-400 torr. This corresponds approximately to the following boiling temperatures at atmospheric pressure: x=1.000, T=680°C; x=0.750(2), T=760°C; x=0.500(5), T=840°C; x=0.000, T=990°C. The $A_2G_2(t)$ functions for these data are displayed in figure 4-2.

The tellurium and alloy data are fit to a single EFG site that is strongly damped, $\delta_1 \approx 0.18$. As the selenium content is increased, the fits for the alloy get worse, because the data show additional structure or wiggles. For the selenium sample, the data are better fit to two sites, but the fit is not very good. Though the fits are not very good, the frequency of the first wiggle can be determined with an accuracy of better than 10% for the alloys and better than 20% for the selenium sample. This frequency is related

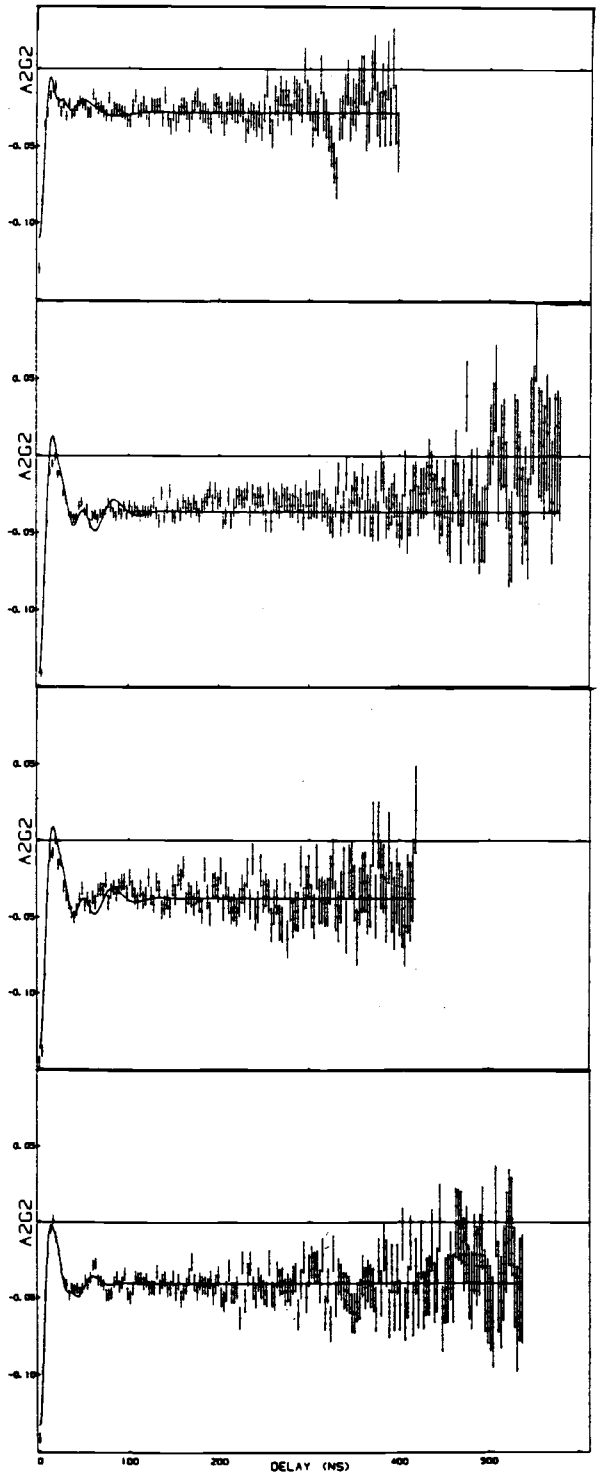

Figure 4-2 The function $A_2G_2(t)$ for the amorphous splats. The top is Se, next is $Se_{0.75}Te_{0.25}$, then $Se_{0.5}Te_{0.5}$ and Te. The solid line is a computer least squares fit.

to the quadrupole frequency, and the accuracy of this number represents the overall confidence of these fitted values.

The numerical results for the quadrupole frequency are summarized in table 4.1. Figure 4-3 demonstrates that the quadrupole frequency increases with increasing tellurium concentration.

Table 4-1 Results of Computer Fits to the Amorphous Splat Data

Alloy	ω_1 (10^6 Rad/s)	ω_2 (10^6 Rad/s)	δ	η	ω_Q (10^6 Rad/s)
Te	151(3)	230(7)	0.22(2)	0.48(5)	25.1(5)
$Se_{0.5}Te_{0.5}$	118(12)	188(19)	0.15(3)	0.43(12)	19.7(20)
$Se_{0.75}Te_{0.25}$	108(11)	178(18)	0.18(3)	0.38(11)	17.9(18)

Se	ω_1^1	ω_2^1	δ_1	η_1	ω_Q^1
fraction=0.7	(10^6 Rad/s)	(10^6 Rad/s)			(10^6 Rad/s)
	67.2(134)	134(27)	0.15(3)	0.0	11.2(22)
fraction=0.3	ω_1^2	ω_2^2	δ_2	η_2	ω_Q^2
	102(24)	189(38)	0.15(3)	.25(13)	17.0(34)

Numerical results of fits to Se_xTe_{1-x} amorphous splats. Te and the alloys are fit to a heavily damped one site model. Se is fit to a heavily damped two site model.

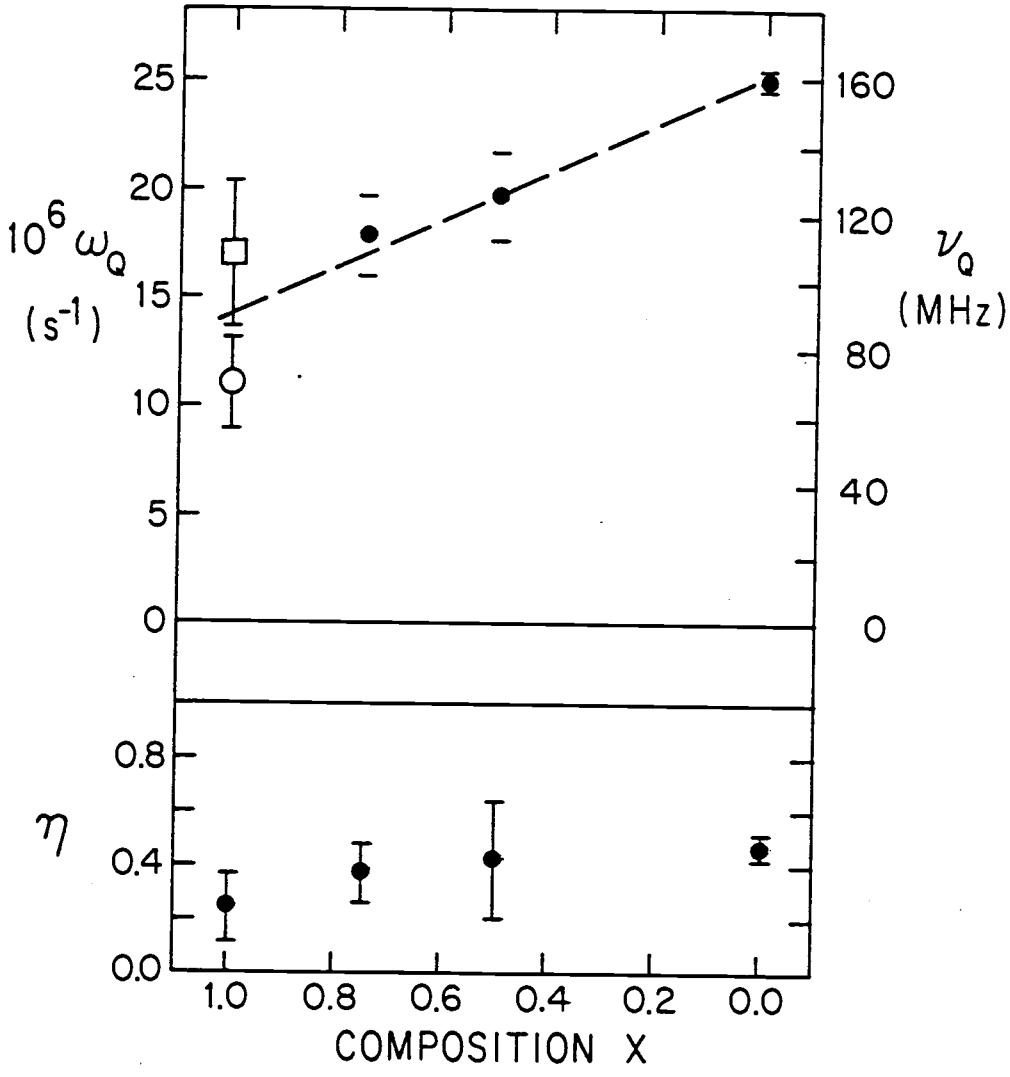

Figure 4-3 Quadrupole frequency and asymmetry parameter as a function of composition for amorphous splats. The top is the quadrupole frequency. The bottom is the asymmetry parameter. The lines are a guide to the eye.

CHAPTER V

DATA ANALYSIS

5.1 Models for the Fitted Values of λ_2

Presented in Chapter II is the theory of perturbed angular correlations with a randomly fluctuating EFG or a PRM. These model Hamiltonians produce an exponentially damped perturbation factor. The data presented in Chapter IV are the results of fitting the accumulated $A_2G_2(t)$ spectra to an exponentially damped function for liquid Se_xTe_{1-x} alloys. The randomly fluctuating EFG and a PRM will be the models used for analyzing the liquid results. The implication of these models will be used to decide which is the most likely explanation since it cannot be concluded a priori whether the measured values of λ_2 are due to a fluctuating EFG, a PRM, or a combination of the two.

There are three cases to consider. The first case is when a quadrupolar interaction dominates the decorrelation. The second case is when both quadrupolar and spin interaction yield approximately equal contributions to λ_2. The third case is when only spin interactions are important.

If the quadrupolar coupling is the dominant mechanism for destroying the angular correlation, then equation 2-35 is used with I=5/2 and k=2.

$$\lambda_2^Q = 25.2 \langle\omega_Q^2\rangle_{E.A.} \tau_Q \qquad 5\text{-}1$$

The coupling parameter ω_Q was defined in equation 2-16.

If the measured correlation function is due to random spin fluctuations, then equation 2-40 is used with I=5/2, k=2, and S=1/2.

$$\lambda_2^S = 1.5 \langle\omega_S^2\rangle_{E.A.} \tau_S \qquad 5\text{-}2$$

The coupling parameter ω_S was defined in equation 2-40 and 2-36.

If the two effects are to be considered together, then the analysis of Chapter II should be repeated with the Hamiltonian $H=H_Q+H_S$. This gives the result

$$\lambda_2^{Q+S} = \lambda_2^Q + \lambda_2^S = 25.2\langle\omega_Q^2\rangle_{E.A.} \tau_Q + 1.5\langle\omega_S^2\rangle_{E.A.} \tau_S \ . \qquad 5\text{-}3$$

The cross terms in $|\langle m|H|m'\rangle|^2$ do not contribute because they involve ensemble averages of S and V_{zz}, which are zero. The sub and superscripts, Q and S, have been added to delineate the mechanisms. Note that in all three cases, the average of the square of the coupling parameter must be known to give a value for the correlation time of the respective fluctuating fields.

It is important to point out that the angular correlation can be influenced by electron capture aftereffects. This is because the parent of the probe, ^{111}In, decays to ^{111}Cd by capturing an electron. This leaves a hole in the K shell which rapidly moves to the outermost shell, through the emission of soft X-rays, and Auger transitions, in times of the order of 10^{-14}s. If the probe nucleus

is embedded in a poor conductor, the hole may persist in the outer shell for times long enough to influence the experiment. (Recall that the half life of the initial state of ^{111}Cd is 120 ps.) Gardner and Krusch[39] did not observe any aftereffects due to electron capture in In_2Se_3, which is a worse conductor than liquid Se. Thus, it is unlikely that aftereffects play any role in this work.

The measured angular correlation could not be influenced by the changing chemistry of the probe from trivalent indium to divalent cadmium, since the time scale of this change in bonding is dominated by a few phonon vibration periods, typically of order picoseconds.

Since the probe atom is cadmium, it may be found in the following forms in the selenium-tellurium alloys. It may be imbedded in a chain, with bonding similar to that of the chalcogenides in the chain. It may also form dangling bonds, like selenium or tellurium, on chain ends. Cadmium may bond to a single chalcogenide, forming a double bond and a small molecular unit. Cadmium may also bond to an indium atom or itself, with no direct bonding to a chalcogenide, though this bond strength is weak and therefore unlikely.

5.2 Case 1: Correlation Times of an EFG

The perturbed angular correlation is destroyed when the symmetry and the strength of the EFG coupled to the quadrupole moment of the

probe nucleus fluctuates in a random manner. The value of the coupling parameter allows calculation of the correlation time τ_Q. Three possible mechanisms that could effect the symmetry and magnitude of the EFG are diffusion, rotation, and bond breaking.

If the probe is randomly diffusing through the liquid, then it can sample EFGs of a wide range of magnitude and symmetry. Similarly, if the probe nucleus is imbedded in a structure that is rotating, but with a random axis of rotation, then the overall symmetry of the EFG at the probe site would be randomly changing with time.

If the bonds of the probe atom are breaking and reforming with a variety of partners, the surrounding electric charges would vary greatly in magnitude and position, hence changing the EFG at the probe site. Likewise, if a near neighbor's bonds were breaking and reforming then the EFG at the probe site would also change. Contributions to the EFG at the probe site from the next near neighbor will be smaller because of the increased distance. These additional contributions from far neighbors can be ignored when compared to the effects of random fluctuations from near neighbors or overall symmetry change due to rotation.

The spectra of the amorphous splats of the Se_xTe_{1-x} alloys can be used to estimate the value of the coupling parameter $\langle(\omega_Q)^2\rangle_{E.A.}$ This is because selenium-tellurium alloys can easily be made in the glassy state[14] and a measure of ω_Q^{splat} will be a measure of the size of the coupling parameter if the local order in the splat is

similar to the liquid. Since the splats contain the probe parent, ^{111}In, the short order symmetry may be dominated by the chemical nature of indium, not cadmium. In this instance ω_Q^{splat} may not be a good measure of the liquid-state coupling parameter. Yet typical values of ω_Q for ^{111}Cd impurities in a wide selection of materials yield values within a factor of two of the given values for ω_Q^{splat}[40] found in Chapter IV. It should be remembered that for this worst instance, the values of ω_Q will be incorrect by a systematic scaling error and any temperature dependence will be unaffected.

The correlation time of the fluctuating EFG has been calculated under the assumption that the splat frequency can be used to evaluate the coupling parameter through $(\omega_Q^{splat})^2=\langle(\omega_Q^{liquid})^2\rangle_{E.A.}$. The values of ω_Q^{splat} used are presented in table 4-1. For those compositions not directly measured, the value of ω_Q^{splat} was interpolated from figure 4-3. The results of this calculation are displayed in figure 5-1. The values of τ_Q display the same temperature dependence as λ_2.

Consider the possibility that the EFG fluctuation is due to random rotations of large molecules to which the tracer is bonded, such as those found in selenium-rich selenium-tellurium alloys. The probe nuclei may exist in any of the chemical forms mentioned at the end of the last section. As figure 5-1 indicates, these correlation times fall in the range of 0.1 to 2ns. But typical rotation times for large extended polymers can at best be as small as 1μs[41], much too slow to be consistent with τ_Q.

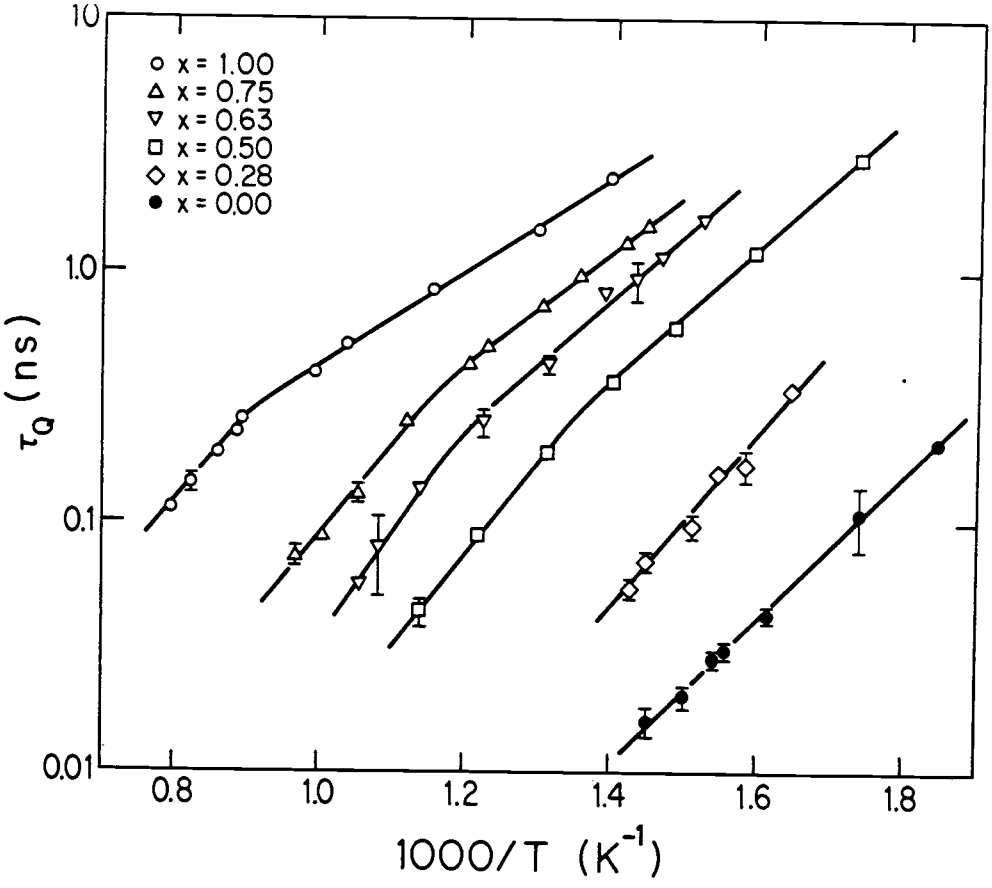

Figure 5-1 τ_Q as a function of 1000/T(K).
The lines are a guide to the eye.

Suppose the EFG fluctuation is caused by smaller structures, such as those found in the midrange of selenium-tellurium alloys, again rotating in some random manner. The cadmium may be in any of the chemical forms previously mentioned. In this region τ_Q takes on values ranging from 15 to 3000 ps. These are consistent with typical rotation times for small polymers[41]. Fixman[42] has given a theory predicting 1-10 ps autocorrelation times for 10 atom chains with 90° bond angles in mixtures with a viscosity of 1 cp, roughly consistent with mid-range selenium-tellurium compositions.

But the τ_Q data varies in a regular manner from these mid-range compositions to pure selenium, which consists only of long chains. As already argued, long chains cannot have rotation times of such short time scales, and thus the EFG fluctuations caused by medium scale structures randomly rotating have physically unreasonable consequences.

Suppose the fluctuating EFG is caused by the random rotation of a very small structure, such as a cadmium-chalcogenide unit. This unit could be randomly diffusing through the selenium-tellurium "soup" of chains, where the correlation time is a measure of the random walk or tumbling of the unit. The range of values of τ_Q is perfectly consistent with autocorrelation times of other small molecular units[41].

As discussed in Chapter I, the viscosity of the sample decreases as the tellurium concentration or temperature is

increased[12]. According to Ferry[41], the autocorrelation time decreases with a decrease in the viscosity, consistent with the τ_Q data presented.

The drawbacks of this model are twofold. As indicated in Chapter IV and shown by the data in figure 5-1, the observed values of τ_Q have a strong activated temperature dependence of approximately 0.68 eV. Random diffusions and rotations of small molecules should have small activation energies, ranging up to a few tenths of an eV in extreme cases[41]. Furthermore, the physical picture of activated motion involves a vibration frequency, approximately a phonon frequency, times a Boltzmann factor. The activation energy represents a barrier to movement. The τ_Q data have extrapolated vibration frequencies ranging from 10^{-13} to 10^{-15} s. Even if $(\omega_Q^{splat})^2$ is incorrect by a factor of 10, τ_Q is still too fast to be considered reasonable.

The last possibility to consider is that the attenuation of the angular correlation function is due to bonds breaking and reforming in the vicinity of the probe nuclei in a random manner. The dominant contributions to this mechanism would be the bond between the probe and its nearest neighbor or between the bonds of near neighbors. As discussed in Chapter I, chalcogenide liquids are made up of chains which contain dangling bonds and other defect states. These thermally generated defect states, created in pairs when bonds break, are in chemical equilibrium with the normal two-fold bonded species.

Thus all species have some characteristic lifetime. The continual creation and destruction of the defect states is a mechanism that can cause the EFG to fluctuate at the probe site. Note that defect states involving the cadmium-chalcogen bond may also play a role.

Detailed balance indicates that the lifetime of any defect bond divided by the lifetime of the original bond is related to the ratio of the defect concentration to the bond concentration. The ratios are directly proportional if the defect pairs are in close proximity to each other. The lifetimes become proportional to the square of the concentration ratio if the defect pairs have diffused apart and are randomly distributed throughout the sample. (The true situation is likely to lie between these limits.)

For the first possibility, the proportionality constant contains geometrical factors and is of order unity. This gives the relation $\tau_{defect} \approx \tau_{bond}(N_{defect}/N_{bond})$, where N_{defect} and N_{bond} are the concentrations of the defect and bond centers respectively. If the mechanism of defect bond formation is responsible for the decorrelation, the correlation time will be approximately the lifetime of the original bond. The concentration of defects range from 10^{-4}, for low temperature selenium, to 10^{-2}, for high temperature tellurium where the density of bonds has been taken to be one. This yields defect lifetimes of 10^{-12} to 10^{-13} s, the size of a phonon period. Thus, at best the measured values of τ_Q imply defect lifetimes that are essentially phonon periods. In addition, the temperature dependence of τ_Q suggests that the intrinsic vibration frequency (the prefactor for τ_Q^{-1}) is much too

fast compared with phonon frequencies.

For the second possibility, where the defect pairs have a high probability of diffusing apart, the predicted lifetimes are ludicrously short.

For the case where the cadmium-chalcogen bond creates a defect pair, the predicted bond lifetimes are not unreasonable if all the cadmium atoms were in a defect state ($N_{defect} \approx 1$). The correlation time is then a measure of the cadmium-chalcogen bond lifetime, but the intrinsic frequency prefactor is still faster than phonon frequencies.

It is clear that τ_Q cannot be a measure of the bond lifetimes of the chalcogen-chalcogen or cadmium-chalcogen bonds. Thus it seems that the experimentally measured values of λ_2 cannot be readily explained by random fluctuations of an EFG due to any simple mechanism.

5.3 Case 2: Correlation Times of an EFG Plus a PRM

It would be too much of a coincidence for both fluctuating EFGs and a PRM to be simultaneously of such size to be responsible for the measured value of λ_2 over the temperature and composition range of this work.

Although figure 4-1 suggests two activated regions for λ_2, it is unlikely that two independent relaxation processes, EFG and PRM, are responsible. Examination of equation 5-3 indicates that the largest contribution to λ_2 will dominate. In this case the

temperature dependence of λ_2 would be opposite at the cross-over from that which is measured. The implication is that the experimental results for λ_2 cannot be explained by competition between two independent relaxation processes.

5.4 Case 3: Correlation Times of a PRM

The angular correlation may be destroyed by a nearby spin, coupled to the probe nucleus, undergoing random reorientation or spin flipping. The correlation time, τ_S, would be a measure of the correlation time of spin fluctuations. As equation 5-2 indicates, the values of τ_S may be extracted from the measured values of λ_2 if the coupling parameter, $\langle\omega_S^2\rangle_{E.A.}$, is known.

Nuclear magnetic resonance (NMR) measurements of τ_S have been performed in pure selenium by Warren and Dupree[26] as a function of temperature and pressure. These data can be scaled to the measured values of λ_2 for pure selenium. If the data scale well, then the coupling parameter can be found for pure selenium.

Figure 5-2 shows the results of scaling the λ_2 data to the NMR τ_S data. The data scale very well together. The apparent discrepancies exhibited by the NMR data are due to pressure differences between the NMR data, taken at 400 bar, 100 bar, and 1 atmosphere, and the λ_2 data, taken at essentially 1 atmosphere. It is clear that τ_S from the NMR data exhibits a slight pressure dependence, characterized by the isobars that can be envisaged on figure 5-2.

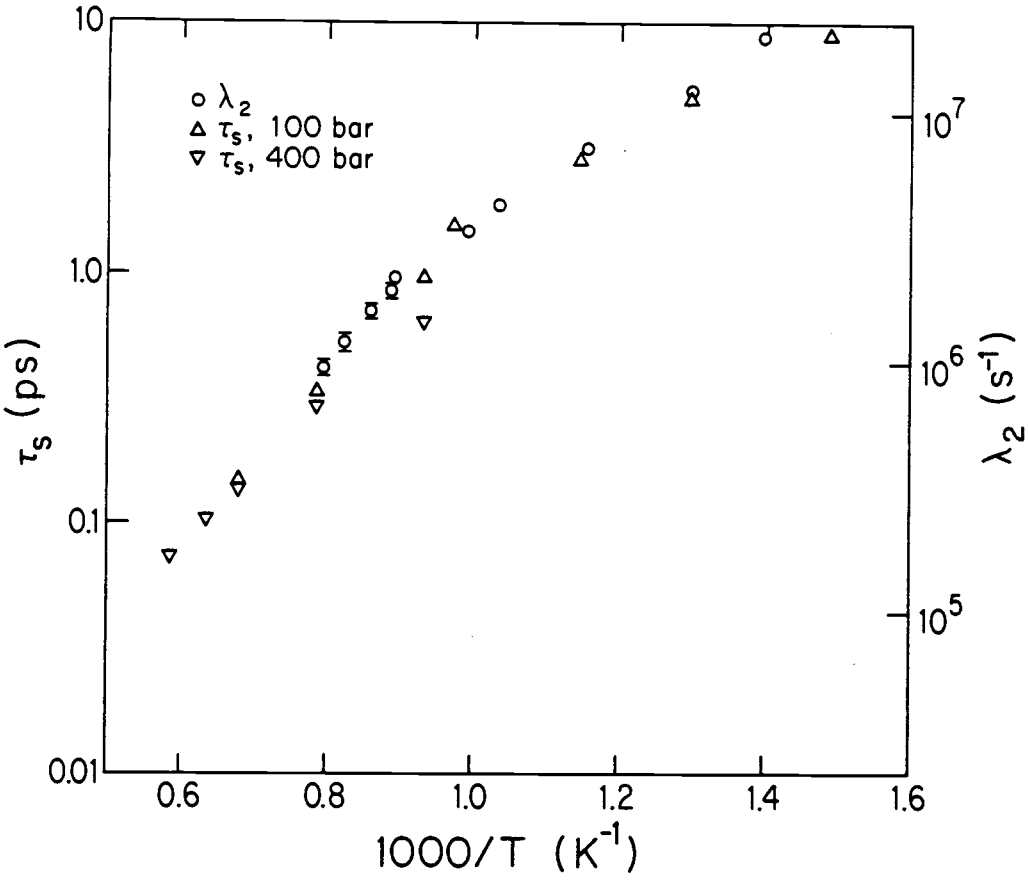

Figure 5-2 Plot of λ_2 scaled to NMR τ_S data vs. 1000/T(K).

The value of the coupling parameter, $\langle\omega_S^2\rangle_{E.A.}$, derived from figure 5-2 is $9.05 \times 10^{17} s^{-2}$. To understand the implications of the size of the coupling parameter, the physical meaning of "ensemble average" must be examined. The ensemble average represents a weighted sum of the various average coupling parameters that the probe nucleus experiences from neighboring spins. The weights are the probabilities that the spin resides at that location. This coupling parameter can be written as the sum of the contributions from each of the near neighbors,

$$\langle\omega_S^2\rangle_{E.A.} = \sum_{i=0} P_i \, \overline{\omega}_{S_i}^2 \quad , \qquad 5\text{-}4$$

where P_0 is the probability that the spin resides at the probe atom, and P_i, $i>0$, is the probability that the spin is on the $i^{\underline{th}}$ neighbor. Since the strength of spin-spin coupling falls off very rapidly with distance[32] only the first two terms need be considered,

$$\langle\omega_S^2\rangle_{E.A.} = P_0 \, \overline{\omega}_{S_0}^2 + P_1 \overline{\omega}_{S_1}^2 \quad . \qquad 5\text{-}5$$

The measured value of $\langle\omega_S^2\rangle_{E.A.}$ is large and is consistent with the spin residing on or very near the cadmium probe nucleus[43]. This implies that P_0 and P_1 are not random probabilities proportional to spin density but that one or both are near unity.

One possible model consistent with the experimental results is a singly ionized CdSe molecular unit. If this were the major cadmium unit in pure selenium, the coupling constant obtained is of reasonable magnitude.

Furthermore, this small molecule could rotate rapidly and have a small τ_Q. If $(\omega_Q^{splat})^2 \approx \langle\omega_Q^2\rangle_{E.A.}$, an upper limit for τ_Q is 10^{-10}s for pure selenium and 10^{-11}s for pure tellurium, because λ_2^Q would be negligible compared to λ_2^S, consistent with the experimental results. These limits are consistent with autocorrelation times for small molecules.

It is reasonable to assume that the above value of the coupling parameter does not change greatly as the tellurium content is increased, because tellurium is chemically similar to selenium. Typically, a spin coupling parameter changes by approximately 10-20% upon substitution of a chemically similar species provided the short range order is the same in the two cases.[43]

Figure 4-1 displays the calculated values of τ_S vs 1000/T(K) assuming that the coupling parameter in the alloys is the same as for pure selenium. The data indicate that the correlation time of the fluctuating spin decreases with increasing temperature and tellurium concentration.

Attempts to measure τ_S in liquid selenium-tellurium alloys have been made by Kirby[27] using NMR. That work measured the relaxation time and Knight shift as a function of temperature for two compositions, $Se_{0.5}Te_{0.5}$ and $Se_{0.4}Te_{0.6}$. These values were used

to calculate τ_S according to the standard model in Abragam[32]. The results of the NMR experiment showed τ_S decreasing as the temperature and tellurium content increased, consistent with the results of this work. The magnitude of τ_S varied by factors of 3-5 compared with the values in this work. These differences may well be due to errors in determining the relevant coupling constants in the NMR experiment. For this reason, Kirby's results can be considered consistent with the values of τ_S presented here.

5.5 Implications of τ_S

Warren and Dupree presented evidence that τ_S in pure selenium depends only on the average distance between spins with no explicit pressure or temperature dependence[26]. The data presented here raise the question of how τ_S in the selenium-tellurium alloys depends on spin density. Values of spin density were calculated from magnetic susceptibility data of Cutler and Gardner[24], and figure 5-3 is a plot of τ_S *vs.* the average volume per spin, N_S^{-1}, for all compositions of Se_xTe_{1-x} measured in this work except pure tellurium. (This is because no good measurement of N_S exists for tellurium[44].) The coupling parameter from pure selenium is assumed to hold for the alloys. The data of Warren and Dupree are included in figure 5-3 for completeness.

The curves in figure 5-3 appear linear in nature and clearly show two branches for large spin densities. The left branch

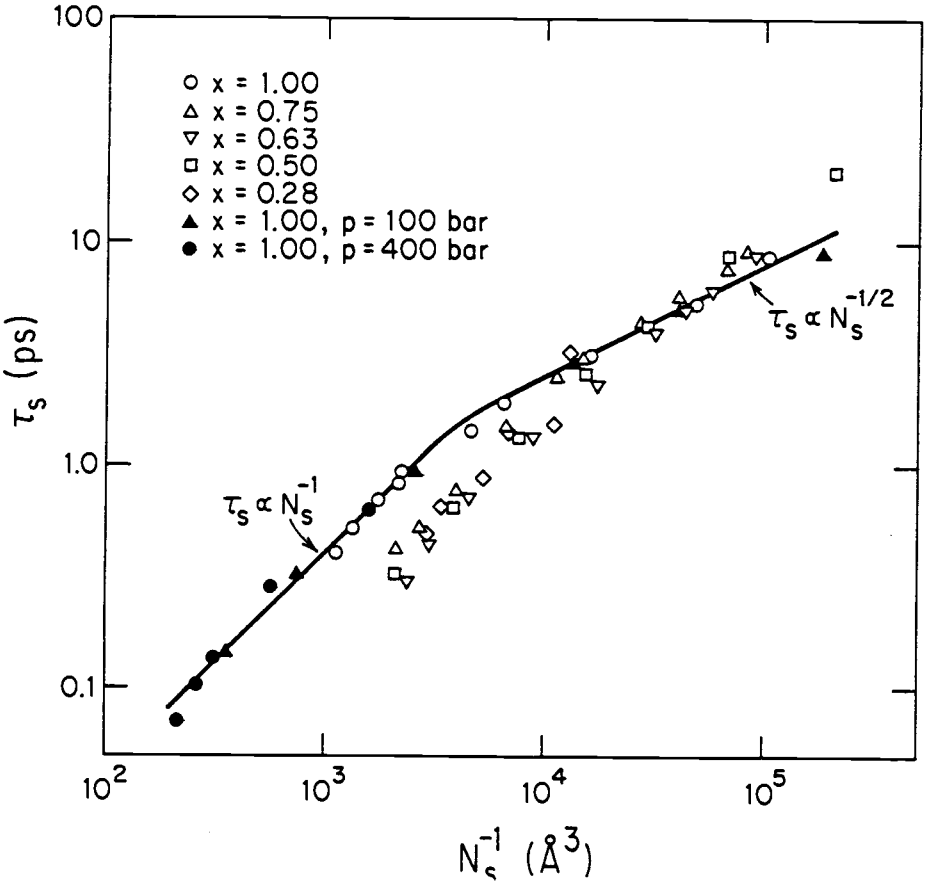

Figure 5-3 A plot of the calculated τ_s values as a function of the inverse spin density. A constant coupling parameter was assumed for all the alloys. The key is as follows: open circles, x = 1.00; open triangles, x = 0.75; open squares, x = 0.50; open diamonds, x = 0.28; closed triangles, x = 1.00 NMR results at 100 bar; closed circles, x = 1.00 NMR results at 400 bar.

contains data only from selenium measurements. The right branch contains all data from alloy measurements. As the spin density decreases, the curves apparently coalesce.

At large spin densities, the linear relation between τ_S and N_S^{-1} suggests that τ_S is directly proportional to N_S^{-1} and at small spin densities τ_S is more nearly proportional to $\sqrt{N_S^{-1}}$. These results are expressed numerically as,

large densities: Se branch $\tau_S = 3.9 \times 10^{-16} N_S^{-1}$ (in A^3)

alloy branch $\tau_S = 1.7 \times 10^{-16} N_S^{-1}$ (in A^3) 5-6

small densities: $\tau_S = 2.2 \times 10^{-14} \sqrt{N_S^{-1}}$ (in A^3) .

The discrepancy between the two τ_S branches at large spin densities in figure 5-3, about a factor of two, could be a real effect or may be due to a violation in the major assumption that the coupling parameter is constant for all the alloys. But, as pointed out in the last section, the square of the coupling parameter for any particular ionic configuration should not vary by as much as a factor of two when tellurium is substituted for selenium. It is possible that the addition of tellurium to form the alloys induces a competing chemical reaction, changing the equilibrium constant which governs the concentration of charged species. The concentration of charged species may change in such a way that the probability that a spin is near the probe, or on the probe itself (refer to equation 5-5), is reduced by about a factor of two as displayed by the

curve. The effect on the model of ionized CdSe molecules would be an increase in the concentration of neutral molecules in the large spin density (or high temperature) region of the alloys.

The magnetic susceptibility measurements of Gardner and Cutler[24] in liquid selenium-tellurium alloys exhibited Arrhenius type behavior in the semiconducting region. This behavior is thought to be caused by the thermal generation of magnetic defects, particularly the creation of D_1^* centers. The data were used to calculate the spin density in this region, and the activation energy of the susceptibility is a measure of one-half the energy to break a chalcogen bond to form a center. The spin density for tellurium could not be calculated at temperatures low enough to reach the semiconducting region.

The correlation times in figure 5-3 are approximately proportional to the spin density at high spin densities. Thus, the activation energies in this work (which are independent of the coupling parameter) are the same as the activation energies of the susceptibility measurements in the semiconducting region. If the correlation times of tellurium are also proportional to the spin density, which is expected to be large, then twice the activation energy, about 1.1(1) eV, is a measure of the tellurium-tellurium bond strength. This value is slightly less than the bond strengths measured in the selenium-rich alloys, about 1.37 eV.

Figure 5-3 can be employed to estimate what the paramagnetic susceptibility is for pure tellurium using either the selenium or alloy branch. The results of this estimate for both branches are displayed in figure 5-4. Plotted are the measured values of susceptibility for pure tellurium and $Se_{.10}Te_{.90}$ corrected by subtracting away the diamagnetic portion. Values estimated from the τ_S vs N_S^{-1} curve for each branch are also plotted. The estimate of susceptibility using the curve of figure 5-3 assumes a Curie model. Those values estimated from the selenium branch appear to be high compared to the susceptibility data at high temperatures. The estimated values from the alloy branch appear low over the whole temperature range and are just above the $Se_{.10}Te_{.90}$ data. At temperatures above 350°C, the density of spins in tellurium is very high and the measured susceptibility should be smaller than the Curie susceptibility of non-interacting spins because of spin-spin coupling. Thus, the values used from the selenium branch of figure 5-3 are more consistent with the measured susceptibility than those taken from the alloy branch.

Therefore, figure 5-4 implies that the coupling parameter is about the same for pure selenium or tellurium but is reduced in the alloys. If the reduction is due to a chemical reaction which reduces the probability that the cadmium impurity is near a spin, then the CdSe or CdTe molecules are more completely ionized in pure selenium and tellurium than in the alloys.

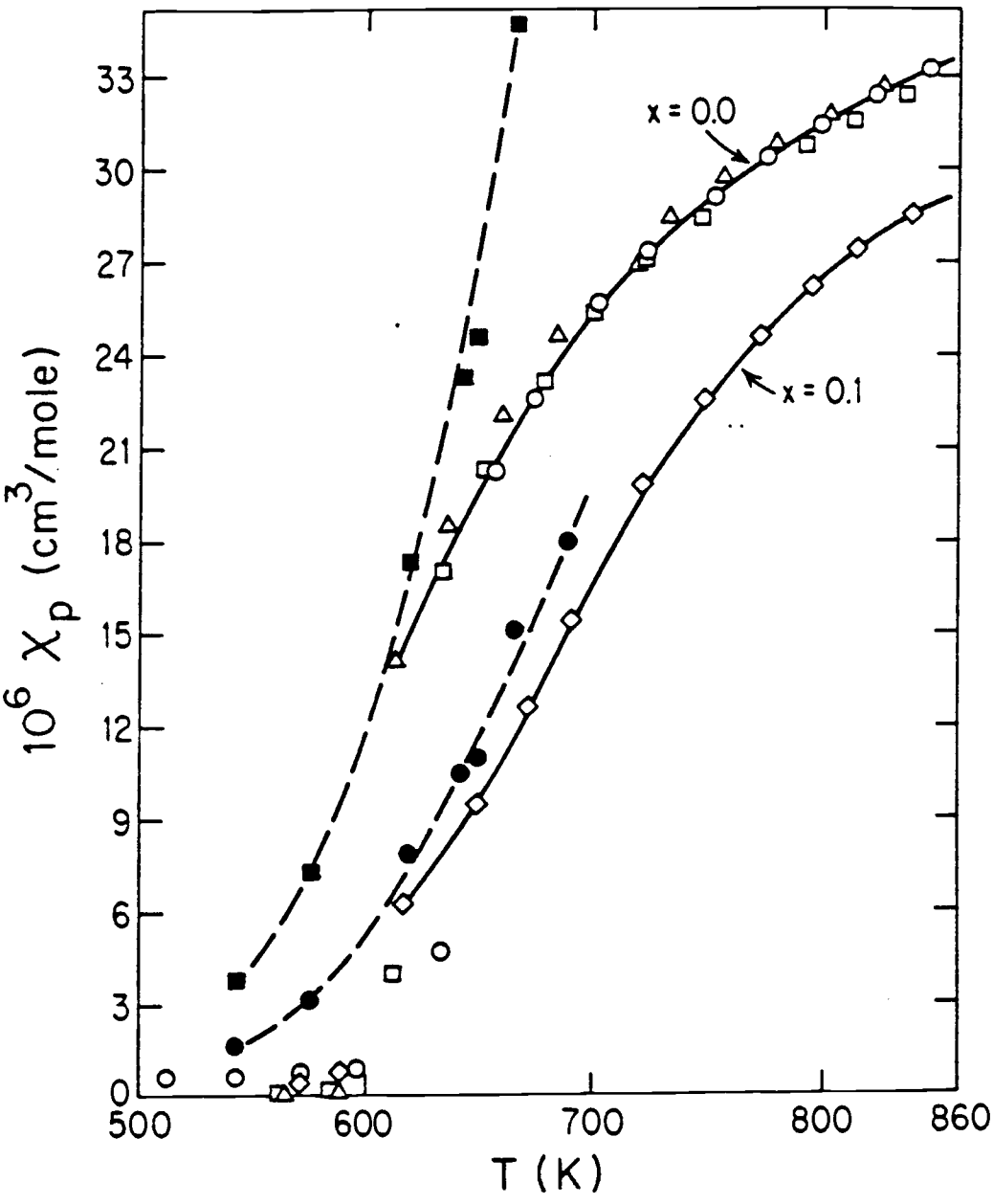

Figure 5-4 Plot of the magnetic susceptibility as a function of temperature. The diamagnetic portion has been subtracted off. The open circles, triangles and square are for Te, open diamonds for $Se_{0.1}Te_{0.9}$. The solid squares is the Curie estimate from the Se branch and the solid circles from the alloy branch of the τ_S vs N_S^{-1} curve, figure 5-3.

CHAPTER VI

CONCLUSION

6.1 Summary of Experimental Results

Perturbation of angular correlations (PAC) has been used to examine the correlation time of randomly fluctuating fields present at the sites of dilute ^{111}Cd impurities in liquid Se_xTe_{1-x} alloys. The measured perturbation factor, $G_{22}(t)$, was found to be exponentially attenuated with fitted values of the attenuation factor, λ_2, presented in figure 4-1. The attenuation factor decreases with increasing temperature and tellurium composition. The set of λ_2 curves exhibit two regions of activated behavior with high-temperature activation energy of about 0.68 eV and low-temperature energies of about half this value.

Perturbation factors were also measured for amorphous splats of Se_xTe_{1-x} alloys, made by quenching the melt at approximately 10^6K/s. The quadrupolar splitting energy, characterized by ω_Q, and the asymmetry parameter η were found to increase by about 30% as the composition varied from pure selenium to pure tellurium. The results are displayed in figure 4-3 and compiled in table 4-1.

The correlation time of the randomly fluctuating fields at the probe site can be determined by employing relations 5-1 and 5-2,

$$\lambda_2^Q = 25.2\ \tau_Q\ \langle\omega_Q^2\rangle_{E.A.} \qquad 5\text{-}1$$

$$\lambda_2^S = 1.5\ \tau_S\ \langle\omega_S^2\rangle_{E.A.} \quad , \qquad 5\text{-}2$$

where τ_Q and τ_S are the correlation times due to a randomly fluctuating electric field gradient (EFG) or a paramagnetic relaxation mechanism (PRM). These relations require knowledge of the coupling parameters $\langle\omega_Q^2\rangle_{E.A.}$ for fluctuating EFG and $\langle\omega_S^2\rangle_{E.A.}$ for a PRM. The derivation and physical meaning of these attenuation factors can be found in Chapter II and the Appendix.

The aftereffects of the decay of the parent ^{111}In to ^{111}Cd via e^- capture and the dynamics of the changing chemistry of In to Cd during this decay occur on a time scale small compared to the half life of the first excited state of ^{111}Cd, 120 ps. Thus, these effects cannot contribute to the measured perturbation factor.

It was assumed that $(\omega_Q^{splat})^2$ is a good measure of $\langle\omega_Q^2\rangle_{E.A.}$ for the liquids. Experimental measurements of quadrupolar splittings at ^{111}Cd sites in a wide variety of hosts differ from ω_Q^{splat} by less than a factor of two, and are weakly dependent on temperature. Thus $(\omega_Q^{splat})^2$ is probably a good estimate of the coupling parameter. If λ_2 is due entirely to EFG fluctuations, the correlation time, τ_Q, of a fluctuating EFG at the probe site can be calculated, and the results are displayed in figure 5-1. The correlation time is found to decrease with increasing temperature and tellurium concentration.

The coupling parameter between the spin of the probe nuclei and a randomly fluctuating nearby spin was not measured in this work. If magnetic fluctuations dominate, it can be found by scaling the NMR measurements of the fluctuating spin correlation time in selenium to the values of λ_2 in this work. Figure 5-2 graphically depicts this scaling which results in a value of $\langle\omega_S^2\rangle_{E.A.} = 9.05 \times 10^{17} s^{-2}$. The coupling parameter was assumed to be constant as the tellurium concentration was increased and was used to calculate the correlation time of the spin fluctuation as a function of temperature and composition. The resulting correlation time decreased as the temperature and tellurium concentration was increased. The results of this calculation are displayed in figure 4-1.

Since it was not known a priori which mechanism would dominate, the implications of the analyses were used to make that determination. The location of the probe nucleus is important and must be deduced from the data. Since the cadmium probe is divalent, it could be bonded within the chalcogen chains or in small molecular units outside the chains.

The calculated values of τ_Q cannot be due to random rotations of large structures such as found in liquid selenium since the autocorrelation or rotation times of these structures are large compared to τ_Q, 1 μs *vs.* 1 ns. Since the values of τ_Q change in a regular and continuous manner, it seems unlikely that rotations in the less viscous alloys are responsible for the EFG relaxation.

The calculated values of τ_Q are small, and their magnitude is consistent with small molecular units diffusing through the alloy liquid. But the temperature dependence of τ_Q is too strong - the fundamental vibration frequencies of the activated behavior are faster than phonon frequencies.

The behavior of λ_2 cannot be explained by approximately equal contributions of a fluctuating EFG and PRM. Not only would it be too coincidental for the contributions to be approximately equal over such a large temperature and composition range, but the values of τ_Q would still be unphysically fast.

The behavior of λ_2 cannot be explained by the dominance of an EFG fluctuation mechanism at one temperature range and a PRM mechanism in another range. This would require the slope of log τ_S *vs.* log (1000/T) (figure 4-1 or 5-1) to increase at the crossover whereas it is found to decrease.

Therefore, because the values of τ_Q do not lend themselves to reasonable physical interpretation, it is suggested that the angular correlation is attenuated through a paramagnetic relaxation mechanism due to the random fluctuation of a nearby spin and that EFG fluctuations are negligible.

6.2 Implications of τ_S

The size of the coupling parameter, $\langle\omega_S^2\rangle_{E.A.}$, is consistent with a spin in close proximity to the cadmium probe. The spin

fluctuates by coupling to the surrounding lattice. Since the concentration of the probe atoms is small, it should have negligible effect on the fluctuating mechanism.

The correlation time has been plotted as a function of volume per spin in figure 5-3. It was found that the data fell into three relatively well defined regions. For small volumes, all the pure selenium data fell in an approximate straight line with $\tau_S \propto N_S^{-1}$, where N_S is the spin density. The alloy data fell in a straight line paralleling the selenium data, but with τ_S approximately twice as fast for the same volume per spin. For small spin densities, all the data fell in an approximate straight line with $\tau_S \propto \sqrt{N_S^{-1}}$. Spin density data for pure tellurium was unavailable.

Because values of τ_S are inversely proportional to the spin density, the activation energies for the alloys in the high temperature τ_S data are the same energies as those measured in the magnetic susceptibility experiments. These values are one-half the chalcogenide bond strength. By assuming that the correlation times for supercooled tellurium is proportional to N_S^{-1} and that the values lie in the semiconducting region, then an estimate of half the tellurium-tellurium bond strength can be made from the activation energy of the data. This yields a value of 0.56 eV, slightly smaller than published values for the alloys, about 0.68 eV.

The 2 branches of the τ_S vs N_S^{-1} curve may be a real effect - the addition of tellurium reducing the fluctuation time. A second

possibility is that the coupling parameter changes with the addition of tellurium. Ordinarily, coupling parameters change by small percentages if the element about the probe is changed to another element from the same column. A third possibility is that the addition of tellurium causes a chemical reaction which in some way reduces the probability that a spin is near the probe. This work cannot definitely establish which of these possibilities is the correct explanation.

The data of the τ_S vs N_S^{-1} curves can be used to predict the susceptibility of highly supercooled tellurium. Figure 5-4 shows the estimates of the Curie susceptibility by assuming that the correlation times calculated for tellurium, using the above coupling parameter, lies on one of the two branches. The predicted values from the selenium branch lie near and above the best available susceptibility for tellurium. Those values from the alloy branch lie far below the tellurium values. Since the density of spins for tellurium-rich Se_xTe_{1-x} alloys is large for temperatures where the susceptibility has been measured, spin-spin interactions cannot be neglected, and the Curie model will yield values larger than the actual measured values. Therefore, the susceptibility estimated from the selenium branch are more consistent with the experimental susceptibility of pure tellurium.

This observation leads to the speculation that the coupling parameter is approximately constant for all composition and that in the alloys a chemical reaction reduces the spin density at the Cd probe.

A model consistent with the calculated values of τ_S is proposed in which the cadmium probe bonds with high probability to a single selenium or tellurium atom in a positive or negative diatomic ion. This would imply large values for the spin-spin coupling parameters, because of the proximity of the spin. The small size of the molecule implies small values of τ_Q. Both are consistent with the experimental data. Since no τ_Q effect is observed, the upper limit to its value is roughly the lower limit of measurable λ_2 values. Using the amorphous splat coupling parameter previously outlined, the upper limit for τ_Q is 10^{-10} to 10^{-11} s for compositions selenium to tellurium, with an expected weak temperature dependence. It is speculated that in pure selenium and tellurium, the cadmium-containing molecules are strongly ionized whereas in the alloys, a higher proportion are neutral. Such a mechanism could explain the of branches of the τ_S *vs.* N_S^{-1} curve.

The analysis of this work suggests the following experiments.

Perturbed angular correlation experiments on selenium with a few percent of tellurium and tellurium with minor selenium additions should be performed to determine if the data fall on one branch of the τ_S *vs.* N_S^{-1} curve or another or the middle. These experiments would probe the switchover from selenium-like to alloy-like behavior. The selenium-rich experiments should not be difficult. Accurate susceptibility values would be required for the concentration studied. Values for selenium-rich alloys and $Se_{0.1}Te_{0.9}$ have been published ($Se_{0.1}Te_{0.9}$ is displayed in

figure 5-4). Additional attempts to measure the very low-temperature susceptibility of tellurium and tellurium-rich alloys should also be made.

The possibility of a concentration or temperature-dependent coupling parameter could be resolved by doing a PAC experiment on liquid Se_xTe_{1-x} in a magnetic field. The Larmor frequency can be measured by perturbed angular correlation[28] and its Knight Shift with field can be plotted to yield the coupling parameter[33] as a function of temperature and composition. Not only could this determine the origin of the two branches of the τ_S *vs.* N_S^{-1} curve, but good estimates of the Curie susceptibility of tellurium-rich alloys could be made. Some questions on the NMR coupling strength in other experiments[26,27] may be resolved by combining these results with the NMR results.

NMR experiments on Se_xTe_{1-x} lightly doped with cadmium could also be performed to decide if τ_S or τ_Q is measured by this work. This is because the NMR cadmium isotope (^{111}Cd in its ground state) is a spin 1/2 nucleus, not susceptible to quadrupolar fields.

The proposed model implies that divalent impurities form small ionized molecular species in Se_xTe_{1-x}. It has been predicted by bond equilibrium theory that monovalent impurities exhibit measurable conductivity, susceptibility and thermopower effects differing from the undoped Se_xTe_{1-x} liquids. Recently this prediction has been verified by Fischer *et al.*[23] with an interesting additional development. One of the dopants, copper, may have been in a divalent state. The copper data presented did not quite

conform to the predictions of BET, leading Fischer et al. to propose a successful modification to BET for divalent materials. Additional experimental work needs to be done with divalent dopants before BET can be extended reliably to the divalent doping case.

It is interesting to note that the original goal to learn about chemical dynamics and the role of defects in liquid chalcogenides produced fundamental results relating to the correlation time of spins and the appealingly simple concept that τ_S may depend only on the spin density in the Se_xTe_{1-x} system. This provides an additional piece to the puzzle connecting the Pauli magnetic regime with the Curie magnetic regime through the values of τ_S for tellurium-rich alloys. Coincidentally, this work provides information on the tellurium bond strength and how a divalent impurity exists in liquid Se_xTe_{1-x}, which will contribute to understanding the chemical dynamics in these liquids.

REFERENCES

1 M. Cutler, Liquid Semiconductors, Academic Press (1977).

2 V. M. Glazov, S. N. Chizhevskaya, and N. N. Glagoleva, Liquid Semiconductors, Plenium (1969).

3 R. C. Keezer and M. V. Bailey, Mater. Res. Bull. 2, 185 (1967).

4 M. Misawa and K. Suzuki, Trans. Jpn. Inst. Met. 18, 427 (1977).

5 G. Tourand, J. de Physique, 34, 937 (1973).

6 G. Tourand, Physics Letters, 54A, 209 (1975).

7 M. Misawa and K. Suzuki, Res. Rep. Lab. Nucl. Sci., Tohoku U., 12, 200 (1979).

8 M. Hansen and K. Anderko, Constitution of Binary Alloys, 2nd ed. McGraw-Hill (1958).

9 G. Locovsky, Selenium and Tellurium, ed. E. Gerlach and P. Grosse, Springer-Verlag (1979).

10 R. Fisher, Thesis, U. of Marburg (1978), unpublished.

11 H. Turn and J. Ruska, J. Non-Cryst. Sol. 22, 331 (1976).

12 J. F. Rialland and J. C. Perron, Rev. Phys. Appl. (Paris) 11, 263 (1976).

13 J. Ruska, Amorphous and Liquid Semiconductors, ed. J. Stuke and W. Brenig, Taylor and Francis, London (1974).

14 A. Koma and S. Tanaka, J. of Non-Cryst. Sol. 8-10, 251 (1972).

15 M. Kastner, D. Adler, and H. Fritzsche, Phys. Rev. Lett. 37, 1504 (1976).

16 R. A. Street and N. F. Mott, Phys. Rev. Lett. 35, 1293 (1975).

17 J. C. Perron, Adv. Phys. 16, 657 (1967).

18 J. C. Perron, Thesis, U. of Paris (1969).

19 H. Rasolondramanitra, Thesis, Oregon State U. (1983), unpublished.

20 M. Cutler, Phys. Rev. B20, 2981 (1979).

21 M. Cutler and W. G. Bez, Phys. Rev. B23, 6223 (1981).

22 H. Radscheit, R. Fischer, and M. Cutler, J. Phys., Paris, 42, C4, 1051 (1981).

23 R. Fischer, M. Cutler and H. Rasolondramanitra, Phil. Mag. B48, 6, 537 (1983).

24 J. A. Gardner and M. Cutler, Phys. Rev. B20, 529 (1979).

25 D. Brown, D. S. Moore, and E. F. W. Seymour, J. Non-Cryst. Solids 8-10, 256 (1972).

26 W. W. Warren, Jr. and R. Dupree, Phys. Rev. B22, 2257 (1980).

27 D. J. Kirby, thesis, Univ. of Warwick (1981). unpublished.

28 H. Frauenfelder and R. M. Steffen, "Angular Distribution of Nuclear Radiations," in Alpha, Beta, and Gamma-Ray Spectroscopy, ed. K. Siegbahn, North Holland (1965).

29 Nucl. Data 27, 490 and 494 (1979).

30 Los Alamos Scientific Laboratory Report, #LA-4677 by K. Krane (1971).

31 S. Raman and H. J. Kim, Nucl. Data B6, 39 (1971).

32 A. Abragam, The Principles of Nuclear Magnetism, Oxford (1970).

33 C. P. Slichter, Principles of Magnetic Resonance, Springer-Verlag (1980).

34 E. Gerdau, T. A. Theil and G. Netz, Hyperfine Interactions 10, 1155 (1981).

35 A. R. Arends, C. Hohennemser, F. Pleiter, H. DeWaard, L. Chow, and R. M. Suter, Hyperfine Interactions, 8, 191 (1980).

36 P. C. Lopiparo and R. L. Rasera, Angular Correlations in Nuclear Disintegration, ed. H. V. Krugten and B. v. Nooijen, Rotterdam University Press (1971).

37 Private communication from R. L. Rasera and C. Cooke (1979).

38 R. L. Rasera and J. A. Gardner, Phys. Rev. B18, 6856 (1978).

39 J. A. Gardner and K. Krusch, Phys. Rev. B24, 4587 (1981).

40 H. Haas and D. A. Shirley, J. Chem. Phys. 58, 3339 (1973).

41 J. D. Ferry, Viscoelastic Properties of Polymers, John Wiley, 1980.

42 M. Fixman, J. Chem. Phys. 68, 2983 (1978).

43 A. J. Freeman and R. E. Watson, Magnetism Vol. IIA, ed. G. T. Rado and H. Suhl, Academic Press (1965).

44 J. A. Gardner and M. Cutler, Phys. Rev. B14, 4488 (1976).

45 A. Abragam and R. V. Pound, Phys. Rev. 92, 942 (1953).

46 M. E. Rose, Angular Momentum, Wiley (1957).

47 A. Edmonds, Angular Momentum in Quantum Mechanics, Princeton University Press (1957).

48 A. Messiah, Quantum Mechanics, Volume II, John Wiley (1958).

49 K. Gottfried, Quantum Mechanics, Volume I, Benjamin (1977).

50 C. N. Yang, Phys. Rev. 74, 764 (1948).

51 A. A. Moszkowski, "Theory of Multipole Radiations" in Alpha, Beta, and Gamma-Ray Spectroscopy, ed. K. Siegbahn, North-Holland (1965).

52 E. Matthias, W. Schneider, and R. M. Steffen, Phys. Rev. 125, 261 (1962).

53 E. Gerdau, J. Wolf, H. Winkler and J. Braunsfurth, Proc. Roy. Soc. A311, 197 (1969).

54 Biedenharn, Blatt, and Rose, Revs. Mod. Phys. 24, 249 (1952).

APPENDIX

APPENDIX

MATHEMATICAL DEVELOPMENT OF ANGULAR CORRELATIONS

This appendix provides the mathematical details which lead to the perturbed angular correlation formulas for two successive gamma decays given in chapter 2. It closely follows the development in Frauenfelder and Steffen's, "Angular Correlations" article in Alpha, Beta and Gamma Spectroscopy[28], and Abragam and Pound[45].

This appendix begins with the necessary mathematical conventions, then develops the angular correlation function. Static perturbative fields are treated followed by the formalism for time dependent fields. Time dependent random electric field gradients and paramagnetic spin relaxation mechanisms are then applied in evaluating perturbative factors.

A. Mathematical Conventions

The Condon-Shortley phase convention for Clebsch-Gordan coefficients is used with the following definition of the 3j symbol:

$$\begin{pmatrix} j_1 j_2 j_3 \\ m_1 m_2 m_3 \end{pmatrix} = \frac{(-1)^{j_1 - j_2 - m_3}}{(\hat{j}_3)^{\frac{1}{2}}} \langle j_1 m_1 j_2 m_2 | j_3 - m_3 \rangle \qquad \text{A-1}$$

(the symbol $\hat{K} = 2K+1$ will be used throughout). Note the sum convention $m_1+m_2+m_3 = 0$.

The 3j symbols are invariant under even permutations of columns,

$$\begin{pmatrix} j_1 j_2 j_3 \\ m_1 m_2 m_3 \end{pmatrix} = \begin{pmatrix} j_2 j_3 j_1 \\ m_2 m_3 m_1 \end{pmatrix} = \begin{pmatrix} j_3 j_1 j_2 \\ m_3 m_1 m_2 \end{pmatrix} , \qquad \text{A-2a}$$

and equal within a phase for the interchange of columns or negating the z projection row

$$\begin{pmatrix} j_1 j_2 j_3 \\ m_1 m_2 m_3 \end{pmatrix} = (-1)^{j_1+j_2+j_3} \begin{pmatrix} j_2 j_1 j_3 \\ m_2 m_1 m_3 \end{pmatrix} = (-1)^{j_1+j_2+j_3} \begin{pmatrix} j_1 j_2 j_3 \\ -m_1 -m_2 -m_3 \end{pmatrix} . \qquad \text{A-2b}$$

The orthogonality relations are:

$$\sum_{j_3 m_3} \hat{j}_3 \begin{pmatrix} j_1 j_2 j_3 \\ m_1 m_2 m_3 \end{pmatrix} \begin{pmatrix} j_1 j_2 j_3 \\ m_1' m_2' m_3 \end{pmatrix} = \delta_{m_1 m_1'} \delta_{m_2 m_2'} , \qquad \text{A-3a}$$

$$\sum_{m_1 m_2} \hat{j}_3 \begin{pmatrix} j_1 j_2 j_3 \\ m_1 m_2 m_3 \end{pmatrix} \begin{pmatrix} j_1 j_2 j_3' \\ m_1 m_2 m_3' \end{pmatrix} = \delta_{j_3 j_3} \delta_{m_3 m_3'} . \qquad \text{A-3b}$$

The Wigner-Eckart Theorem is:

$$\langle I m | T_q^{(\lambda)} | I_i m_i \rangle = (-1)^{I-m} \begin{pmatrix} I & \lambda & I_i \\ -m & q & m_i \end{pmatrix} \langle I \| T^{(\lambda)} \| I_i \rangle \qquad \text{A-4}$$

which serves to define the reduced matrix element, $\langle I \| T^{(\lambda)} \| I_i \rangle$, which is independent of m states (geometry).

The contraction of three 3j symbols is

$$\sum_{m_4 m_5 m_6} (-1)^{j_4+j_5+j_6+m_4+m_5+m_6} \begin{pmatrix} j_1 j_5 j_6 \\ m_1 m_5 -m_6 \end{pmatrix} \begin{pmatrix} j_4 j_2 j_6 \\ -m_4 m_2 m_6 \end{pmatrix} \begin{pmatrix} j_4 j_5 j_3 \\ m_4 -m_5 -m_3 \end{pmatrix}$$

$$= \begin{pmatrix} j_1 j_2 j_3 \\ m_1 m_2 m_3 \end{pmatrix} \begin{Bmatrix} j_1 j_2 j_3 \\ j_4 j_5 j_6 \end{Bmatrix} \qquad \text{A-5}$$

where the 6j symbol, $\{^{j_1 j_2 j_3}_{j_4 j_5 j_6}\}$, is related to the Racah coefficient through

$$W(j_1 j_2 j_5 j_4;\ j_3 j_6) = (-1)^{j_1+j_2+j_4+j_5} \begin{Bmatrix} j_1 j_2 j_3 \\ j_4 j_5 j_6 \end{Bmatrix} \quad . \qquad \text{A-6}$$

The symmetry properties of the 6j symbols are:

$$\begin{Bmatrix} j_1 j_2 j_3 \\ j_4 j_5 j_6 \end{Bmatrix} = \begin{Bmatrix} j_2 j_3 j_1 \\ j_5 j_6 j_4 \end{Bmatrix} = \begin{Bmatrix} j_1 j_5 j_6 \\ j_4 j_2 j_3 \end{Bmatrix} = \ldots \qquad \text{A-7}$$

Complete details concerning 3j, 6j, and Racah coefficients can be found in Rose[46] and Edmonds[47]. A short synopsis of various properties and relations can be found in Messiah.[48]

The rotation matrix, $D^L_{\mu m}(\vec{K} \to \hat{z})$, represents the quantum mechanical rotation of a state with angular momentum L with some quantization axis $\vec{K}$ rotated into the axis $\hat{z}$. Some properties of the D matrices are:

inversion $\quad D^L_{\mu m}(\vec{K} \to \hat{z}) = D^{L\,*}_{m\mu}(\hat{z} \to \vec{K}) \quad , \qquad \text{A-8a}$

projection $\quad D^{L\,*}_{\mu m}(\vec{K} \to \hat{z}) = (-1)^{\mu-m} D^L_{-\mu -m}(\vec{K} \to \hat{z}) \quad , \qquad \text{A-8b}$

contraction $\quad \sum_{m'} D^L_{\mu m'}(\vec{K} \to \hat{z}')\, D^L_{m'm}(\hat{z}' \to \hat{z}) = D^L_{\mu m}(\vec{K} \to \hat{z}). \qquad \text{A-8c}$

The Clebsch-Gordan series is

$$D^L_{\mu m}\, D^{L'}_{\mu' m'} = \sum_k \langle L\mu L'\mu' | k\tau \rangle \langle LmL'm' | kN \rangle D^k_{\tau N} \qquad \text{A-9}$$

with the usual angular momentum sum rule $|L-L'| \leq k \leq L+L'$. Additional details can be found in most graduate quantum mechanics textbooks such as Gottfried.[49]

B. The Density Matrix

Let $|m\rangle$ be a complete orthonormal set of states, and let $|n\rangle$ be a state with well defined eigenvalues, a statistically pure state of an ensemble. Then $|n\rangle$ can be represented by a superposition of the states $|m\rangle$,

$$|n\rangle = \sum_m a_{nm} |m\rangle \quad . \tag{A-10}$$

A mixed state, $|n'\rangle$, is an incoherent sum over the pure states $|n\rangle$ with weights g_n. Thus the expectation value of some operator, F, over the ensemble is

$$\langle F\rangle \equiv \langle n'|F|n'\rangle = \sum_{nmm'} g_n \, a^*_{nm'} \, a_{nm} \langle m'|F|m\rangle \quad , \tag{A-11}$$

where F is diagonal in the m representation.

This suggests the creation of a matrix element in the form:

$$\langle F\rangle = \sum_{mm'} \langle m|\rho|m'\rangle\langle m'|F|m\rangle$$

$$= \mathrm{Tr}\,(\rho F) = \mathrm{Tr}\,(F\rho) \tag{A-12}$$

where the matrix elements

$$\langle m|\rho|m'\rangle = \sum_n a^*_{nm'} \, g_n \, a_{nm} \tag{A-13}$$

contain information about the mixture of states in an ensemble and $\langle m'|F|m\rangle$ contains the quantum mechanical information for the operator F. Since $a_{nm} = \langle m|n\rangle$, then

$$\rho = \sum_n |n\rangle\, g_n\, \langle n| \quad . \tag{A-14}$$

The quantum mechanical interpretation is that $|a_{nm}|^2$ is the probability of finding the pure state $|n\rangle$ in the state $|m\rangle$. Similarly the probability, P(m), of finding any member of a mixed ensemble, described by an incoherent superposition of the pure state $|n'\rangle$, in the state $|m\rangle$ is

$$P(m) = \sum_n g_n\, a^*_{nm}\, a_{nm} = \langle m|\rho|m\rangle \quad . \tag{A-15}$$

Thus, the diagonal elements of the density matrix give the probability of finding the ensemble in the state $|m'\rangle$.

Consider a two level system consisting of states $\{|m_i\rangle\}$ and $\{|m_f\rangle\}$. Let H(t) be the Hamiltonian which induces the transition $|m_f\rangle = H|m_i\rangle$. Let $|n\rangle$ be the pure state of an ensemble made up of the above systems. The density matrix for a mixed initial state is then

$$\rho_i = \rho\ (t=0) = \sum_n |n\rangle\, g_n\, \langle n| \tag{A-16}$$

At t = 0 the Hamiltonian is turned on, giving

$$\rho_f = \rho(t) = \sum_n H(t)\ |n\rangle\, g_n\, \langle n|H(t)^\dagger \tag{A-17}$$

Evaluating the matrix elements of $\rho(t)$ in terms of the complete set $\{|m_f\rangle\}$ yields

$$\langle m_f|\rho(t)|m_f'\rangle = \sum_n \langle m_f|H(t)|n\rangle g_n \langle n|H(t)^\dagger|m_f'\rangle$$

inserting unity $= \sum_{m_i} |m_i\rangle\langle m_i|$ twice gives

$$\langle m_f|\rho(t)|m_f'\rangle = \sum_{m_i m_i'} \langle m_f|H(t)|m_i\rangle\langle m_i|\rho_A|m_i'\rangle\langle m_f'|H(t)|m_i'\rangle^* \quad . \quad \text{A-18}$$

If the above final state is really an intermediate state of some two step process, then it can be shown in a similar manner that

$$\langle m_f|\rho(i\to I\to f)|m_f'\rangle =$$

$$\sum_{\substack{m_i m_i' \\ m_I m_I'}} \langle m_f|H_2|m_I\rangle\langle m_I|H_1|m_i\rangle\langle m_i|\rho_i|m_i'\rangle \langle m_I'|H_1|m_i'\rangle^* \langle m_f'|H_2|m_I'\rangle^* \quad \text{A-19}$$

Now consider the initial density operator. Let the pure states all have equal weight f

$$\langle m_i|\rho_i|m_i'\rangle = f \sum_n \langle m_i|n\rangle\langle n|m_i'\rangle = f\,\delta_{m_i m_i'} \quad . \quad \text{A-20}$$

That is, the initial density matrix is diagonal in this case. It should be remembered that the result given is perfectly general.

C. Evaluating the Angular Correlation Function

The angular correlation function, $W(\vec{k}_1,\vec{k}_2)d\Omega_1 d\Omega_2$, is the probability that a nucleus decaying through the cascade $I_i\to I\to I_f$ emits two radiations, R_1 and R_2 in the directions $\vec{k}_1$, $\vec{k}_2$, in the

solid angle $d\Omega_1$, $d\Omega_2$. In equation A-18, with $\rho = \rho(\vec{K}_1,\vec{K}_2)$, $m_f'=m_f$ yields the probability that the nucleus is in the final state m_f after emitting radiations $\vec{K}_1,\vec{K}_2$. The sum over all final states is the angular correlation function $W(\vec{K}_1,\vec{K}_2)$. The matrix element becomes

$$\langle m|H_1|m_i\rangle = \langle Im\vec{K}_1\sigma|H_1|I_im_i\rangle \qquad \text{A-21}$$

where I, m is the spin and spin projection of angular momentum of the intermediate state and σ is the polarization of the radiation emitted in the direction $\vec{K}_1$. A similar understanding exists for the other matrix elements involving the radiation Hamiltonian H_2.

Further, the initial state is assumed to have no preferred orientation. This means $\langle m_i|\rho_i|m_i'\rangle = \delta_{m_im_i'}/\hat{I}$. Thus

$$W(\vec{K}_1,\vec{K}_2) = S_1S_2 \sum_{\substack{m_fm_i \\ mm'}} \langle m_f|H_2|m\rangle\langle m|H_1|m_i\rangle\langle m'|H_1|m_i\rangle^*\langle m_f|H_2|m'\rangle^* \quad , \quad \text{A-22}$$

where S_1S_2 represents the sums over any observed states, e.g., polarizations, and unimportant constants have been divided out.

It has been assumed that the intermediate states, $|Im\rangle$, do not change before the emission of the second radiation. (Note: to avoid redundancy, the angular momentum, I, will be dropped from the kets, $|Im\rangle$, in the mathematics that follows. It should be clear to the reader what the value of I is for a particular ket from the context of the mathematics.) The angular correlation function can be rewritten as

$$W(\vec{K}_1,\vec{K}_2) = \sum_{mm'} \langle m|\rho(\vec{K}_1)|m'\rangle\langle m'|\rho(\vec{K}_2)|m\rangle \quad , \qquad \text{A-23a}$$

where

$$\langle m|\rho(\vec{K}_1)|m'\rangle = S_1 \sum_{m_i} \langle m|H_1|m_i\rangle\langle m'|H_1|m_i\rangle^* \qquad \text{A-23b}$$

and

$$\langle m'|\rho(\vec{K}_2)|m\rangle = S_2 \sum_{m_f} \langle m_f|H_2|m\rangle\langle m_f|H_2|m'\rangle^* \quad . \qquad \text{A-23c}$$

To evaluate the above expressions first consider the matrix elements $\langle Im\vec{K}\sigma|H|I_i m_i\rangle$ which describe the radiation in terms of its direction and polarization. Expand the matrix element in terms of the angular momentum of the radiation and its parity

$$\langle Im\vec{K}\sigma|H|I_i m_i\rangle = \sum_{LM\pi} \langle\vec{K}\sigma|LM\pi\rangle\langle ImLM\pi|H|I_i m_i\rangle \quad , \qquad \text{A-24}$$

where M is the z component of L along some arbitrary z axis and π is the parity of the radiation. Rewriting the first matrix with the aid of the D-matrices

$$\langle\vec{K}\sigma|LM\pi\rangle = \sum_{\mu} \langle o\sigma|L\mu\pi\rangle\, D^{L*}_{M\mu}(\hat{z}\to\vec{K}) \quad . \qquad \text{A-25}$$

The term $\langle o\sigma|L\mu\pi\rangle$ represents the matrix element $\langle\vec{K}\sigma|L\mu\pi\rangle$ where the direction of $\vec{K}$ coincides with the axis of quantization, $\hat{z}$. The second matrix element in the sum, $\langle ImLM\pi|H|I_i m_i\rangle$, involves the radiation Hamiltonian of multiple order L. Using the Wigner-Eckart Theorem the result becomes

$$\langle m|H|m_i\rangle = \sum_{L M \pi\mu} (-1)^{L-I-m_i} \begin{pmatrix} I & L & I_i \\ m & M & -m_i \end{pmatrix} \langle o\sigma|L\mu\pi\rangle \, D^{L*}_{M\mu}(\hat{z}\to\hat{K}) \langle I\|L\pi\|I_i\rangle. \quad \text{A-26}$$

Inserting the relations found for $\langle m|H|m_i\rangle$ to evaluate $\langle m|\rho|m'\rangle$. This leads to

$$\langle m|\rho(\hat{K})|m'\rangle = S \sum_{m_i} \sum_{\substack{L M \\ \pi\mu}} \sum_{\substack{L' M' \\ \pi'\mu'}} (-1)^{L+L'-2(I+m_i)} \langle o\sigma|L\mu\pi\rangle\langle o\sigma'|L'\mu'\pi'\rangle^*$$

$$\begin{pmatrix} I & L & I_i \\ m & M & -m_i \end{pmatrix} \begin{pmatrix} I & L' & I_i \\ m' & M' & -m_i \end{pmatrix} \langle I\|L\pi\|I_i\rangle\langle I\|L'\pi'\|I_i\rangle^* \, D^{L*}_{M\mu}(\hat{z}\to\hat{K}) D^{L'}_{M'\mu'}(\hat{z}\to\hat{K}). \quad \text{A-27}$$

Use equation A-8b to convert $D^{L*}_{m\mu}$ and then apply the Clebsch-Gordan series, equation A-9. Evaluating all the phases (note that I+m is always an integer) gives the result:

$$\langle m|\rho(\hat{K})|m'\rangle = S \sum_{\substack{L L' \\ \mu\mu'}} \sum_{k N\tau} (-1)^{2I-I_i+m-\mu'} \hat{k} \langle o\sigma|L\mu\pi\rangle\langle o\sigma'|L'\mu'\pi'\rangle^*$$

$$\begin{pmatrix} I & L & I_i \\ m & M & -m_i \end{pmatrix} \begin{pmatrix} I & L' & I_i \\ m' & M' & -m_i \end{pmatrix} \begin{pmatrix} L & L' & k \\ M & -M' & N \end{pmatrix} \begin{pmatrix} L & L' & k \\ \mu & -\mu' & \tau \end{pmatrix}$$

$$\langle I\|L\pi\|I_i\rangle\langle I\|L'\pi'\|I_i\rangle^* D^{k}_{N\tau}(\hat{z}\to\hat{K}) \quad . \quad \text{A-28}$$

This can be simplified by using the contraction relation for 3j symbols to a product of a 3j and 6j symbol, equation A-5.

$$\langle m|\rho(\vec{K})|m'\rangle = S \sum_{\substack{LL' \\ \mu\mu'}} \sum_{k\tilde{N}\tau} (-1)^{2I-I_i+m-\mu'} \hat{k}\langle o\sigma|L\mu\pi\rangle\langle o\sigma'|L'\mu'\pi'\rangle^*$$

$$\langle I\|L\pi\|I_i\rangle\langle I\|L'\pi'\|I_i\rangle^* D^k_{N\tau}(\hat{z}\to\vec{K}) \begin{pmatrix} L & L' & k \\ \mu-\mu' & \tau & \end{pmatrix}\begin{pmatrix} I & I & k \\ m' & -m & N \end{pmatrix}\begin{Bmatrix} I & I & k \\ L & L' & I_i \end{Bmatrix}. \quad \text{A-29}$$

Defining the Racah Radiation Parameter

$$C_{k\tau}(LL') = S \sum_{\mu\mu'} (-1)^{-L+\mu} \hat{k} \begin{pmatrix} L & L' & k \\ \mu & -\mu' & -\tau \end{pmatrix}\langle I\|L\pi\|I_i\rangle^*\langle I\|L'\pi'\|I_i\rangle^* \quad \text{A-30}$$

This produces the result, where the subscript 1 denotes the first radiation,

$$\langle m|\rho(\vec{K}_1)|m'\rangle = \sum_{\substack{L_1L_1' \\ \pi_1\pi_1'}} \sum_{k_1\tilde{N}_1\tau_1} (-1)^{2I-I_i+m-L'} \hat{k}_1 \; C_{k_1\tau_1}(L_1'L_1)$$

$$\begin{pmatrix} I & I & k_1 \\ m' & -m & N_1 \end{pmatrix}\begin{Bmatrix} I & I & k_1 \\ L_1 & L_1' & I_i \end{Bmatrix}\langle I\|L_1\pi_1\|I_i\rangle\langle I\|L_1'\pi_1'\|I_i\rangle^* D^{k_1}_{N_1\tau_1}(\hat{z}\to\vec{K}_1) \; . \quad \text{A-31}$$

Performing similar mathematical manipulations for the density matrix element involving the second radiation gives

$$\langle m'|\rho(\vec{K}_2)|m\rangle = \sum_{\substack{L_2L_2' \\ \pi_2\pi_2'}} \sum_{k_2\tilde{N}_2\tau_2} (-1)^{k_2-m-L_2'-I_f} \hat{k}_2 \; C^*_{k_2\tau_2}(L_2L_2')$$

$$\begin{pmatrix} I & I & k_2 \\ m' & -m & N_2 \end{pmatrix}\begin{Bmatrix} I & I & k_2 \\ L_2 & L_2' & I_f \end{Bmatrix}\langle I_f\|L_2\pi_2\|I\rangle\langle I_f\|L_2'\pi_2'\|I\rangle^* D^{k_2}_{\tau_2N_2}(\vec{K}_2\to\hat{z}) \quad . \quad \text{A-32}$$

The results for the two density matrix elements can be put together to form the angular correlation function, equation A-23a. The expression contains the term

$$\sum_{mm'} \begin{pmatrix} I & I & k_1 \\ m' & -m & N_1 \end{pmatrix} \begin{pmatrix} I & I & k_2 \\ m' & -m & N_2 \end{pmatrix} \hat{k}_1 \hat{k}_2 = \delta_{k_1 k_2} \delta_{N_1 N_2}$$

which contracts under the orthogonality of the 3j symbols, equation A-3b. The resulting expression contains the product of two D matrices. This simplifies because of the contraction property of the D matrices, equation A-8c. The final expression becomes

$$W(\vec{k}_1,\vec{k}_2) = (-1)^{2I-I_i-I_f} \sum_{k} \sum_{\tau_1\tau_2} \sum_{\substack{L_1 L_1' \\ \pi_1 \pi_1'}} \sum_{\substack{L_2 L_2' \\ \pi_2 \pi_2'}} (-1)^{k-L_1'-L_2'} C_{k\tau_1}(L_1' L_1)$$

$$C^*_{k\tau_2}(L_2 L_2') \langle I \| L_1 \pi_1 \| I_i \rangle \langle I \| L_1' \pi_1' \| I_i \rangle^* \langle I_f \| L_2 \pi_2 \| I \rangle \langle I_f \| L_2' \pi_2' \| I \rangle^*$$

$$\begin{Bmatrix} I & I & k \\ L_1 & L_1' & I_i \end{Bmatrix} \begin{Bmatrix} I & I & k \\ L_2 & L_2' & I_f \end{Bmatrix} D^k_{\tau_2\tau_1}(\vec{k}_2 \to \vec{k}_1) \quad . \qquad \text{A-33}$$

It is important to point out that the result depends only on the angles between $\vec{k}_2$ and $\vec{k}_1$ and not the choice of the arbitrary quantization axis $\hat{z}$.

Furthermore, the 6j symbol $\{\begin{smallmatrix} I & I & k \\ L & L' & I_i \end{smallmatrix}\}$ contains the two vector triangle inequalities involving (IIk) and (LL'k). This places a fundamental limit on the value of the index k,

$$0 \leq k \leq \text{Min}(2I, L_1+L_1', L_2+L_2') \quad , \qquad \text{A-34}$$

otherwise the 6j symbols are zero. It has also been pointed out that these selection rules follow directly from the invariance of the correlation process under rotation and inversion.[50]

Experimental observation of the directions of the radiations and not the polarization is made in this work. Thus the observed correlation function is independent of rotations about the directions $\vec{K}_1$ and $\vec{K}_2$. Also, $C_{k\tau}(LL')$ is an eigenfunction of the angular momentum $\vec{K}$ with z component τ, where the z axis is in the K direction. Because of rotational invariance, only the $\tau = 0$ component is non-zero. Using the relation between reduced matrix elements

$$\langle I_f \| L\pi \| I \rangle \hat{I} = (-1)^{I_f - I + L} \langle I \| L\pi \| I_f \rangle^* I_f \quad ,$$

defining the A_k coefficient,

$$A_k(L_1 L_1' I_i I) =$$

$$\sum_{\substack{L_1 L_1' \\ \pi_1 \pi_1'}} (-1)^{L_1} C^*_{k0}(L_1 L_1') \langle I \| L_1 \pi_1 \| I_i \rangle \langle I \| L_1' \pi_1' \| I_i \rangle^* \begin{Bmatrix} I & I & k \\ L_1 & L_1' & I_i \end{Bmatrix} , \qquad \text{A-35}$$

and using the fact that $D^k_{oo}(\vec{K}_2 \to \vec{K}_1) = P_k(\cos\theta)$, where θ is the angle between $\vec{K}_1$ and $\vec{K}_2$, the important formula results:

$$W(\vec{K}_1, \vec{K}_2) = \sum_k A_k(L_1 L_1' I_i I) A_k(L_2 L_2' I_f I) \, P_k(\cos\theta)$$

or

$$W(\vec{K}_1,\vec{K}_2) = \sum_k A_k(\gamma_1)A_k(\gamma_2)P_k(\cos\theta) \quad . \qquad \text{A-36}$$

To evaluate the Racah radiation parameters, and hence the A_k coefficients, only two multipoles need be considered. This is because the transition probabilities for nuclear radiations have the approximate form.[51]

$$\frac{T^{M(L+1)}}{T^{EL}} \sim \left(\frac{\hbar\omega}{mc^2}\right)^2$$

and

$$\frac{T^{E(L+1)}}{T^{ML}} \sim \frac{ma\omega}{\hbar}$$

where T^{ML}, T^{ME} is the transition probability for radiation of magnetic L-pole (ML) or electric L-pole (EL) character, $\hbar\omega$ is the energy of the transition, m is the proton mass and $a=1.2\times10^{-13}A^{1/3}$cm is the average nuclear radius. It can be seen that the transition probability for a third multipole radiation mixed into a transition is reduced by many orders of magnitude. As an example the ratio of M1:E2:M3 for the 7/2 → 5/2 171 Kev transition in ^{111}Cd is $1:2\times10^{-4}:6\times10^{-12}$.

Evaluation of the Racah coefficients under the condition that polarization is not observed gives the important result that only even k values contribute.

Evaluation of the A_k coefficients is best done using the F coefficient defined as

$$F_k(LL'I_iI) = (-1)^{I_i+I-1}(\hat{L}\hat{L}'\hat{k}\hat{I})^{\frac{1}{2}} \begin{pmatrix} L & L' & k \\ 1 & -1 & 0 \end{pmatrix} \begin{Bmatrix} L & L' & k \\ I & I & I_i \end{Bmatrix} \quad \text{A-37}$$

using

$$A_k(LL'I_iI) = \frac{F_k(LLI_iI)+2\delta F_k(LL'I_i-I)+\delta^2 F_k(L'L'I_iI)}{1+\delta^2}, \quad \text{A-38}$$

where the mixing ratio is defined as

$$\delta = \frac{\langle I\|L'\pi'\|I_i\rangle}{\langle I\|L\pi\|I_i\rangle} . \quad \text{A-39}$$

Values of the F coefficients are tabulated in references such Krane.[30] (This reference uses the same phase conventions as this work.) See table 2-1 for the pertinent values for the ^{111}Cd cascade used in this work.

D. The Effect of Extranuclear Perturbations

Let the intermediate state of the nuclear cascade interact with some external perturbing field, represented by an interaction Hamiltonian K(t). This field acts on the intermediate state just after the first radiation is emitted, at t=0, and persists until the second radiation is emitted, at time t. The time evolution operator formalism is the prescription for evaluating the interaction,

$$\Lambda(t)|m_a\rangle = |m_b\rangle, \quad \Lambda(t) = \exp\left[\frac{-i}{\hbar}\int_0^t K(t')dt'\right],$$

$$\Lambda(t=0) = \delta_{m_a m_b} \quad \text{A-40}$$

where the integral has Feynman time ordering.

Under these conditions we modify equation A-22 to

$$W(\vec{K}_1,\vec{K}_2,t) =$$

$$\sum_{\substack{m_i m_f \\ m_a m'_a}} \langle m_f|H_2\Lambda(t)|m_a\rangle\langle m_a|H_1|m_i\rangle\langle m'_a|H_1|m_i\rangle^*\langle m_f|H_2\Lambda(t)|m'_a\rangle \quad . \quad \text{A-41}$$

Inserting unity in the form of a sum over complete states $|m_b\rangle$ and $|m'_b\rangle$ and using the definition of the density matrix elements as used in equation A-23b,c gives the result

$$W(\vec{K}_1,\vec{K}_2,t) =$$

$$\sum_{\substack{m_a m'_a \\ m_b m'_b}} \langle m_a|\rho(\vec{K}_1)|m'_a\rangle\langle m'_b|\rho(\vec{K}_2)|m_b\rangle\langle m_b|\Lambda(t)|m_a\rangle\langle m'_b|\Lambda(t)|m'_a\rangle^* \quad . \quad \text{A-42}$$

Evaluation requires insertion of the values of the density matrix elements as previously calculated in equation A-31 and A-32 along with the experimental condition that polarizations are not observed ($\tau = 0$) and using the equalities,

$$D^L_{\mu 0}(\phi,\theta,\gamma) = \left(\frac{4\pi}{\hat{L}}\right)^{\frac{1}{2}} Y^{\mu *}_L(\theta,\phi) \qquad \text{A-43a}$$

$$D^L_{0m}(\rho,\theta,\gamma) = \left(\frac{4\pi}{\hat{L}}\right)^{\frac{1}{2}} Y^{-m}_L(\theta,\phi) \quad . \qquad \text{A-43b}$$

After performing algebra similar to that of the previous section, and using the definitions of $A_k(LL'II)$ (equation A-35), the result is

$$W(\vec{K}_1,\vec{K}_2,t) =$$

$$\sum_{\substack{k_1N_1\\k_2N_2}} A_{k_1}(\gamma_1)A_{k_2}(\gamma_2)(\hat{k}_1\hat{k}_2)\ G_{k_1k_2}^{N_1N_2}(t)\ Y_{k_1}^{N_1\,*}(\theta_1,\phi_1)\ Y_{k_2}^{N_2}(\theta_2,\phi_2)\ , \quad \text{A-44}$$

where the attenuation factor is

$$G_{k_1k_2}^{N_1N_2}(t) = \sum_{m_am_b} (-1)^{2I+m_a+m_b}\ (\hat{k}_1\hat{k}_2)^{\frac{1}{2}} \begin{pmatrix} I & I & k_1 \\ m_a & -m_a & N_1 \end{pmatrix} \begin{pmatrix} I & I & k_2 \\ m_b & -m_b & N_2 \end{pmatrix}$$

$$\langle m_b|\Lambda(t)|m_a\rangle\langle m_b'|\Lambda(t)|m_a'\rangle^* \quad \text{A-45}$$

and θ_i,ϕ_i are the emission direction coordinates of the radiations referred to some arbitrary $\hat{z}$ axis.

The expression for $G_{k_1k_2}^{N_1N_2}(t)$ can be simplified by considering the two limiting cases of interest, a single crystal sample and a powdered sample of randomly oriented microcrystals. In both cases the Hamiltonian K(t) is assumed static on the time scale of the experiment, i.e., the decay lifetime of the intermediate state.

In general, the interaction is not diagonal and must be diagonalized by some unitary matrix U,

$$U\ K\ U^{-1} = E, \text{ where E is diagonal.} \quad \text{A-46}$$

It follows that

$$\Lambda(t) = \exp\ [-iKt/\hbar] = U^{-1}\ \exp[-iEt/h]\ U$$

with matrix elements

$$\langle m_b|\Lambda(t)|m_a\rangle = \sum_n \langle m_b|U^{-1}|n\rangle\langle n|e^{-iE_n t/h}|n\rangle\langle n|U|m_a\rangle \quad .$$

For convenience, let $\langle n|m_a\rangle = \langle n|U|m_a\rangle$. The attenuation factor becomes

$$G^{N_1N_2}_{k_1k_2}(t) = \sum_{\substack{m_a m_b \\ N\ N'}} (-1)^{2I+m_a+m_b}(\hat{k}_1\hat{k}_2)^{\frac{1}{2}} \begin{pmatrix} I & I & k_1 \\ m_a & -m_a & N_1 \end{pmatrix} \begin{pmatrix} I & I & k_2 \\ m_b & -m_b & N_2 \end{pmatrix}$$

$$\langle n|m_b\rangle^* \langle n|m_a\rangle\langle n'|m_b'\rangle\langle n'|m_a'\rangle^* \exp\,[-i(E_n-E_{n'})t/h] \quad . \qquad \text{A-47}$$

If the interacting field is axially symmetric, i.e., a pure magnetic field or an axially symmetric electrostatic field, then the z-axis of all previous expressions can be chosen to coincide with the symmetry axis of the field. Thus K and $\Lambda(t)$ are diagonal and U=1. This yields

$$G^{N_1N_2}_{k_1k_2}(t) = \sum_{mm'} (\hat{k}_1\hat{k}_2)^{\frac{1}{2}} \exp[-i(E_m-E_{m'})t/h]$$

$$\begin{pmatrix} I & I & k_1 \\ m' & -m & N_1 \end{pmatrix} \begin{pmatrix} I & I & k_2 \\ m' & -m & N_1 \end{pmatrix} \delta_{N_1N_2} \quad . \qquad \text{A-48}$$

If one of the radiations propagates in a direction parallel to the symmetry axis, then one of the spherical harmonic terms in

is the spherical tensor operator of the classical external electric gradient (EFG). The sum is over all lattice point charges and their coordinates.

The components of the EFG tensor can be written in terms of cartesian derivatives in some arbitrary coordinate system.

$$V_0^{(2)} = \frac{1}{4}\sqrt{\frac{5}{\pi}}\, V_{z'z'}$$

$$V_{\pm1}^{(2)} = \mp\frac{1}{2}\sqrt{\frac{5}{6\pi}}\,(V_{x'z'} \pm iV_{y'z'})$$

$$V_{\pm2}^{(2)} = \frac{1}{4}\sqrt{\frac{5}{6\pi}}\,(V_{x'x'} - V_{y'y'} \pm 2iV_{x'y'}) \quad . \qquad \text{A-65}$$

where $V_{x_i x_j} = \dfrac{\partial^2 V}{\partial x_i \partial x_j} = \dfrac{\partial^2}{\partial x_i \partial x_j}\sum_c \dfrac{e_c}{r_c}$.

These relations simplify in the principle axis coordinate system where mixed derivatives disappear,

$$V_0^{(2)} = \frac{1}{4}\sqrt{\frac{5}{\pi}}\, V_{zz}$$

$$V_{\pm1}^{(2)} = 0$$

$$V_{\pm2}^{(2)} = \frac{1}{4}\sqrt{\frac{5}{6\pi}}\,\eta\, V_{zz} \quad , \qquad \text{A-66}$$

where

$$\eta = (V_{xx} - V_{yy})/V_{zz} \quad , \quad 0 \leq \eta \leq 1 \quad ,$$

is the asymmetry parameter. The allowed values of η come about because of the particular choice of principal axis such that $|V_{zz}| \geq |V_{yy}| \geq |V_{xx}|$. When the EFG has axial symmetry $\eta=0$. To solve for the eigenenergies for the $\eta \neq 0$ case, one must diagonalize the matrix elements of K_Q, $\langle m|K_Q|m'\rangle$. These elements are straightforward to evaluate. The result is

$$\langle m|K_Q|m'\rangle = \frac{eQV_{zz}}{4I(2I-1)} [3m^2-I(I+1)] \delta_{m'm}$$

$$+ \eta/2 \sqrt{(I-m+2)(I-m+1)(I+m)(I+m-1)}\ \delta_{m',m-2}$$

$$+ \eta/2 \sqrt{(I+m+2)(I+m+1)(I-m)(I-m-1)}\ \delta_{m',m+2} \quad , \qquad \text{A-67}$$

where the quadrupole moment is defined through the following matrix element for the highest valued m-state:

$$eQ = \langle II| \sum_p e_p(3z_p^2-r_p^2)|II\rangle = 4\left(\frac{\pi}{5}\right) \langle II|T_0^{(2)}|II\rangle \quad . \qquad \text{A-68}$$

Note that the elements $\langle m|K_Q|m'\rangle$ are symmetrical with respect to $m \rightarrow -m$. Thus the quadrupole interaction is always degenerate for $\pm$ m states.

Because of the form of the K_Q matrix, diagonalization is a non-trivial task. The usual prescription is to diagonalize the matrix for a particular value of I. The I = 5/2 case in this work produces the following matrix:

$W(\vec{K}_1,\vec{K}_2,t)$ simplifies to

$$Y_k^N(0,\phi) = \delta_{NO}\left(\frac{\hat{k}}{4\pi}\right)^{\frac{1}{2}}$$

which implies N=0. This in turn implies m'=m through the sum rule of m-states for 3j symbols. Thus $E_m - E_{m'}=0$ and applying the orthogonality relation A-3b gives the results

$$G_{k_1k_2}^{N_1N_2}(t) = \delta_{k_1k_2}\,\delta_{N_1N_2}\,\delta_{N_1O}$$

and

$$W(\vec{K}_1,\vec{K}_2,t) = \sum_k A_k(\gamma_1)A_k(\gamma_2)P_k(\cos\theta) \quad , \qquad \text{A-49}$$

indicating that the perturbing external field has no effect on the angular correlation. This is because the external field does not induce transitions among the m states of the intermediate state.

For a powdered sample made up of large numbers of randomly oriented microcrystals the observed effect is found by averaging over the random directions of the symmetry axes of the microcrystals. The general case where the perturbing field is not axially symmetric but rhombic in character is treated as follows. Let D be the rotation matrix which rotates from a microcrystal's general coordinates of orientation to the arbitrary z axis frame of the perturbed angular correlation formalism. Let R be the rotation matrix which rotates from a microcrystal's principle axis to its general coordinates of orientation. Let U^{-1} be the particular unitary matrix which transforms the diagonal Hamiltonian, E, to the

principle axis Hamiltonian. (Then U is the matrix which diagonalized the principle axis Hamiltonian, consistent with the rotation of A-47). Thus, $K=DRU^{-1}EUR^{-1}D^{-1}$. Likewise,

$$\Lambda(t) = DRU^{-1} \exp[-iEt/\hbar]\, UR^{-1}D^{-1} \qquad \text{A-50}$$

For simplicity, let the rotation operator X=DR, a product of two rotations. The matrix elements of X are then $X^{(k_1)}_{P_1N_1} = \sum_{\lambda} D^{(k_1)}_{P_1\lambda} R^{(k_1)}_{\lambda N_1}$. The matrix elements required are,

$$\langle m_b|\Lambda(t)|m_a\rangle = \sum_{mn_1n_2} \langle m_b|X|n_1\rangle\langle n_1|n\rangle \exp[-iE_nt/\hbar]\langle n|n_2\rangle\langle n_2|X^{-1}|m_a\rangle$$

$$= \sum_{nn_1n_2} X^{(I)}_{m_bn_1} X^{(I)^*}_{m_an_2} \langle n|n_1\rangle^*\langle n|n_2\rangle \exp[-iE_nt/\hbar] \quad . \qquad \text{A-51}$$

Similarly

$$\langle m'_b|\Lambda(t)|m'_a\rangle^* = \sum_{n'n'_1n'_2} X^{(I)^*}_{m'_bn'_1} X^{(I)}_{m'_an'_2} \langle n'|n'_1\rangle\langle n'|n'_2\rangle^* \exp[+iE_{n'}t/\hbar] \quad . \qquad \text{A-52}$$

Insert the matrix elements into the expression for $G^{N_1N_2}_{k_1k_2}(t)$, equation A-45,

$$G^{N_1N_2}_{k_1k_2}(t) = \sum_{m_a m_b} \sum_{\substack{nn_1n_2 \\ n'n'_1n'_2}} (-1)^{2I+m_a+m_b} (\hat{k}_1\hat{k}_2)^{\frac{1}{2}} \begin{pmatrix} I & I & k_1 \\ m'_a & -m_a & N_1 \end{pmatrix} \begin{pmatrix} I & I & k_2 \\ m'_b & -m_b & N_2 \end{pmatrix}$$

$$\chi^{(I)}_{m_b n_1} \chi^{(I)*}_{m_a n_2} \chi^{(I)*}_{m'_b n'_1} \chi^{(I)}_{m'_a n'_2} \langle n|n_1\rangle^* \langle n'|n_2\rangle \langle n'|n'_1\rangle \langle n'|n'_2\rangle$$

$$\exp[-i(E_n - E_{n'})t/\hbar] \quad . \qquad \text{A-53}$$

To simplify this equation consider the m_a sum

$$\sum_{m_a} (-1)^{m_a} \chi^{(I)*}_{m_a n_2} \chi^{(I)}_{m'_a n'_2} \begin{pmatrix} I & I & k_1 \\ m'_a & -m_a & N_1 \end{pmatrix} = \sum_{m_a} (-1)^{n_2} \chi^{(I)}_{-m_a -n_2} \chi^{(I)}_{m'_a n'_2} \begin{pmatrix} I & I & k_1 \\ m'_a & -m_a & N_1 \end{pmatrix},$$

by A-8b

$$= (-1)^{n_2} \chi^{(k_1)*}_{P_1 N_1} \begin{pmatrix} I & I & k_1 \\ n'_2 & -n_2 & P_1 \end{pmatrix} \quad . \qquad \text{A-54}$$

Similarly for the m_b sum

$$\sum_{m_b} (-1)^{n_b} \chi^{(I)}_{m'_b n'_1} \chi^{(I)*}_{m'_b n'_1} \begin{pmatrix} I & I & k_2 \\ m'_b & -m_b & N_2 \end{pmatrix}$$

$$= (-1)^{n_1} \chi^{(k_2)}_{P_2 N_2} \begin{pmatrix} I & I & k_2 \\ n'_1 & -n_1 & P_2 \end{pmatrix} \quad . \qquad \text{A-55}$$

Inserting the above results into A-53 gives

$$G^{N_1N_2}_{k_1k_2}(t) = \sum_{\substack{nn_1n_2\\ n'n_1'n_2'}} (-1)^{2I+n_1+n_2}(\hat{k}_1\hat{k}_2)\; X^{(k_1)^*}_{P_1N_1} X^{(k_2)^*}_{P_2N_2}$$

$$\begin{pmatrix} I & I & k_1 \\ n_2' & -n_2 & P_1 \end{pmatrix} \begin{pmatrix} I & I & k_2 \\ n_1' & -n_1 & P_2 \end{pmatrix} \langle n|n_1\rangle^* \langle n|n_2\rangle \langle n'|n_1'\rangle \langle n'|n_2'\rangle^*$$

$$\exp\,[-i(E_n - E_{n'})t/\hbar] \quad . \qquad \text{A-56}$$

The average over all the microcrystal orientations must now be performed. These are the Euler angles, α,β,γ, contained in the D matrices. The average is

$$\overline{G^{N_1N_2}_{k_1k_2}(t)} = \sum_{\substack{nn_1n_2\\ n'n_1'n_2'}} \sum_{\lambda\lambda'} (-1)^{2I+n_1+n_2}(\hat{k}_1\hat{k}_2)\; R^{(k_1)^*}_{\lambda N_1} R^{(k_2)}_{\lambda' N_2} \langle n|n_1\rangle^* \langle n|n_2\rangle$$

$$\langle n'|n_1'\rangle \langle n'|n_2'\rangle^* \exp[-i(E_n - E_{n'})t/\hbar] \begin{pmatrix} I & I & k_1 \\ n_1' & -n_2 & P_1 \end{pmatrix} \begin{pmatrix} I & I & k_2 \\ n_1' & -n_1 & P_2 \end{pmatrix}$$

$$\frac{1}{8\pi^2} \int D^{(k_1)^*}_{P_1\lambda}(\alpha,\beta,\gamma)\, D^{(k_2)}_{P_2\lambda}(\alpha,\beta,\gamma)\, d\alpha\, d\cos\beta\, d\gamma \quad . \qquad \text{A-57}$$

Because of the orthogonality properties of the D matrices, the integral yields $\frac{8\pi^2}{\hat{k}_1}\,\delta_{k_1k_2}\,\delta_{P_1P_2}\,\delta_{\lambda\lambda'}$. This gives

$$\overline{G_{k_1k_2}^{N_1N_2}(t)} = \delta_{k_1k_2} \sum_{\substack{nn_1n_2 \\ n'n'_1n'_2}} (-1)^{2I+n_1+n_2} \langle n|n_1\rangle^* \langle n|n_2\rangle \langle n'|n'_1\rangle \langle n'|n'_2\rangle^*$$

$$\begin{pmatrix} I & I & k_1 \\ n'_2 & -n_2 & P_1 \end{pmatrix} \begin{pmatrix} I & I & k_1 \\ n'_1 & -n_1 & P_1 \end{pmatrix} \exp[-i(E_n - E_{n'})t/\hbar] \sum_{\lambda} R_{\lambda N_1}^{(k_1)^*} R_{\lambda N_2}^{(k_1)} \quad . \quad \text{A-58}$$

The sum over λ produces $\delta_{N_1N_2}$. The final result is

$$\overline{G_{k_1k_2}^{N_1N_2}(t)} = \delta_{k_1k_2}\delta_{N_1N_2} \sum_{mm'} \exp[-i(E_m - E_{m'})t/\hbar] \; S_{mm'}^{k_1k_1}$$

$$\equiv G_{kk}(t) \quad (k_1 = k_2 = k) \; , \qquad \text{A-59a}$$

where

$$S_{mm'}^{k_1k_2} = \sum_{n_1n_2n_3} (-1)^{2I+n_1+n_2} \langle m|n_1\rangle^* \langle m|n_2\rangle \langle m'|n'_1\rangle \langle m'|n'_2\rangle^*$$

$$\begin{pmatrix} I & I & k_1 \\ n'_2 & -n_2 & P \end{pmatrix} \begin{pmatrix} I & I & k_2 \\ n'_1 & -n_1 & P \end{pmatrix} \quad . \qquad \text{A-59b}$$

Applying the addition theorem of spherical harmonics to the perturbed angular correlation function gives the simple result,

$$W(\vec{k}_1,\vec{k}_2,t) = \sum_{k} A_k(\gamma_1) \; A_k(\gamma_2) \; G_{kk}(t) \; P_k(\cos\theta) \quad . \qquad \text{A-60}$$

The simple form of the perturbed angular correlation function is due entirely to the averaging process. Note that $G_{kk}(t)$ can be rewritten in a more revealing form

$$G_{kk}(t) = \sum_{nn'} S_{nn'}^{k\,k} \cos[(E_n - E_{n'})t/\hbar] \qquad \text{A-61}$$

The n=n' term, $S^{k_1 k_1}_{nn}$, is independent of time. This is the so-called hardcore term. This term indicates that the angular correlation pattern is never completely wiped out by static crystalline fields of any type. The origin of this effect is as follows. The powder sample has microcrystals oriented randomly in all directions. This means a small but finite number of these microcrystals are nearly aligned with respect to the propagation direction of one of the radiations. As shown earlier (equation A-49) the angular correlation pattern is unperturbed in this case.

E. The Static Electric Field Gradient

The interaction Hamiltonian for the static electric field interacting with the quadrupole moment of a nucleus is[52]

$$K_Q = \frac{4\pi}{5} T^{(2)} V^{(2)} = \frac{4\pi}{5} \sum_q (-1)^q T_q^{(2)} V_{-q}^{(2)} \quad . \qquad \text{A-62}$$

where the nuclear quadrupole spherical tensor operator is

$$T_q^{(2)} = \sum_p e_p r_p^2 Y_2^q (\theta_p, \phi_p) \quad . \qquad \text{A-63}$$

The sum is over all (point) nuclear changes and their coordinates. The term

$$V_q^{(2)} = \sum_c \frac{e_c}{r_c^3} Y_2^q (\theta_c, \phi_c) \qquad \text{A-64}$$

$$\underset{\sim}{K}_Q = \frac{eQV_{zz}}{4I(2I-1)} \begin{bmatrix} 10 & 0 & \eta\sqrt{10} & 0 & 0 & 0 \\ 0 & -2 & 0 & \eta 3\sqrt{2} & 0 & 0 \\ \eta\sqrt{10} & 0 & -8 & 0 & \eta 3\sqrt{2} & 0 \\ 0 & \eta 3\sqrt{2} & 0 & -8 & 0 & \eta\sqrt{10} \\ 0 & 0 & \eta 3\sqrt{2} & 0 & -2 & 0 \\ 0 & 0 & 0 & \eta\sqrt{10} & 0 & 10 \end{bmatrix} . \quad \text{A-69}$$

The energy eigenvalues are the solutions, λ, to the equation

$$\left(\frac{\lambda}{2}\right)^3 - 7\left(\frac{\lambda}{2}\right)(3+\eta^2) - 20(1-\eta^2) = 0 \quad . \quad \text{A-70}$$

The secular equation is of order three instead of the expected six because of the m-state degeneracy. Solution for the limiting cases are: $\eta = 0$, axially symmetric, $\lambda = 10, -2, -8$ (in units of $\frac{eQV_{zz}}{4I(2I-1)}$); $\eta = 1$, extreme asymmetry, $\lambda = 4\sqrt{7}, 0, -4\sqrt{7}$. Explicit solutions for the energy eigenvalues can be found in Gerdau et al.[53] Fig. A-1 schematically shows the simple behavior of the roots λ as a function of η.

As indicated in the previous section (see equation A-59a or A-61) $G_{kk}(t)$ depends on the energy differences, $E_m - E_{m'}$, which are experimentally measured quantities. Because of the degeneracy in the m states, only three energy differences need be considered for the I = 5/2 case. (For integer spin there are I+1 differences, for half integer I there are I+1/2 differences.) As figure A-1 indicates, the largest energy difference is equal to the

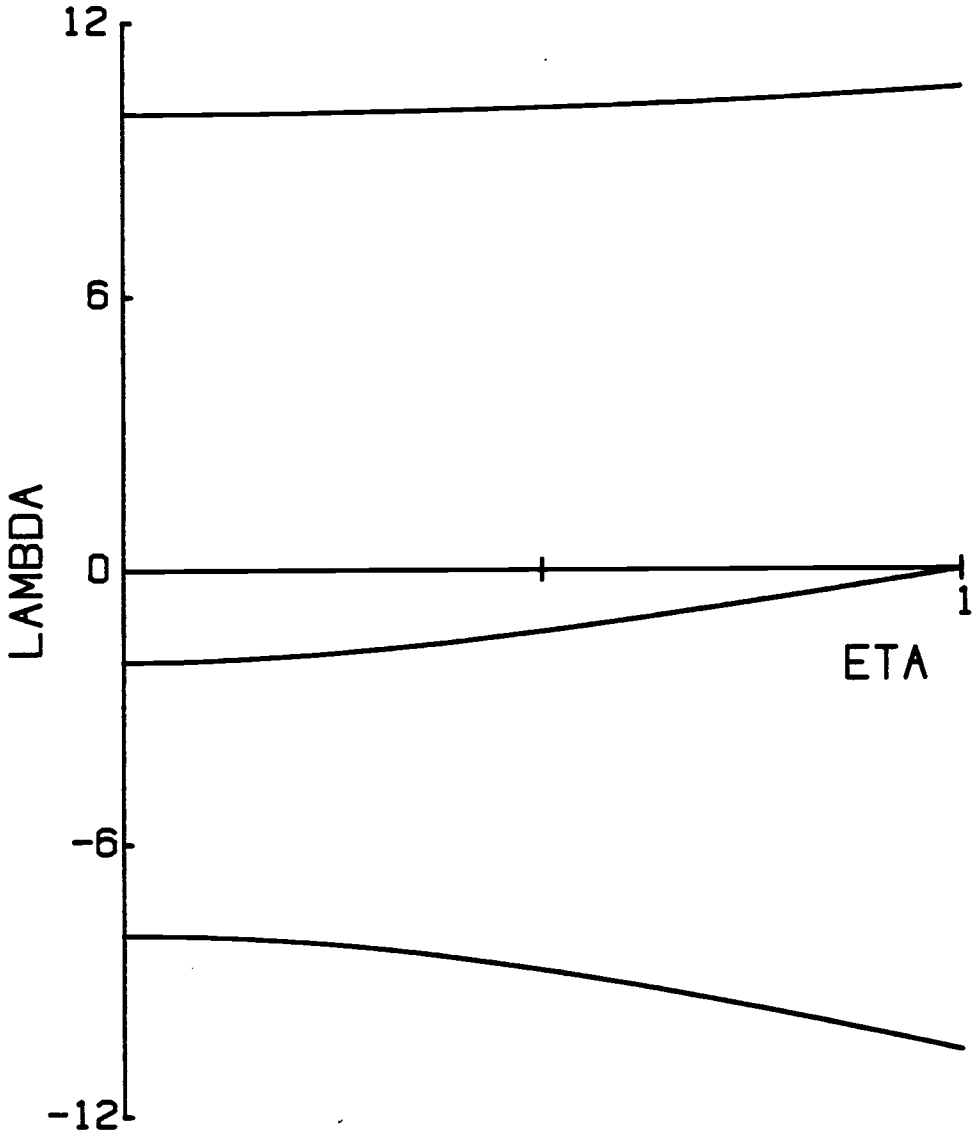

Figure A-1 A plot of the roots λ from equation A-70 as a function of the asymmetry parameter η.

sum of the smaller two. Note that these differences depend on the value of η.

Let $h\omega_1$ be the smallest energy difference and $h\omega_2$ be the next largest difference. Let $R = \omega_2/\omega_1$. Solving the I = 5/2 secular equation in polar coordinates gives the connection between R and η,

$$\theta = 3 \cot^{-1}\left[\frac{2\sqrt{3}(R+1)}{3}\right] \quad , \quad 0 \leq \theta \leq \frac{\pi}{2}$$

and

$$\cos\theta = \frac{10(1-\eta^2)3^{3/2}}{7^{3/2}(3+\eta^2)^{3/2}} \quad . \qquad \text{A-71}$$

In this way an experimental value of R can be related to the asymmetry parameter, η. Note the limiting cases:

$$R = 2 \quad \text{yields } \eta = 0$$

$$R = 1 \quad \text{yields } \eta = 1 \quad .$$

The factor, $eQV_{zz}/4I(2I-1)$, is the fundamental size of the energy splitting for the nuclear levels. The quadrupole coupling parameter and frequency of the quadrupolar interaction are defined as

$$\omega_Q = -\frac{eQV_{zz}}{4I(2I-1)\hbar} \text{ and } \nu_Q = \frac{4I(2I-1)}{2\pi}\omega_Q \quad . \qquad \text{A-72}$$

Consider the axially symmetric EFG. Equation A-61 and A-59b are in this case

$$G_{kk}(t) = \sum_{mm'} \begin{pmatrix} I & I & k \\ m' & -m & p \end{pmatrix}^2 \cos[(m^2-m'^2)3\omega_Q t] \quad .$$

Let the index n take on all positive integer values of $|m^2-m'^2|$ for integer I and $1/2|m^2-m'^2|$ for half integer I. Let the fundamental frequency $\omega_f = 3\omega_Q$ for integer I and $6\omega_Q$ for half integer I. Then the attenuation factor can be written

$$G_{kk}(t) = \sum_n s_n^{k\ k}{}_p \cos(n\omega_f t) \qquad \text{A-73}$$

where

$$s_n^{k_1 k_2}{}_p = \sum_{mm'} \begin{pmatrix} I & I & k_1 \\ m' & -m & p \end{pmatrix} \begin{pmatrix} I & I & k_2 \\ m' & -m & p \end{pmatrix} , \qquad \text{A-74}$$

with the sum over those m values which satisfy the above equality for the index n. For I = 5/2 the expansion takes the form,

$$G_{kk}(t) = \frac{1}{5} + \frac{13}{35} \cos \omega_f t + \frac{10}{35} \cos 2\omega_f t + \frac{5}{35} \cos 3\omega_f t . \qquad \text{A-75}$$

For the general case of axially asymmetric EFG, the explicity form of $G_{kk}(t)$ is difficult to calculate. As figure A-1 indicates, the energy difference changes continuously and monotonically as n increases from zero. (For example, explicit expressions can be used from Gerdau et al.[53]) In the same spirit as in the preceding development, the attenuation factor can be expressed as

$$G_{kk}(t) = \sum_n {}^{kk}S(\omega_n)\cos(\omega_n t) \qquad \text{A-76}$$

where $\omega_0 = 0$, $\omega_1 + \omega_2 = \omega_3$, $\omega_1 = \omega_f$ and

$$S^{k_1k_2}(\omega_n) = \sum_{mm'} S^{k_1k_2}_{mm'} \qquad \text{A-77}$$

with the sum over those values of m and m' that satisfy the particular energy difference ω_n. The expression for $S^{k_1k_2}_{mm'}$ is given in equation A-59b.

In reality, the magnitude and symmetry of the EFG varies from site to site. By assuming that the energy differences vary according to a normal probability distribution law,

$$\frac{1}{\sigma\sqrt{2\pi}} \exp\left[-\left\{\frac{(\omega-\omega_f)}{\sigma\sqrt{2}}\right\}^2\right] \quad ,$$

the average attenuation constant becomes

$$\overline{G_{kk}(t)} = \sum_n S^{k_1k_1}(\omega_n) \cos(\omega_n t)\, e^{-\delta^2\omega_n{}^2/2} \qquad \text{A-78}$$

with $\delta = \sigma/\omega_f$, σ being the standard deviation of the distribution of ω about the fundamental frequency ω_f. This relation assumes that only V_{zz} is distributed and not necessarily V_{xx} or V_{yy}.

F. Time Dependent Perturbations of Randomly Fluctuating Fields

The perturbing field is assumed to be fluctuating randomly both in magnitude and direction. At any instantaneous time t, a local configuration or field exists about the nucleus that has some average value acting in some direction z'. This local field continually reorients as time passes. If many reorientations occur in the lifetime τ_N of the intermediate state, then there exists

Thus, a convenient quantization axis z can be chosen for the perturbed angular correlation formalism which simplifies the mathematics. Let the z direction be parallel to the propagation direction of one of the radiations, i.e., the first. The spherical harmonics in equation A-44 can be simplified,

$$Y^{N_1}_{k_1}{}^{*}(\theta_1,\phi_1) \rightarrow 1$$

Furthermore, since the azimuthal angle is unimportant in describing the direction of the second radiation, let $\phi_2 = 0$. The other spherical harmonic becomes

$$Y^{N_2}_{k_2}(\theta_2,0) \rightarrow \sqrt{\frac{\hat{k}_2}{4\pi}}\, P_{k_2}\,(\cos\theta)$$

and θ is the angle between the two radiations. The results indicate that it is unnecessary to keep the n_1 and n_2 dependence in the formulas, so they have been conveniently set to the value zero. With these modifications, equations A-44 and A-45 become

$$W(\vec{k}_1,\vec{k}_2,t) = \sum_{k_1 k_2} A_{k_1}(\gamma_1)\, A_{k_2}(\gamma_2)\, G^{00}_{k_1 k_2}(t)\, P_{k_2}\,(\cos\theta) \qquad \text{A-79}$$

and

$$G^{00}_{k_1 k_2}(t) = \sum_{mm'} (-1)^{2I+m+m'} (\hat{k}_1\hat{k}_2)^{\frac{1}{2}} \begin{pmatrix} I & I & k_1 \\ m & -m & 0 \end{pmatrix} \begin{pmatrix} I & I & k_2 \\ m' & -m' & 0 \end{pmatrix} \left|\langle m' \left| \Lambda(t) \right| m \rangle\right|^2 . \qquad \text{A-80}$$

The term $|\langle m'|\Lambda(t)|m'\rangle|^2$ is the probability, $W_{mm'}(t)$, that if a nucleus was in the state $|m\rangle$ at t = 0 then it will be in the state $|m'\rangle$ at a time t. The transition is brought about by the time evolution operator, $\Lambda(t)$, which contains the interaction Hamiltonian K(t).

Using first order time dependent perturbation theory the transition probability is found to be

$$W_{mm'}(t) = \frac{1}{h^2} \left| \int_0^t K_{mm'}(t') \, e^{-i\omega_{mm'}t'} \, dt' \right|^2 , \qquad \text{A-81}$$

where $\omega_{mm'} = (E_m - E_{m'})/h$ and $K_{mm'}(t) = \langle m|K(t')|m\rangle$.

Expand the absolute square to simplify $W_{mm'}(t)$.

$$W_{mm'}(t) = \frac{1}{h^2} \int_0^t dt' \int_0^t dt'' \, K_{mm'}(t') \, K_{mm}^*(t'') \, e^{-i\omega_{mm'}(t'-t'')}$$

Now change the integration variables - letting $t'-t'' = \tau$ and keep t'. The resulting equation is

$$W_{mm'}(t) = \frac{1}{h^2} \left[\int_0^t d\tau \int_\tau^t dt' \, K_{mm}(t') \, K_{mm'}^*(t'-\tau) \, e^{-i\omega_{mm'}\tau} \right.$$
$$\left. + \int_{-t}^{0} d\tau \, e^{-i\omega_{mm'}\tau} \int_0^{t+\tau} dt' \, K_{mm'}(t') \, K_{mm'}^*(t'-\tau) \right] . \qquad \text{A-82}$$

An ensemble of nuclei is being subjected to the interaction K(t) and thus the ensemble averaged transition probability is required. Hence the expression, $\langle K_{mm'}(t')K_{mm'}^*(t'-\tau)\rangle_{E.A.}$, must be evaluated. This expression is proportional to the correlation function of the random fluctuating field contained in the

Hamiltonian K(t). Additional information on correlation functions and their properties can be found in Abragam.[32]

By assuming that the fluctuating perturbing fields are stationary random fields (that is, the fluctuations are independent of the origin of time), then the correlation function depends only on the time difference between observations,

$$R_{mm'}(\tau) = \langle K_{mm'}(t')\, K^{*}_{mm'}\, (t'-\tau)\rangle_{E.A.} \quad . \qquad \text{A-83}$$

Further, assuming that the direction in which time is measured has no effect on the value of the correlation function, then $R_{mm'}(t)$ is real and must be an even function of τ.[32]

Notice that for $\tau = 0$,

$$R_{mm'}(0) = \langle \left| K_{mm'}(t') \right|^{2} \rangle_{E.A.} \geq 0 \quad . \qquad \text{A-84}$$

Also, for very long times the value of the field in the future is independent of or uncorrelated with the field in the distant past. Thus for $\tau \to \infty$, $R_{mm'}(\tau) \to 0$. Let τ_c be a characteristic time, the correlation time, where the value of the correlation function is approximately midway between zero and the maximum value at $\tau = 0$. Thus for $|\tau| >> \tau_c$, $R_{mm'}(\tau)$ is essentially zero.

Abragam's model[32] for the correlation function due to Brownian type motion or fluctuating fields is

$$R_{mm'}(\tau) = R_{mm'}(0)\, e^{-|\tau|/\tau_e}$$

Slichter[33] gives a simple example of a correlation function due to a fluctuating elementary spin,

$$R_{mm'}(\tau) = R_{mm'}(0)\ e^{-|\tau|/\tau_c} \qquad \text{A-85}$$

with $\tau_c = 1/2W$, where W is the spin flip transition rate.

Assuming the correlation function to be a stationary even function of τ, then the integrations over t' can be performed. This leads to the result,

$$\langle W_{mm'}(t)\rangle_{E.A.} = \frac{1}{\hbar^2}\left[t\int_{-t}^{+t} d\tau e^{-i\omega_{mm'}\tau} R_{mm'}(\tau) \right.$$

$$\left. -2\int_{0}^{t} d\tau\ \tau \cos \omega_{mm'}\tau\ R_{mm'}(\tau)\right] \quad . \qquad \text{A-86}$$

Using the assumption that the experimental observation time is very long compared to the correlation time, then the above two integrals can be easily compared and the first term dominates by virtue of the coefficient t in front of the integral. For $t>\tau_c$, $R_{mm'}(t)$ is essentially zero and the limits of the integral can be extended to infinity with little overall contribution. This gives

$$\langle W_{mm'}(t)\rangle_{E.A.} = \frac{t}{\hbar^2}\int_{-\infty}^{\infty} e^{-i\omega_{mm'}\tau} R_{mm'}(\tau) \quad . \qquad \text{A-87}$$

The integral is in fact the spectral density function, $J(\omega_{mm'})$, which can be measured under some circumstances with other experimental techniques such as nuclear magnetic resonance.[33]

Using the Abragam or Slichter model for the correlation function, the spectral density function can be evaluated. With the relation that the transition probability per unit time is just the

averaged transition probability divided by time, then the transition rate for the ensemble becomes,

$$Q_{mm'}(t) = \frac{\langle W_{mm'}(t)\rangle_{E.A.}}{t} = \frac{2\tau_c}{h^2}\frac{\langle |K_{mm'}(0)|^2\rangle_{E.A.}}{1 + (\omega_{mm'}\tau_c)^2} \quad . \qquad \text{A-88a}$$

With the assumption that $W_{mm'}\tau_c << 1$ (there are many fluctuations occurring during the transition frequency time scale $W_{mm'}$) then the simple result for the transition rate is

$$Q_{mm'}(t) = \frac{2\tau_c}{h^2} < |K_{mm'}(t)|^2>_{E.A.} \quad . \qquad \text{A-88b}$$

where $<|K_{mm}(t)|^2>$ has been substituted for $<|K_{mm'}(0)|^2>$ because of the independence of the origin of time previously assumed.

The above result is correct to first order, and is not correct when the transition probability is not small compared to unity. In this case the occupation probability of a state $|m>$ changes with time and must be calculated from the master equation,

$$\frac{dP_m}{dt} = \sum_{m'=-I}^{+I} Q_{mm'}(P_{m'}-P_m) \quad ,$$

which is valid when the transition rate is small compared to the field fluctuation rate, $Q_{mm'}\tau_c << 1$. (Note that $Q_{mm'}t \lesssim 1$ is possible since $t>>\tau_c$ under the previous assumptions.)

The solution to the master equation must be found under the initial condition that the state $|m>$ is initially occupied, $P_{m'}(0) = \delta_{mm'}$.

At this point an explicit form for the term $\langle|K_{mm'}(t)|^2\rangle_{E.A.}$ must be calcuated. The following two sections makes this calculation under the cases of fluctuating electric field gradients and a paramagnetic relaxation mechanism respectively.

G. The Attenuation Factor for Randomly Fluctuating EFGs

The quadrupolar Hamiltonian for the laboratory axis z is

$$K_Q(z,t) = \frac{4\pi}{5} \sum_q (-1)^q T_q^{(2)} V_{-q}^{(2)}(z,t) \quad . \qquad \text{A-89}$$

But the EFG is best described in its own time independent coordinates z'. Using the rotation matrix with time dependent Euler angles to rotate into the principal axis frame of the EFG produces,

$$K_Q(z,t) = \frac{4\pi}{5} \sum_{qq'} (-1)^q T_q^{(2)} D^{(2)}_{-q',-q}(\alpha(t),\beta(t),\gamma(t)) V^{(2)}_{-q'}(z'). \qquad \text{A-90}$$

For an axially symmetric EFG, the sum over q' reduces to only one contributing value at q' = 0. In the general case with rhombic fields, additional terms are present and cannot be ignored.

Simplifying the product,

$$\langle m_b|K_Q(t)|m_a\rangle\langle m_b|K_Q(t)|m_a\rangle^* = \left(\frac{4\pi}{5}\right)^2 \sum_{\substack{qq' \\ q_1 q_1'}} (-1)^{q+q_1} V^{(2)}_{-q'}(z') V_{-q_1'}(z')$$

$$\langle m_b|T_q^{(2)}|m_a\rangle\langle m_b|T_{q_1}^{(2)}|m_a\rangle^* D^{(2)}_{-q',-q} \; D^{(2)}_{-q_1',-q_1}{}^*$$

by applying the Wigner-Eckart Theorem and the definition of the quadrupole moment (see equations A-4 and A-68) gives

$$\left|\langle m_b|K_a(t)|m_a\rangle\right|^2 = \frac{\pi}{5} \sum_{\substack{qq' \\ q_1 q_1'}} (-1)^{q+q_1}(eQ)^2\, V^{(2)}_{-q'}(z')\, V^{(2)}_{-q_1'}(z')$$

$$\begin{pmatrix} I & 2 & I \\ -m_b & q & m_a \end{pmatrix}\begin{pmatrix} I & 2 & I \\ -m_b & q_1 & m_a \end{pmatrix}\begin{pmatrix} I & 2 & I \\ -I & 0 & I \end{pmatrix}^{-2} D^{(2)}_{-q'-q}\, D^{(2)}_{-q_1'-q_1}\,, \quad \text{A-91}$$

where the z projection sum rule of the 3j symbols implies $q_1 = q$. The ensemble average is taken over all the random orientations of the Euler angles,

$$\frac{1}{8\pi^2}\int D^{(2)}_{-q'-q}\,(\alpha(t),\beta(t),\gamma(t))\, D^{(2)*}_{-q'-q}(\alpha(t),\beta(t),\gamma(t))\,d\alpha\, d\cos\beta\, d\gamma\,.$$

The square of the matrix element now has the form

$$\left\langle\left|\langle m_b|K_Q(t)|m_a\rangle\right|^2\right\rangle_{E.A.}$$

$$= \frac{\pi}{25}\sum_q (eQ)^2\begin{pmatrix} I & 2 & I \\ -m_b & q & m_a \end{pmatrix}^2\begin{pmatrix} I & 2 & I \\ -I & 0 & I \end{pmatrix}^{-2}\sum_q \left[V^{(2)}_{-q'}(z')\right]^2\,. \quad \text{A-92}$$

Referring to equation A-66 to evaluate the sum

$$\sum_{q'}\left[V^{(2)}_{-q'}(z')\right]^2 = \frac{5}{16\pi}\, V^2_{z'z'}\left(1+\frac{1}{6}\eta^2\right)$$

yields the completed result

$$\left\langle \left| \langle m_b | K_Q(t) | m_a \rangle \right|^2 \right\rangle_{E.A.}$$

$$= \frac{\pi}{80} (eQ)^2 V^2_{z'z'} \left(1 + \frac{\eta^2}{6}\right) \begin{pmatrix} I & 2 & I \\ -I & 0 & I \end{pmatrix}^{-2} \sum_q \begin{pmatrix} I & 2 & I \\ -m_b & q & m_a \end{pmatrix}^2 \quad . \quad \text{A-93}$$

The term $V_{zz'}(1 + \eta^2/6)$ should be interpreted as the ensemble average of the square of magnitude of the local field strength.

With the above result we can rewrite the master equation as

$$\frac{dP_{m_a}}{dt} = a \sum_{m_b} \begin{pmatrix} I & 2 & I \\ -m_b & q & m_a \end{pmatrix}^2 (P_{m_b} - P_{m_a}) \qquad \text{A-94}$$

where

$$a = \frac{\tau_c}{40\hbar^2} \frac{(eQ)^2 V^2_{z'z'} \left(1 + \frac{\eta^2}{6}\right)(I+1)(2I+3)(2I+1)}{I(2I-1)} \quad .$$

(The explicit expression for $\begin{pmatrix} I & 2 & I \\ -I & 0 & I \end{pmatrix}^{-2}$ has been calculated from Messiah's expression[48] and inserted into the equation.)

Using the orthogonality property of the 3j symbol (equation A-36) and trying the solution form

$$P_{m_i}(t) = P_{m_i}(0) e^{-\lambda t} \quad , \qquad \text{A-95}$$

gives the result

$$C\, P_{m_a}(0) = \sum_{m_b} \begin{pmatrix} I & 2 & I \\ -m_b & q & m_a \end{pmatrix}^2 P_{m_b}(0) \quad , \qquad \text{A-96}$$

where

$$C = \frac{1}{\hat{I}} - \frac{\lambda}{a} \quad .$$

If $P_{m_i}(0)$ were a suitable chosen 3j symbol then the contraction relation for three 3j symbols (equation A-6) yields another 3j multiplied by a 6j symbol, this 6j could then be equal to the constant C above. The solution form

$$P_m^{(r)}(0) = \text{constant}(-1)^{r-I-m} \begin{pmatrix} I & r & I \\ m & 0 & -m \end{pmatrix} \qquad \text{A-97}$$

where $P_m(0) = \sum_r \alpha_r P_m^{(r)}(0)$ is inserted. After performing the contraction over the three 3j's the result found is

$$C\, P_{m_a}^{(r)}(0) = P_{m_a}^{(r)}(0)(-1)^{2I+r} \begin{Bmatrix} I & r & I \\ I & 2 & I \end{Bmatrix} \qquad \text{A-98}$$

or

$$C = (-1)^{2I+r} \begin{Bmatrix} I & r & I \\ I & 2 & I \end{Bmatrix} = W(Ir2I;\ II)$$

By demanding orthogonality of the components of the vector $p^{(r)}(0)$ the constant can be evaluated to be $\hat{r}$. Furthermore, orthogonality of the total probability vector $P(0) = \sum_r \alpha_r p^{(r)}(0)$ implies

$$\alpha_r = (-1)^{r-I-m_a} \hat{r} \begin{pmatrix} I & r & I \\ m_a & 0 & -m_a \end{pmatrix} \quad , \qquad \text{A-99}$$

where the initial condition, $P_m(0) = \delta_{mm_a}$ has been used. In this way the total probability vector for any time t is

$$P(t) = \sum_{r,m_b} (-1)^{2r-2I-m_a-m_b} \hat{r} \begin{pmatrix} I & r & I \\ m_a & 0 & -m_a \end{pmatrix} \begin{pmatrix} I & r & I \\ m_b & 0 & -m_b \end{pmatrix} \quad . \qquad \text{A-100}$$

The solution required is $P_{m_b}(t)$, the probability that the state m_b is occupied at time t. This is substituted for $\left|\langle m_b|\Lambda(t)|m_a\rangle^2\right|$ in the expression for $G^{00}_{k_1k_2}(t)$ (equation A-80). After using the orthogonality properties of the 3j symbols two more times the result found is

$$G^{00}_{k_1k_2}(t) = e^{-\lambda_{k_1} t} \delta_{k_1k_2} \quad , \qquad \text{A-101}$$

which means that the perturbed angular correlation function has the form

$$W(\vec{k}_1,\vec{k}_2,t) = \sum_k A_k(\gamma_1)\, A_k(\gamma_2)\, G^{00}_{kk}(t)\, P_k(\cos\theta) \quad . \qquad \text{A-102}$$

The attenuation constant

$$\lambda_k = a(\underline{\underline{\frac{1}{\hat{I}}}} - C)$$

can be evaluated using the tables by Biedenharn, Blatt and Rose[54] for evaluating Racah coefficients. After a lengthy calculation, the attenuation constant takes the form

$$\lambda_k = \frac{3}{80} \frac{\tau_c (eQ)^2}{\hbar^2} \frac{V^2_{z'z'}(1+\frac{\eta^2}{6})k(k+1)[4I(I+1)-k(k+1)-1]}{I^2(2I-1)^2} \quad . \qquad \text{A-103}$$

H. The Attenuation Factor for a Paramagnetic Relaxation Mechanism

The model Hamiltonian for a paramagnetic interaction is

$$K_s = a_s \vec{I}(z) \cdot \vec{S}(z,t) \quad , \qquad \text{A-104}$$

where the paramagnetic center is represented by the term $\vec{S}(z,t)$ which fluctuates in time due to relaxation effects with other nearby spins in the material (the material is usually a liquid) and z is the laboratory axis. The spin of the paramagnetic center is effectively 1/2 (one electron) which couples to the nuclear spin of the intermediate state through the coupling constant a_s. Additional details can be found in Abragam.[32]

Rewriting the Hamiltonian in tensor form

$$K_s = a_s \sum_n (-1)^n I_n^{(1)}(z) S_{-n}^{(1)}(z,t) \qquad \text{A-105}$$

and rotating the spin term to the local coordinate system of the paramagnetic center through the Euler angles $\alpha(t)$, $\beta(t)$, and $\gamma(t)$, whose fluctuations in time represent the random reorientation of the local coordinate system exactly as in the previous EFG case. The Hamiltonian is now

$$K_s = a_s \sum_{nn'} (-1)^n I_n^{(1)}(z) D_{-n'-n}^{(1)}(\alpha,\beta,\gamma) S_{-n'}^{(1)}(z') \quad . \qquad \text{A-106}$$

As before, the matrix elements $\langle m|K_s|m'\rangle\langle m|K_s|m'\rangle^*$ must be formed. Evaluation of this product is similar to the EFG case.

$$\left|\langle m\left|K_S\right|m'\rangle\right|^2 = \left|a_S\right|^2 \sum_{\substack{nn' \\ \ell\ell'}} (-1)^{n+\ell} I^2 \, S^{(1)}_{-n'}(z') \, S^{(1)}_{-\ell'}(z')$$

$$\begin{pmatrix} I & 1 & I \\ -m & n & m \end{pmatrix} \begin{pmatrix} I & 1 & I \\ -m' & \ell & m \end{pmatrix} \begin{pmatrix} I & 1 & I \\ -I & 0 & I \end{pmatrix}^{-2} D^{(1)}_{-n'-n}(\alpha,\beta,\gamma) \, D^{(1)*}_{-\ell'-\ell}(\alpha,\beta,\gamma) \quad . \text{A-107}$$

Averaging over the Euler angles produces the factor $1/3 \, \delta_{n\ell}\delta_{n'\ell'}$. Inserting this result gives

$$\left\langle\left|\langle m\left|K_S\right|m'\rangle\right|^2\right\rangle_{E.A.} =$$

$$\frac{\left\langle\left|a_S\right|^2\right\rangle_{E.A.}}{3} I^2 \begin{pmatrix} I & 1 & I \\ -I & 0 & I \end{pmatrix}^2 \sum_{n'} [S^{(1)}_{-n'}(z')]^2 \sum_{n} \begin{pmatrix} I & 1 & I \\ -m' & n & m \end{pmatrix}^2 \quad . \text{A-108}$$

The spin sum is simply the expectation value of S^2 in the local configuration. Substituting the value of the 3j symbol and letting $\left\langle\left|a_S\right|^2\right\rangle_{E.A.} = \hbar^2\omega_S{}^2$ yields

$$\left\langle\left|\langle m\left|K_S\right|m'\rangle\right|^2\right\rangle_{E.A.} = \frac{\hbar^2\omega_S{}^2}{3} S(S+1)I(I+1)(2I+1) \sum_{n} \begin{pmatrix} I & 1 & I \\ -m' & n & m \end{pmatrix}^2 \quad . \text{A-109}$$

Using the time dependent perturbation theory developed in section F where the correlation time become the characteristic fluctuation or relaxation time of the paramagnetic center, the master equation can be written

$$\frac{dP_{m_a}}{dt} = a \sum_{m_b} \begin{pmatrix} I & 1 & I \\ -m_b & q & m_a \end{pmatrix}^2 (P_{m_b} - P_{m_a}) \qquad \text{A-110}$$

where

$$a = \frac{2}{3} \tau_c \omega_S^2 \, S(S+1)I(I+1)(2I+1)$$

This relation should be contrasted with that of equation A-94 for the EFG, the difference being only the constant a, and the unit index in the 3j symbol instead of the "2" in the EFG case. The similarity also includes all assumptions that were used in developing the EFG result; the correlation function having the Abragam form, the observation time being very large compared to the correlation time, and the master equation validity relation. The solution technique is exactly the same as before, except for some minor phase differences.

The eigenvalue is

$$C = (-1)^{2I+k+1} \begin{Bmatrix} I & 1 & I \\ I & k & I \end{Bmatrix} = W(I1kI;II) \quad , \qquad \text{A-111}$$

with attenuation factor

$$G^{00}_{k_1 k_2}(t) = e^{-\lambda_{k_1} t} \delta_{k_1 k_2} \quad , \qquad \text{A-112}$$

where $\lambda_k = a(\frac{1}{1} - C)$.

Again using Biedenharn *et al.*[54] to evaluate the Racah coefficient gives the final result,

$$\lambda_k = \frac{1}{3} \tau_c \omega_S^2 \, S(S+1) \, k(k+1) \qquad \text{A-113}$$